ANGIOGENESIS AS A PATHOLOGIC MECHANISM AND NOVEL THERAPEUTIC TARGET IN AN ANIMAL MODEL OF MULTIPLE SCLEROSIS

by

Carolyn Jo-Anne MacMillan

Submitted in partial fulfilment of the requirements
for the degree of Doctor of Philosophy

at

Dalhousie University
Halifax, Nova Scotia
March 2013

DALHOUSIE UNIVERSITY

DEPARTMENT OF PATHOLOGY

The undersigned hereby certify that they have read and recommend to the Faculty of Graduate Studies for acceptance a thesis entitled "ANGIOGENESIS AS A PATHOLOGIC MECHANISM AND NOVEL THERAPEUTIC TARGET IN AN ANIMAL MODEL OF MULTIPLE SCLEROSIS" by Carolyn Jo-Anne MacMillan in partial fulfilment of the requirements for the degree of Doctor of Philosophy.

Dated: March 4, 2013

External Examiner: _____

Research Supervisor: _____

Examining Committee: _____

_____

_____

Departmental Representative: _____

DALHOUSIE UNIVERSITY

DATE: March 4, 2013

AUTHOR: Carolyn Jo-Anne MacMillan

TITLE: ANGIOGENESIS AS A PATHOLOGIC MECHANISM AND NOVEL THERAPEUTIC TARGET IN AN ANIMAL MODEL OF MULTIPLE SCLEROSIS

DEPARTMENT OR SCHOOL: Department of Pathology

DEGREE: PhD CONVOCATION: May YEAR: 2013

_____

Signature of Author

In loving memory of my dear friend and mentor, Dr. Duane L. Guernsey.

TABLE OF CONTENTS

LIST OF TABLES

LIST OF FIGURES

ABSTRACT

Multiple sclerosis (MS) is an inflammatory autoimmune disease of the central nervous system. We hypothesize that angiogenesis results in new vessels which serve as a conduit for immune cell recruitment in MS, and contribute to inflammation through the pro-inflammatory properties of angiogenic regulators. This study is one of the first to explore regulation of angiogenesis in a murine model of MS (experimental autoimmune encephalomyelitis, EAE), and its potential as a therapeutic target.

Angiogenesis was apparent 21 days following disease induction and correlated with clinical and pathologic scores. We documented alterations in the VEGF and Ang/Tie signaling pathways. Expression of VEGF increased at day 14 then reduced by day 21. At this time point, Ang-2 levels were elevated due to expression by infiltrating macrophages. Ang-1 was significantly reduced at day 14 and increased at day 21 due to expression by CD3+ T-cells. The same expression pattern was validated in inflammatory cells within human MS tissue. Vascular permeability increased at day 14 and returned to control levels at day 21. The volume of permeable tissue weakly correlated with angiogenesis.

VEGF blockage with bevacizumab suppressed angiogenesis and reduced clinical scores and vascular permeability. Retention of CD4+ T-cells in peripheral lymph nodes and reduced T-cell proliferation was noted following treatment. Bevacizumab reduced mononuclear cell infiltration into spinal cord. Isolated CD4+ T-cells showed reduced expression of IL-17 and IFN-γ. B20-4.1.1 (a monoclonal antibody against murine VEGF) reduced clinical scores and suppressed angiogenesis as did treatment with angiostatin (an inhibitor of endothelial cell proliferation). B20-4.1.1 reduced vascular permeability, induced retention of CD4+ T-cells in peripheral lymph nodes, and inhibited T-cell proliferation, while angiostatin had no effect. Isolated lymphoid cells from mice treated with both agents showed reduced secretion of IL-17, but B20-4.1.1 had no effect on T-cell proliferation or IL-17 secretion when combined with angiostatin.

We conclude that these angiogenesis inhibitors are effective in EAE and act by suppressing angiogenesis with a secondary effect on peripheral T-cell activation. To the extent that EAE replicates changes occurring in MS, we have demonstrated that modulation of angiogenesis may represent a promising strategy in the management of disease progression.

LIST OF ABBREVIATIONS USED

°C	degrees Celcius
µg	microgram
µl	microlitre
µm	micrometer
ADEM	acute disseminated encephalomyelitis
aEAE	active experimental autoimmune encephalomyelitis
ALS	amytrophic lateral sclerosis
Ang	angiopoietin
APC	antigen presenting cell
ATP	adenosine triphosphate
BBB	blood-brain barrier
BM	bone marrow
BMDC	bone marrow-derived dendridic cell
BSB	blood-spinal cord barrier
cDNA	complementary deoxyribonucleic acid
CFA	complete Fruend's adjuvant
cm	centimetre
CNS	central nervous system
CO_2	carbon dioxide
dH_20	distilled water
DMT	disease modifying therapy
DNA	deoxyribonucleic acid
DRG	dorsal root ganglion
EAE	experimental autoimmune encephalomyelitis
EBV	Epstein-Barr virus
ECM	extracellular matrix
ELISA	enzyme-linked immunosorbent assay
FCS	fetal calf serum
FDA	Food and Drug Administration

FGF	fibroblast growth factor
FITC	fluorescein isothiocyanate
g	gram
Gd	gadolinium
GFAP	glial fibrillary acidic protein
GM-CSF	granulocyte macrophage colony-stimulating factor
H&E	hematoxylin & eosin
H_2O_2	hydrogen peroxide
HEPES	4-(2-hydroxyethyl)-1-piperazineethanesulfonic acid
HLA	human leukocyte antigen
hr	hour(s)
HRP	horseradish peroxidase
HSPG	heparan sulfate proteoglycan
HUVEC	human umbilical vein endothelial cells
i.p.	intraperitoneal
ICAM	intercellular adhesion molecule
IFN	interferon
IgG	immunoglobulin G
IL	interleukin
JAM	junctional adhesion molecule
kg	kilogram
l	litre
LFB/CV	luxol fast blue/cresyl violet
LPS	lipopolysaccharide
LY	Lucifer Yellow
mAb	monoclonal antibody
MBP	myelin basic protein
mg	milligram
MHC	major histocompatibility complex
min	minute(s)
ml	millilitre

mM	millimolar
MMP	matrix metalloprotease
MOG	myelin oligodendrocyte glycoprotein
MRI	magnetic resonance imaging
mRNA	messenger ribonucleic acid
MS	multiple sclerosis
n	number
ng	nanograms
NO	nitric oxide
P	permeability
PBS	phosphate buffered saline
PCR	polymerase chain reaction
PDGF	platelet-derived growth factor
pEAE	passive experimental autoimmune encephalomyelitis
P_{estLY}	Lucifer Yellow-estimated permeability
PlGF	placental growth factor
PLP	proteolipid protein
P_{LY}	Lucifer Yellow permeability
PPMS	primary progressive multiple sclerosis
PS	permeability surface area
qPCR	real time/quantitative PCR
qRT-PCR	real time reverse-transcription PCR
r^2	regression coefficient
RNA	ribonucleic acid
RRMS	relapsing-remitting multiple sclerosis
RT	room temperature
DAB	diaminobenzidine
S	surface area
s.c.	subcutaneous
sec	second(s)
SPMS	secondary progressive multiple sclerosis

TBST	tris buffered saline with Tween 20
TcR	T-cell receptor
TGF	transforming growth factor
T_h	T helper
TNF	tumor necrosis factor
U	units
VCAM	vascular cell adhesion molecule
VEGF	vascular endothelial growth factor
VEGFR	vascular endothelial growth factor receptor

ACKNOWLEDGEMENTS

I would first and foremost like to express my most sincere gratitude to my supervisor Dr. Alexander Easton. His constant guidance, encouragement, and support have been absolutely vital to my growth as a researcher. I will be eternally grateful for his mentorship.

I am very thankful to my supervisory committee members Drs. David Hoskin, Virender Bhan, and Tim Lee for their time, direction, and support throughout my program. I would also like to express thanks to my external examiner, Dr. Jacqueline Quandt, for graciously making time to lend her wisdom to the final stages of my degree.

I am tremendously thankful for the support and training provided to me by Patricia Colp and Dr. Geoff Rowden from Histology Research Services. I am grateful to the many individuals at the Carleton Animal Care Facility who have spent a great deal of time throughout my program training and assisting me with the handling and treatment of my research animals. The success of this project can be attributed in large part to the individuals of these two facilities. I am also grateful to Drs. Carolyn Doucette and Suzanne Furlong for their contributions to this project, and to Eileen Kaiser in the departmental office for her support.

I would like to make note of the incredible support I have received from the endMS Regional Research and Training Centre and the Atlantic Division of the MS Society throughout my program. I would specifically like to thank Dr. John Fisk, Jodi Reid, and Dena Simon for their constant encouragement.

Finally, I am thankful for the love and support of my family and close friends throughout my time at Dalhousie University. Thank you to Dr. Linda Chen, Kathleen Atwood, Dale Corkery, Sara Lahsee, and Jordan Warford for making everyday in the lab so enjoyable.

CHAPTER 1: INTRODUCTION

1.1 Natural History of MS: Epidemiology and Pathogenesis

Multiple sclerosis (MS) is a chronic immune-mediated inflammatory disease of the central nervous system (CNS) that affects approximately 2.1 million people globally [1]. The disease was first described in 1838 by Robert Carswell when he noted "remarkable lesions of the spinal cord accompanied with atrophy" [2]. In 1955, the disease was given the name MS and has since come to be characterized by the destruction of myelin, the protective coating around nerve axons, and varying degrees of axonal injury [3].

Clinically, MS is characterized by the development of acute neurologic deficits and typically the progressive accumulation of neurological dysfunction [4]. The presentation of these deficits are separated in time, and can be attributed to lesions within the myelinated white matter of the CNS, the location of which are separated in space [5]. While the disease can present at any age, it most commonly presents in females during child-bearing years (age 20-45) [3]. Approximately twice as many women are affected as men, and individuals of northern European descent are at highest risk [3]. Onset during childhood or after the age of 50 is relatively rare although this has been documented [5].

Current therapies attempt to alter the disease course and its progression by manipulating the immune pathways responsible for demyelination and inflammation. Unfortunately, there is a great deal of heterogeneity in the response to these disease modifying therapies (DMTs). This may be attributable, at least in part, to the fact that the etiology of the disease remains unknown. An increased understanding of the mechanisms underlying MS pathogenesis is required to identify novel therapeutic targets, and improve treatment regimens and therapeutic outcomes.

1.1.1 Pathogenesis

It is generally believed that the inflammatory disease, MS, is initiated when the integrity of the blood-brain and blood-spinal cord barrier (BBB, BSB) is breached in a person who is genetically predisposed to the disease. The BBB (depicted in Fig. 1.1) is a concept based on the composition of small blood vessels in the CNS. These vessels are lined by endothelial cells whose junctions are tightly sealed, creating very low permeability (hence a barrier).

Post mortem analysis of the tissue from an MS brain by visual inspection will generally reveal multiple, discrete grey areas of discoloration, referred to as plaques or lesions. They have a predilection for periventricular white matter, but also affect the surface of the brain stem [6]. These lesions are hard and rubbery in texture and represent areas of both myelin and oligodendroctye loss, that can be evaluated by microscopic examination.

The lesions also contain inflammatory cells, often in a perivascular location, that include autoreactive T-cells (autoreactivity referring to the inappropriate identification of self antigens by components of the immune system). In addition, there are also plasma cells, macrophages, and activated microglia (the resident macrophages and antigen presenting cells, APCs, of the CNS) with in the lesions [3,7]. This inflammatory population is responsible for the production of a plethora of proinflammatory cytokines and chemokines, reactive oxygen species, glutamate excitotoxicity in nerve cells, and autoantibody production, in which plasma cells secrete antibodies that bind to self antigens. All of these factors have been implicated in the demyelination, axonal and neuronal damage, and BBB disruption that is present in MS patients [8]. Initially the

inflammation will be transient and remyelination can occur; however, over time this recovery lessens, allowing persistent symptoms to accumulate and disability to progress [2].

Several theories exist as to why the initial breach of the BBB occurs. One theory involves exposure to viruses during childhood and early life that result in activation of the CNS endothelium, permitting the entry of peripheral lymphocytes into the CNS [6]. If these infiltrating cells include a myelin-reactive population an acute inflammatory reaction can be initiated which ultimately results in the destruction of the myelin sheath and oligodendrocytes (the cells responsible for myelination) [6,7].

Another commonly accepted paradigm is that a genetic predisposition may result in failure of autoreactive immune cells to undergo apoptosis, resulting in disrupted immune tolerance and regulation [8]. Due to this, autoreactive T-cells which are normally eliminated during development are allowed to clonally expand within the lymph nodes and eventually enter peripheral circulation. For reasons unknown, these cells become activated, and penetrate the BBB. Here they are reactivated and clonally expand through interactions with APCs displaying self-antigens. Several autoimmune disorders, including lupus and rheumatoid arthritis, have been associated with the failure of cells to undergo apoptosis [9,10].

1.1.2 Components of Susceptibility

While the cause of MS remains unknown, there is a growing consensus that the etiology of the disease involves a combination of genetic susceptibility, environmental influence, and/or metabolic triggers. The influence of genetics on disease susceptibility has become increasingly evident. The risk of developing MS has been reported as 1/750

in the general population. This risk increases to 1/40 in individuals who have a first degree relative with the disease [1,2]. In addition, the concordance rate for maternal twins is approximately 25%, this rate being much lower for fraternal twins [5].

This potential for a genetic link was first highlighted by the observation that different ethnic groups have distinct rates of MS [5]; for example, MS is most common in Caucasians of northern European decent however Inuit and Aborigines have few (if any) documented cases [1]. This genetic link has been attributed to several causal genes, research most strongly supporting the human leukocyte antigen (HLA) class II locus as playing a role in MS [11]. In addition, as previously discussed, several studies have implicated a genetic alteration in the pro-apototic Fas-mediated pathway and/or anti-apoptotic Bcl-2-related protein that results in a failure to induce apoptosis in autoreactive immune cells as playing a key role [12,13].

Environmental factors that are most commonly implicated in altering susceptibility to the development of MS include sun exposure (and/or Vitamin D), and Epstein-Barr virus [14]. It has long been known that changes in environment also affect the rate of MS relapse, for instance exposure to heat. This initial observation has been extended by recent studies that implicate environmental factors in the rate of disease relapse [15,16].

The geographical spread of MS shows a relationship between latitude and disease prevalence, so that MS incidence increases as one moves away from the equator [14]. While there is a suspected inheritable component based upon ancestry, studies have also suggested that actual geographical location and subsequent exposure to sunlight impact Vitamin D levels in an individual making them more susceptible to the disease [17].

Lending credibility to the notion that Vitamin D may play a significant role in susceptibility to MS, high serum levels of the precursor of the active form of Vitamin D have been shown to be protective in MS, especially in individuals under 20 years old [18]. Beyond altering susceptibility, MRI has shown that the number of active lesions correlated with Vitamin D levels, indicating that this vitamin also acts during the active phase of relapsing-remitting MS [16].

Discussions regarding the relationship between EBV infection and MS have persisted following the discovery that virtually all (99.5%) of MS patients tested are positive for antibodies against EBV [14]. It should be noted, however, that the prevalence of EBV in age and sex matched controls is also very high (90-95%), highlighting the ubiquitous nature of EBV infection. The risk of developing MS appears to be especially high (doubled) in individuals who developed infectious mononucleosis following EBV infection [14]. Following onset of disease, EBV antigens have been correlated with lesion burden as measured by MRI and with measures of disability [19,20]. Studies have shown that adults who are seronegative for EBV have virtually no risk of developing MS, suggesting that perhaps EBV infection is permissive to disease initiation [14,21].

While there are many theories regarding the etiology of MS, it is becoming more apparent that MS cannot be attributed to a single cause, and that environmental and genetic factors may interact in a complex manner to determine overall susceptibility [14]. This is highlighted by several studies showing that individuals who emmigrate younger than 15 years old will adopt the MS risk of the country they relocate to whereas those who emmigrate at an age older than 15 retain the risk of their country of origin [22,23].

1.1.3 Clinical Features

Clinically, the course of MS is quite variable. Generally, MS begins with acute and reversible episodes of neurological disability, and eventually transforms into a progressive and irreversible neurological disease [24]. Initially, patients tend to present with motor, sensory, visual, and/or autonomic involvement [2]. These symptoms most commonly include numbness and tingling (paresthesias), burning or "pins and needles" sensations (dysesthesias), diplopia, ataxia, vertigo, and bladder and bowel disturbances [3]. These disturbances can resolve but may evolve into chronic deficits. These symptoms are typically not unique to the disease with the exception of two that tend to be characteristic: Lhermitte's symptom (electrical sensation that runs down spine and/or limbs when the neck is flexed) and the Uhthoff phenomenon (temporary worsening of symptoms when body temperature increases) [2].

Eighty percent of patients will present with an acute presentation of symptoms termed "Clinically Isolated Syndrome" [2]. A definitive diagnosis of MS can be made based upon clinical findings and using supporting evidence from ancillary tests such as magnetic resonance imaging (MRI) documenting the presence of BBB disruption and white matter lesions [25-27]. Depending on the course of disease the patient is experiencing, there are four major categories of MS [3]:

1. Relapsing-remitting (RRMS): This is the most common category representing approximately 85% of diagnoses. It is marked by unpredicatable "flare-ups" or episodes followed by partial or complete remission of symptoms. In instances where over a defined period of time

symptoms always completely resolve, this may be referred to as Benign MS.

2. Secondary progressive (SPMS): Many patients with RRMS will progress into this form. This category is characterized by progressive neurological deterioration between acute episodes. The median time between onset of RRMS and conversion to SPMS is 19 years [1].

3. Primary progressive (PPMS): This diagnosis can be applied to approximately 10% of MS patients. Symptoms gradually worsen from disease onset without relapse or remission, however, there may be plateaus in progression. PPMS is typically resistant to current DMTs.

4. Progressive-relapsing: This is the rarest diagnosis accounting for less than 5% of MS patients. The disease is progressive from onset with intermittent flare-ups of worsening symptoms and no remission.

In most patients the clinical course evolves as relapsing episodes of deficit during a variable and erratic time period followed by gradual or partial remission [2,5]. The frequency of relapse tends to decrease over time but there is a steady accumulation of neurological deficit [5]. Eventually 65% of patients will enter a secondary progressive phase [2].

The severity of acquired disability over time is variable, and can be dependent upon the disease course. Ultimately, 50% of patients will need assistance with walking within 15 years following disease onset [28]. Fatigue occurs in 90% of patients and is the most common work related disability affiliated with MS [3]. Patients also have increased risk of suicide reflecting an increased lifetime frequency of depression of up to 50%.

There is discussion as to whether this increased risk could be a manifestation of cerebral inflammation or a response to restrictions imposed by progressive disability [2].

MS reduces life expectancy by 5-10 years, with the median time to death approximately 30 years from disease onset. Death can be attributed to MS in two thirds of cases and to an increased risk of infection (most notably skin, chest and bladder in individuals with advanced neurological disability) [2]. However, a recent study also shows a reduced incidence of cancer in patients with MS compared to the general population, which may be related to increased immune surveillance [29].

1.1.4 Current Treatments

Given the prominence of inflammatory cells in MS lesions, targeting immune mechanisms that influence the destruction of myelin have been the focus of most therapeutic interventions [5]. There are eight DMTs currently approved for use in relapsing remitting forms of MS, all of which attempt to interrupt immune processes (Table 1.1). There are several other treatments currently in trials, the majority of which also operate through immune modulatory mechanisms [3].

DMTs are employed in an attempt to minimize the frequency and severity of relapses, and to provide relief from relapse symptoms [3]. Acutely, relapses can be treated with a short course of corticosteroid with rapid onset of action (for example, intravenous methylprednisolone [30]) to shorten the duration and severity of the attack and prevent the accumulation of further disability [3] . However, the long term effects of these therapies on disease progression and the development of disability are questionable [2].

While the majority of currently applied DMTs have been utilized in the treatment of MS for many years, their use comes with many side effects and substantial risk in

some cases. Treatment with interferon beta, for example, increases the risk of of liver abnormalities, leukopenia, thyroid disease and depression. Patients commonly report injection site reactions and worsening of pre-existing spasticity [3]. Glatiramer acetate treatment has been associated with injection site reactions, flu-like symptoms, chest pain, hot flashes, and headaches [3]. Natalizumab therapy, a second line treatment used only for individuals who do not respond to or are not able to tolerate first line therapies, increases the risk of progressive multifocal leukoencephalopathy (PML), an opportunistic viral infection of the brain that leads to severe disability or death [3].

MS is a progressive disease with no currently known cure. Unfortunately, these currently applied therapies are often poorly tolerated by patients, and ultimately they inadequately control the disease course [2]. In light of this, there is a need to identify new therapeutic strategies to be used in adjunct with lower doses of the current therapies, or to replace the current DMTs entirely. Due to ethical considerations of experimentation in humans and the impracticality of lesion sampling from MS patients, animal models that replicate features of the disease can be used to gain a better understanding of disease processes and identify novel potential therapeutic targets [31].

1.2 Experimental Autoimmune Encephalomyelitis (EAE)

Experimental autoimmune encephalomyelitis (EAE) is an inflammatory CNS disease induced in experimental animals to mimic aspects of MS and its pathogenesis. Animals with EAE have become the most widely accepted animal model for MS research. In fact, approximately 20% of all scientific literature published on MS to date utilized an EAE animal model. While it is most commonly used in rodents, EAE can be

induced in a variety of laboratory animals including, but not limited to, guinea pigs, rabbits, sheep, pigs, and primates [32].

The model is based on early observations of vaccination-related encephalitis in patients, which remains a rare complication in children injected with vaccines against mumps, measles and rubella, producing a disease known as acute demyelinating encephalomyelitis (ADEM). In the 1930s researchers were investigating why patients injected with a vaccine composed of spinal cord homogenates from rabies-infected rabbits were developing encephalomyelitis distinct from rabies [33]. Subsequently, through administration to several animal models it was discovered that CNS antigens present in the vaccine were triggering an unexpected autoimmune reaction within the vaccine recipients [34].

While early models of EAE were predominately in rabbits and rats, current protocols generally employ mice due to several factors including cost, simplicity of housing and maintenance, availability of experimental reagents, and the development of transgenic murine models that allow very specific molecular targeting *in vivo*. Over time, modifications have been made to the murine model protocol to allow for more robust and consistent development of encephalomyelitis. These changes included the addition of Complete Freund's adjuvant (CFA; a mixture of mineral oil and inactivated mycobacteria) to prolong and amplify the immune reaction to the CNS antigens, as well as an initial pertussis toxin injection to temporarily open the BBB and allow entry of autoreactive immune cells into the CNS [35,36].

MS is uniquely a human disease and there are currently no other animals known or documented to naturally and spontaneously develop a disease with all of the key

pathologic features (myelin damage, inflammation, and neurodegeneration) [31]. Several animal models have been created or adopted, however, to study specific features and components of MS. These models can be utilized to explore a variety of components of MS including demyelination and axonal damage. Generally, these methods fall into one of three categories: 1. Active induction models, 2. Passive induction models, or 3. Humanized/TCR transgenic models.

1.2.1 Active EAE (aEAE)

Active EAE (aEAE) is one of the earliest developed models for neuroinflammatory research. It involves immunization with CNS homogenates or myelin protein/peptides emulsified in a strong adjuvant [37-41]. This is done to activate peripheral myelin-specific CD4+ T-cells [42]. Both the CNS antigen used as well as the strain of mouse can alter the course and severity of disease. Table 1.2 demonstrates the variety of disease attainable using a combination of these factors, and demonstrates the strain specificity of EAE.

Typically, the pathology and disease course observed is species- or strain-specific and can be acute and monophasic (more representative of clinically isolated syndrome) or chronic and relapsing [31]. All EAE experiments conducted in this thesis were done using active immunization with myelin oligodendrocyte protein (MOG; amino acid sequence 35-55) in the C57Bl/6J murine strain which produces an acute and monophasic illness followed by a prolonged period of partial recovery or death. A chronic model of EAE can be induced using SJL/J mice and typically myelin basic protein (although other antigens have been documented) [42]. The C57Bl/6J – MOG_{35-55} model has become the most broadly applied method due to the simplicity of the induction protocol, the predictability of

disease onset, and the robustness and consistency of disease produced [37]. A significant disadvantage of this model, however, is that a large amount of systemically administered adjuvant is required, which could potentially distort immune responses by activating peripheral innate immunity independently of the desired autoimmune activation [37,43].

Following active induction protocols, animals typically remain asymptomatic for a period of 9-12 days [42]; however, the duration of this period can vary among species and immunization protocol [44]. Following this period of latency, immunized animals will begin to develop symptoms of neurological deficit. Clinically, these symptoms begin with tail weakness and will be followed by ascending paralysis. At the peak of acquired disability, symptoms in immunized animals can range from unilateral walking deficits, hindlimb paralysis, or, in the most extreme cases, forelimb paralysis. Table 1.3 outlines the clinical scoring system used to assess disease severity in the animals; 0 being no apparent disease, and 5 being moribund. Typically, peak disease activity can be observed by day 16-18, and will plateau by day 21 post-immunization. Following this time, animals may partially recover from their symptoms or symptoms will persist without further progression.

In the murine model of MS, the presentation of clinical symptoms can be histologically associated with perivascular inflammatory lesions and mononuclear cell infiltration (perivascular cuffing) [31]. Lesions seen in EAE are often associated with both inflammation and demyelination in the C57Bl/6J model, and are predominantly composed of CD4+ T-cells, macrophages, and neutrophils; however, CD8+ T-cells, and B-cells are also present [45].

The location within the CNS affected by the lesion varies according to the animal strain immunized and the stage of disease; however, the brain of most EAE animals will remain unaffected and the disease is generally contained within the spinal cord. There are, however, a few models that can develop cerebellar lesions [31,46,47]. In the C57Bl/6J – MOG_{35-55} model, peak inflammation can be observed two days following the peak of clinical symptoms, and demyelination will peak several days following that. While some pathology may be found in the forebrain in animals of this model, the disease is predominately in the spinal cord [34].

1.2.3 Passive EAE (pEAE)

In the passive induction model of EAE (pEAE), disease is induced by the adoptive transfer of myelin-specific T-cells from an aEAE animal to a naïve animal [37,48]. This model can be advantageous over the traditional aEAE model in that the effector T-cell population can be both labeled and manipulated *in vitro* prior to the transfer [48]. While this is generally beneficial, appropriate interpretation of mechanisms can be hampered by *in vitro* activation of the pathogenic cell population and the fact that a large number of maximally activated effector cells are bulk transferred into the animal [37]. In addition, this model typically fails to produce the robust and aggressive disease that can be induced with aEAE due to the fact that it is difficult to control the activation state of the T-cells being transferred, and the resulting disease is highly dependent on the number of T-cells transferred [48].

1.2.4 Humanized EAE models

Perhaps the most significant advances to MS experimentation came with the creation of Humanized or T-cell Receptor (TcR) transgenic murine models [31]. This is a

spontaneously occurring model which involves transgenic induction of myelin-specific major histocompatibility class (MHC) I antigen from human T-cell clones. While aEAE and pEAE tend to foster a CD4+ T-cell biased model, this transgenic method allows for the development of a CD8+ T-cell dominated disease which is more reminiscent of the inflammatory milieu observed in MS [31,37]. Unfortunately, the high variability and unpredictability of disease course in these models (ranging from mild deficit to rapidly developing chronic paralysis) make these models difficult to manipulate and therefore less advantageous over existing models unless the focus is to directly test a therapeutic that is targeting the human component of this model [31].

1.2.5 Limitations of EAE

EAE has contributed appreciably to current views on the pathogenesis of MS. In fact, three of the currently applied DMTs (glatiramer acetate, natalizumab, and mitoxantrone) were developed based on results from EAE experiments [49]. In addition, several therapeutics developed in the same manner are currently in late-phase clinical trials. Despite these contributions, it is of great importance that observations made with this model are done with consideration of potential disadvantages and limitations inherent in using an animal model to study a human disease.

One of the most obvious limitations in this model lies in the fact that MS is a spontaneous and unpredictable disease, whereas EAE is inducible, and results in a predictable disease course. In addition, no model of EAE replicates all of the pathological features of MS. Some mechanisms of neurodegeneration that have been associated with MS, such as low-grade microglial inflammation, gliosis and glutamaterigic overloading and neural metabolic dysfunction [31] have not been seen in acute models of EAE or in the

majority of chronic models [31]. As previously mentioned, there are also differences within the predominant inflammatory population in lesions, where CD8+ T-cells are more apparent in MS lesions, but CD4+ T-cells dominate in the majority of EAE models [50].

Another potential limitation revolves around the development of novel therapeutics. As with animal models of other human diseases, many treatments that work exceptionally well in the animal model do not translate to the clinic. For example, tumor necrosis factor (TNF) blockers were shown to ameliorate the disease course in EAE by reducing inflammation and promoting remyelination; however, they led to worsening of disease in MS clinical trials [51].

In light of these limitations, it is important to continually evaluate results with this model against MS patient tissues and samples for corroboration. Given the complexity of MS it is virtually impossible at this stage to replicate all features of this disease in a single model. With this in mind, appropriately used animal models are a critical component and an invaluable tool in exploring pathogenic mechanisms and potential therapeutic targets in MS.

1.3 Angiogenesis and Inflammatory Disease

Despite strong research efforts the cause of MS remains elusive. The pathological mechanisms are not fully understood and the clinical course is highly variable, explaining why treatment options are so limited. Without an established etiology or pathophysiology, the selection of DMTs has concentrated almost exclusively on modifying the immune response, as mentioned earlier. The notion that MS is an autoimmune disease has directed the majority of EAE research to date; however, resulting therapies have failed to fully ameliorate disease [31], indicating there may be other

underlying mechanisms at play. The purpose of this thesis was to explore another mechanism which may be contributing to disease progression in MS, specifically, the phenomenon of angiogenesis, which is the formation of new blood vessels.

Angiogenesis is a physiological process which plays a vital role in growth, development, and wound repair. The formation of vessels is a complex process which requires a delicate and finely maintained balance of several stimulatory and inhibitory signals [52,53]. Several forms of vessel creation have been identified. During embryonic development, vessels arise from endothelial precursor cells (angioblasts). These angioblasts differentiate into endothelial cells to form blood vessels *de novo* [54]. These endothelial cells assemble into a primitive labyrinth to form a rudimentary vascular network in a process known as vasculogenesis [52]. The process of angiogenesis ensures expansion of this network through the sprouting of new capillaries from pre-existing vessels. Through this process the primitive network remodels into a highly organized vascular network of larger vessels which branch into smaller ones [52]. The nascent tubes of endothelial cells then become covered by pericytes and/or vascular smooth muscle cells in a process called arteriogenesis which provides strength to the vessel and allows regulation of perfusion through release of vasoactive substances, such as nitric oxide (NO) [52].

Several other processes of vessel formation have been identified; however, are less understood. Intussusception is the process whereby pre-existing vessels split, giving rise to daughter vessels. In cancer, tumor cells have been shown to have the ability to hijack existing vasculature and create perfusable vessel-like structures in a phenomenon known as vascular mimicry. While debated, it is generally believed that the maintenance

of healthy adult vessels or the expansion of pathological networks of vessels can be assisted by the recruitment of bone marrow-derived cells and/or angioblasts to the vascular wall. These cells can then incorporate themselves into the vascular lining in a process known as postnatal vasculogenesis [55].

1.3.1 Physiological Angiogenesis

Quiescent vascular endothelial cells, in healthy adults, interconnect through junctional adhesion molecules (JAMs) to form a monolayer with a streamlined surface. In a mature vessel, the endothelial cells are covered by pericytes which suppress endothelial cell proliferation through secretion of maintenance and survival signals such as Vascular Endothelial Growth Factor (VEGF), and Angiopoietin-1 (Ang-1) which suppresses endothelial proliferation, a process necessary for angiogenesis to occur. Endothelial cells and pericytes produce a common basement membrane to support the structure [55].

In response to inflammation or hypoxia, angiogenic signals such as VEGF, Placental Growth Factor (PlGF), Angiopoietin-2 (Ang-2), or Fibroblast Growth Factors (FGFs) may be released to promote the recruitment of new vasculature to the area to reestablish homeostasis [56,57] . When this signal is detected by quiescent vessels, pericytes (in response to Ang-2 specifically) will detach from the vessel and use proteolytic degradation to release themselves from the basement membrane. VEGF signaling causes the endothelial cells of the vessel to loosen their cell-cell junctions, increasing permeability, and allowing plasma proteins to move between the vessel lumen and the surrounding tissue. These plasma proteins form a provisional extracellular matrix (ECM) scaffold along which activated endothelial cells will migrate via integrin signaling toward the angiogenic stimuli [55]. Matrix-bound isoforms of VEGF are liberated from the ECM

by proteases and interact with heparan sulfate proteoglycans (HSPGs) in the ECM to form a chemotactic gradient along which activated endothelial cells travel [58].

At the onset of this migration, one endothelial cell becomes the leading cell, referred to as the tip cell. This ensures an organized progression of the endothelial cells towards the angiogenic stimuli. Endothelial cells around the tip cell assume a secondary position and are called stalk cells. These cells divide and elongate behind the tip cell forming a lumen. To maintain this hierarchy, the tip cell exploits the VEGF gradient it is travelling along to control stalk cells. The tip cell upregulates DLL4 expression which activates NOTCH in the stalk cells. This results in the downregulation of VEGF receptor, VEGFR-2, expression by stalk cells rendering them less responsive to VEGF and ensuring the tip cell maintains the dominant leading position [59].

In order for this new immature vessel to stabilize and mature, the activated endothelial cells must resume their quiescent state, and inhibitory signals [60], such as Platelet derived growth factor (PDGF)-B, Ang-1, and Transforming growth factor (TGF)-β, must recruit pericytes to cover the vessel [61,62]. Protease inhibitors then allow the deposition of a basement membrane and junctional connections between the endothelial cells will be reestablished. If any of these steps are not completed, the vessel will not perfuse and it will regress [55].

1.3.2 Angiogenesis in the CNS

The vasculature supplies almost every organ in the body including the CNS. The CNS acquires its blood supply through angiogenesis (rather than vasculogenesis) in a complicated process whereby vessels from the pia mater grow inwards. Some will reach the ventricles then branch; these branches will give rise to more branches which will then

grow back towards the pia [54]. By adulthood, blood flow within the CNS accounts for roughly 20% of cardiac output highlighting the elaborate and vast network of branching that occurs within this system [54].

While the angiogenic process within the CNS is similar to that employed systemically, the resulting capillaries are unique in that they possess tight junctions which do not typically exist in normal circulation. This creates the BBB, separating the circulating blood from the CNS [63]. These tight junctions, created by claudins, occludins, and JAMs, allow endothelial cells of the CNS circulatory system to restrict the movement of molecules into the CNS. Active transport of metabolic products (such as glucose) also occurs through this barrier [55]. In addition to the tight junctions, the barrier is supported by a thick basement membrane and astrocytic end feet (Fig. 1.1).

The role of angiogenesis and its regulators extends beyond the expansion of the vasculature within the CNS. Cross talk between the pathways regulating angiogenesis and neurogenesis has been identified. For example, axon-guidance signals such as ephrin, semaphorins, and netrins allow angiogenic vessels within the CNS to navigate towards their target more efficiently, in addition to controlling vessel morphogenesis [52]. Neuronally-produced VEGF has also been demonstrated to influence vascular development within the CNS [64,65]. In both health and disease, angiogenic signals have been shown to guide axons and influence neuron function [54].

1.3.3 Key Regulators of Angiogenesis

While there are many factors influencing angiogenesis, VEGF has been identified as the predominate regulator of this process in both health and disease. VEGF is a sub-family of the platelet-derived growth factor (PDGF) family, and is a critical signaling

protein involved in both vasculogenesis and angiogenesis. There are five isoforms in the VEGF family: VEGF-A (referred to most commonly and throughout this thesis as simply VEGF), VEGF-B, VEGF-C, VEGF-D, and Placenta growth factor (PlGF).

VEGF is the most important member of the family and (most notably) is the dominant regulator of angiogenesis, a stimulatory signal for monocytes, granulocytes, and neurons, and acts as a vascular permeability factor. VEGF acts through VEGFR-2 signalling to promote endothelial cell proliferation, tube formation, and endothelial cell survival [66,67]. Neuropilins are VEGF co-receptors which enhance the activity of VEGFR-2 but they are also capable of signaling independently [68]. VEGF isoforms that can be cleaved from the ECM (and are therefore soluble) preferentially enlarge vessels, whereas matrix metalloprotease (MMP)-resistant matrix bound isoforms support vessel branching [69]. The critical role of VEGF and VEGFR-2 in angiogenesis is highlighted by the fact that deficiencies in either results in loss of vascular development that cannot be entirely compensated for by other angiogenic factors [52,55].

The other members of the VEGF family play a lesser role in angiogenesis. VEGF-B has been shown to be important for angiogenesis embryonically, specifically for the development of myocardial tissue [70]. VEGF-C and -D play an important role in the formation of lymphatic vessels [71]. PlGF is dispensable for developmental angiogenesis and only relevant in disease [72,73]. While all the isoforms have important functions, their roles in post-embryonic angiogenesis are thought to be insignificant relative to VEGF [58].

VEGF plays a critical role within the CNS. VEGF is trophic for nerve cells, and insufficient levels of VEGF have been shown to contribute to neurodegeneration [52]. By acting through VEGFR-1, VEGF can also stimulate the growth of astrocytes, an

important component of the BBB [54]. Within the CNS, the first actions of VEGF identified were its neurotrophic effects. In cultured cervical and dorsal route ganglion neurons, VEGF was shown to promote axonal outgrowth and cell survival through VEGFR-2 signaling [74]. In cultured neurons, VEGF increased the number and/or length of neurites through VEGFR-2 signaling [75]. Additionally, neuronal survival in explant cultures of the midbrain was increased in the presence of VEGF [76]. Under conditions of hypoxia or serum deprivation, hippocampal neuronal death was reduced in the presence of VEGF [77].

While VEGF-B plays a minimal to non-existent role in post-embryonic angiogenesis, it appears to have neuroprotective effects. Cultured cerebral cortical neurons are protected from hypoxia in the presence of VEGF-B. When VEGF-B knockout mice were exposed to an ischemic injury in the CNS, infarct volume was increased and neurological function was impaired compared to wildtype mice [78].

As previously mentioned, quiescent vessels must retain the ability to respond to angiogenic stimuli when these are presented. The angiopoietin family of growth factors plays an important role in regulating this switch. The angiopoietins are protein growth factors of which there are three members in humans: Ang-1, Ang-2, and Ang-4. Ang-3 is an interspecies ortholog in the mouse of human Ang-4 [79]. Ang-1 and Ang-2 are the most important members of this family and are required for the formation of mature blood vessels [80]. The effects of the angiopoietins are mediated through the Tie receptors (Tie-1, and Tie-2), which are cell surface tyrosine kinases. Ang-1 acts as a Tie-2 agonist, while Ang-2 competitively antagonizes Ang-1 in a context-dependent manner. Little is known about the function of Ang-4 however it is believed to act like Ang-1 [79]. Tie-1 is referred

to as an orphan receptor due to the fact that no ligand has yet been identified for this receptor. It is, however, believed to act as a negative regulator of Tie-2 [81].

Expression of Ang-1 can be attributed to mural cells such as pericytes and smooth muscle cells, however, expression of Ang-2 is predominantly from endothelial cells during angiogenesis. Ang-1 has been shown to influence the formation of cell-cell junctions which is vital for maintaining endothelial quiescence. Ang-1 also stimulates mural coverage and the deposition of basement membrane around the vessel [55]. In the presence of angiogenic signals, such as VEGF, sprouting endothelial cells will secret Ang-2. This antagonizes Ang-1 by competitively binding to Tie-2, enhancing pericyte detachment from the vessel, increasing vascular permeability, and promoting endothelial cell sprouting [55]. In cancer, tumor cell-derived Ang-2 has also been shown to promote angiogenesis by recruiting pro-angiogenic Tie-2 expressing monocytes [82].

1.3.4 Angiogenesis as a Therapeutic Target in Disease

Blood vessels are crucial for the growth and development of organs in the embryo and for wound repair and maintenance in adults. An imbalance in the growth or regulation of the vessels, however, can fuel disease by acting as a conduit for the recruitment of pro-inflammatory cells in the case of inflammatory diseases, or by allowing the movement of invasive cancer cells [52,55]. While angiogenesis is beneficial in some diseases, such as cardiovascular ischemic disease, in many others such as rheumatoid arthritis and psoriasis an increase in the vascular network increases pathology [83,84].

As previously described, quiescent endothelial cells require an angiogenic signal to become active and respond to the stimuli. In many conditions, this stimulus can

become excessive and the balance between pro- and anti-angiogenic signals becomes deregulated resulting in an angiogenic switch [52]. This pathogenic switch is commonly seen in malignancies, ocular disease, and inflammatory disorders [52]. In other conditions, such as ischemic heart disease or preeclampsia, the angiogenic switch required to respond to the insult is inadequate, leading to endothelial cell dysfunction, vessel malformation, and regression. This can result in insufficient revascularization and regeneration, and further pathology [52].

In inflammatory conditions, angiogenesis and inflammation can create a positive feedback relationship [85]. Various cytokines and chemokines are produced, attracting macrophages, neutrophils, dendritic cells, T-cells, and hematopoietic progenitors to the site. Recruited cells (specifically macrophages and neutrophils) can promote angiogenesis through activation of VEGF by releasing it from ECM stores using MMPs (specially MMP-9) [86-88]. In several diseases models, the survival of these cells has been shown to be promoted through locally produced VEGF and PlGF, sustaining their ability to perpetuate the angiogenic response [52]. Leukocyte-attracting chemokines, such as IL-8, can directly stimulate endothelial cell growth in addition to recruiting inflammatory cells, thereby promoting angiogenesis [52]. In cancer models, tumor-associated macrophages and Tie-2-expressing monocytes have been shown to produce pro-angiogenic factors such as VEGF [52]. In contrast to the vascular homeostasis induced by autocrine release of VEGF by endothelial cells [89], paracrine VEGF release by stromal cells (or tumor cells in cancer) results in an increase in vessel branching, and is most at risk of being a pathogenic angiogenic pathway in inflammatory diseases [59]. Intracellular VEGFR-1 signaling in

angiogenic endothelial, stromal and myeloid cells has also been shown to stimulate pathological angiogenesis [90].

Within the CNS, VEGF has been identified as a common factor between angiogenesis and pathogenesis [54]. VEGF has a role in a variety of neurological disorders, including stroke and motor neuron disease [54]. Elevated VEGF levels are significantly elevated in patients with amyotrophic lateral sclerosis (ALS) [91]. In contrast, several studies have suggested that diminished CNS perfusion may precede conditions such as Alzheimer's disease and this may be attributed to reduced VEGF activity in the CNS [58].

Due to its prominent role in angiogenesis, VEGF inhibitors have become the most widely used anti-angiogenic agents [52]. VEGF inhibitors act through a number of mechanisms. They arrest endothelial cell proliferation, preventing vessel growth. They also induce the regression of pre-existing vessels by increasing endothelial cell death [52]. As previously discussed, mature vessels are covered in pericytes for mechanical and biochemical support. The local production of VEGF by these cells renders these vessels resistant to systemic anti-VEGF treatments and protects them; therefore, new vessels which lack pericyte coverage become most affected by these treatments [52].

Several studies have indicated that inhibition of a single angiogenic target such as VEGF can lead to the upregulation of other proangiogenic factors such as PlGF [52]. With this in mind, many studies are now exploring concurrent therapeutics to be applied with VEGF treatments to enhance the restriction of new vessel growth in pathogenic circumstances [52].

1.3.5 Evidence of Angiogenesis in MS

MS research thus far has largely concentrated on alterations in inflammation, demyelination, axonal injury, and oligodendrocyte loss; however, MS lesions have been shown to have a significant vascular component. An association between the vasculature and MS was identified by Edward Rindfleish over 140 years ago when he documented changes in the large and small vessels in the spinal cord during the disease [56,92]. He noted that all MS lesions were associated with abnormal blood vessels and typically, were centered on one or more veins within the white matter [92].

Circulating VEGF levels have also been reported to be elevated in both MS patients, as well as in murine EAE models [93]. One study pointed to a potential pathogenic role for VEGF in MS when EAE rats infused intracerebrally with VEGF developed an increased inflammatory response with subsequent worsening of disease progression [93]. VEGF expression is upregulated in both acute and chronic MS lesions, and vessels within these lesions show irregular morphology consistent with angiogenesis [93]. In acute MS lesions, an increase in the number and size of blood vessels with increases in endothelial cell number and mitotic count has also been documented [94]. In post mortem tissue, VEGF is elevated in MS brains when compared to normal controls. In addition, the lesions within these brains appeared to have an increase in the number of blood vessels [94].

Other well documented components of angiogenesis have also been identified to play important roles in MS. Factors, such as MMPs, intercellular adhesion molecule (ICAM)-1, and vascular cell adhesion molecule (VCAM)-1, that influence the breakdown of the basement membrane during angiogenesis have been shown to play a critical role in facilitating the movement of inflammatory cells across the BBB in MS [95,96]. Mediators of

inflammation, such as interferon (IFN)- γ, and tumor necrosis factor (TNF)-α and –β, are well documented to play a pro-angiogenic role [95,97]. Expression of NO, a well known pro-angiogenic factor in inflammatory and vascular disease, has been shown to correlate strongly with clinical and MRI markers of MS [98,99].

Several studies have examined cerebral perfusion within the brains of MS patients. One study demonstrated an increase in this perfusion in RR- and SPMS patients, potentially pointing to an increase in the number of vessels within the CNS of these patients [56]. A serial MRI study exploring local perfusion in gadolinium (Gd) enhancing MS lesions showed an increase in cerebral blood volume and cerebral blood flow not only at time of Gd enhancement but 3 weeks prior to the enhancement. This could point to a role for the vasculature in normal appearing white matter very early on in lesion formation [56,100]. The existence of ring enhancement on MRI has been assumed to be an increase in the permeability of pre-existing vessels caused by the inflammatory process [101]. This could, however, represent new vessels where the newly formed vessels, not yet fully matured, are permeable to Gd [56].

Despite these indications that angiogenesis is occurring in MS, there has been little investigation into its role or its potential as a therapeutic target. While angiogenesis is a vital component of wound healing, in MS it may promote the destruction of normal tissue by fueling persistent inflammation directed against self-antigen. Inhibition of angiogenesis in other models of autoimmune disease have proven beneficial by limiting immune cell trafficking, reducing the supply of nutrients to inflamed areas, and by reducing endothelial cell activation [56,96].

1.4 Overall Objectives

We hypothesize that the apparent relationship between angiogenesis and MS is not merely a result of the disease process, but a pathological mechanism that is directly contributing to disease progression. The major objective of this thesis was to assess whether angiogenesis is occurring in an aEAE model and if this can be correlated to clinical and pathologic severity. It is important to determine whether the angiogenic events precede the onset of disease, or whether they are merely an epiphenomenon occurring alongside the inflammatory process. We aim to identify what pathways may be contributing to the regulation of this phenomenon, as these may serve as potential therapeutic targets.

The second objective was to target the angiogenic process *in vivo* using bevacizumab (trade name Avastin®), a commercially available monoclonal antibody used clinically to interfere with angiogenesis in cancer patients by binding to the pro-angiogenic factor, VEGF, as well as B20-4.1.1, a research antibody that specifically binds to murine VEGF. And finally, the third objective was to assess the impact of an additional anti-angiogenic agent, angiostatin, which has been demonstrated to interfere with angiogenesis by a mechanism different from bevacizumab.

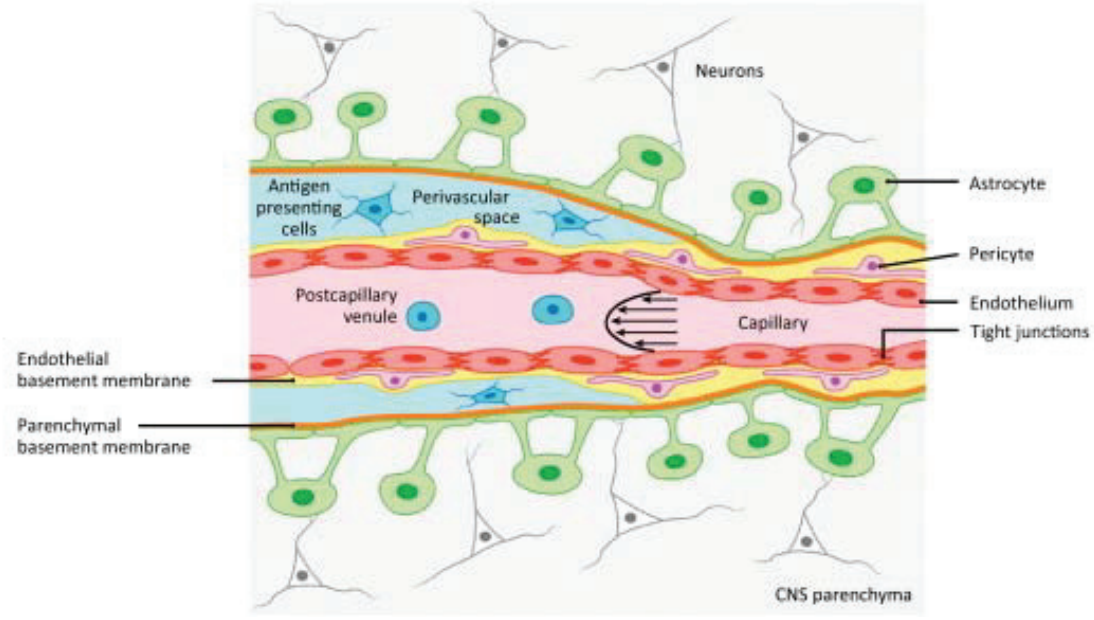

Figure 1.1. Anatomy of the blood-brain barrier. Highly specialized endothelial cells (red) create a barrier using complex tight junctions. The barrier is supported by a thick extracellular matrix (yellow) which is secreted by the endothelial cells and pericytes (pink). At post-capillary venules, the parenchymal basement membrane (orange) which is secreted by astrocytes (green) seperates from the endothelial basement membrane allowing for a cerebrospinal fluid-drained perivascular space (blue). Antigen-presenting cells of the CNS can be found here. *This figure has been reprinted with copyright permission* [102].

Table 1.1. FDA-approved therapies for the treatment of MS. [3]

Drug	Trade Name(s)	Mechanism of action
Interferon beta-1a	Avonex, Rebif	Immune modulator (mechanism unknown); Reduced BBB permeability
Interferon beta-1b	Betaseron, Extavia	Immune modulator (mechanism unknown); Reduced BBB permeability
Glatiramer acetate	Copaxone	Mimics and competes with myelin basic protein; activates suppressor T-cells
Mitoxantrone	Novantrone	Inhibits T-cell, B cell, and macrophage proliferation; impairs antigen presentation
Natalizumab	Tysabri	Inhibits alpha 4-mediated adhesion of leukocytes to the vasculature
Fingolimid	Gilenya	Blocks the egress of lymphocytes from lymph nodes

Table 1.2. Murine models of active EAE [42]. This table summarizes the most frequently used models of aEAE. MBP, myelin basic protein; MOG, myelin oligodendrocyte glycoprotein; PLP, proteolipid protein. Classic refers to a traditional acute and/or relapsing-remitting course of disease. Atypical refers to any course that deviates from the classic pattern, which can include (but is not limited to) a chronic progressive disease course.

Mouse Strain	Immunogen	Clinical Course	Gender Specificity
C57Bl/6J	MOG_{35-55}	Classic	No gender difference
PL/J	MBP_{Ac1-11}	Classic	Male
B10.PL	MBP_{Ac1-11}	Classic	Male
NOD	MOG_{35-55} PLP_{48-70}	Classic Classic	No gender difference
SJL/J	$PLP_{139-151}$	Classic Atypical	Female Male
C3H.SW	MOG_{35-55}	Classic	Not reported
Biozzi	PLP_{56-70} MOG_{8-22}	Classic Classic	Not reported
A.SW	MOG_{92-106}	Atypical	Female
C3H/HeJ	$PLP_{190-209}$ $PLP_{215-232}$	Classic or Atypical Classic or Atypical	Not reported
CBA/J	$PLP_{190-209}$ $PLP_{215-232}$	Atypical Atypical	Not reported
DBA/1	MOG_{79-96}	Classic	Not reported

Table 1.3. Clinical scoring scale for aEAE mice [42].

Grade	Clinical Symptom	Observations
0	Asymptomatic	Normal gait; tail wraps around cylindrical objects; when held up by base of tail hind limbs extend
0.5	Partially limp/weak tail	Normal gait; tip of tail droops (hook tail), and/or does not wrap around cylindrical objects; when held up by base of tail hind limbs extend
1	Paralyzed tail	Normal gait; tail droops and does not wrap around cylindrical objects; when held up by base of tail hind limbs extend
2	Loss in coordinated hind limb movement	Uncoordinated gait; limp tail; hind limbs reflex when toes are pinched; hind limbs contract when held by base of tail
2.5	Unilateral hind limb paralysis	Mouse drags one hind limb; limb does not respond to toe pinch
3	Bilateral hind limb paralysis	Mouse drags both hind limbs; neither limb responds to toe pinch
3.5	Weakness in grip strength of forelimbs	Mouse displays difficulty pulling body with forelimbs; when place on cage lid, mouse displays difficulty gripping bars; forelimbs respond to pinch
4	Forelimb paralysis	Mouse is no longer mobile; forelimbs do not respond to pinch
5	Moribund	No movement; altered breathing; hypothermia

CHAPTER 2: MATERIALS AND METHODS

2.1 EAE Induction

Adult female C57Bl/6J mice (aged 6-8 wk, 16-20g) were purchased from Charles River Laboratories (Saint Constant, Quebec, Canada). Mice were housed for a minimum of 5 days to acclimatize them before inoculation and were allowed free access to pelleted food and water and kept on a 12h light/dark cycle. All animal procedures were conducted in accordance with approval from the Dalhousie University Committee on Laboratory Animals (Dalhousie University, Halifax, Nova Scotia) and complied with guidelines from the Canadian Council on Animal Care.

EAE was induced by injecting a 1:1 mix of MOG_{35-55} (Sheldon Biotechnology Centre, Montreal, PQ) dissolved in 1X PBS (Sigma-Aldrich; Oakville, ON) and CFA containing *Mycobacterium tuberculosis* (5mg/ml) (BD Diagnositics; Mississauga, ON) s.c. at the base of the tail (200µg per mouse in 200µl). This was combined with an i.p. injection of pertussis toxin (Sigma-Aldrich; Oakville, ON) (200ng in 100µl). Pertussis toxin was given again at day 2. On day 7, each mouse was given a second dose of the MOG_{35-55}/CFA mixture by 2 s.c. injections into the lower flanks. Control mice (2 per group) were treated at the time of disease induction with pertussis toxin alone, MOG_{35-55} alone, or combined ovalbumin and pertussis toxin.

2.2 Clinical Scoring and Care of EAE Mice

The mice were weighed and clinically scored daily for the 21 day duration of each experiment. Mice were clinically scored based upon the following scale (Table 1.3): 0, no clinical deficits; 0.5, hook tail/partially limp tail; 1, paralyzed tail; 2, walking deficit; 2.5, unilateral hind limb paralysis; 3, bilateral hind limb paralysis; 3.5, bilateral hind limb paralysis, and weakness in forearms; 4, forelimb paralysis; and 5, moribund. Mice were

provided mash and HydroGel (ClearH_2O; Portland, ME, USA) when their deficits no longer allowed them to reach water and food.

2.3 Drug Administration

For all therapeutic interventions, treatment was initiated within 24h of the onset of clinical symptoms (score of 0.5 or greater). In each experiment, in addition to the animals treated with the respective drug, there were non-treated EAE controls, vehicle-treated EAE controls, and drug-treated wild-type mice. Bevacizumab (5mg/kg diluted in 0.9% saline) was administered i.p. every 3 days until sacrifice. IgG was administered (5mg/kg diluted in 0.9% saline) following the same dosing protocol as an isotype control. B20-4.1.1, an anti-murine VEGF antibody shown to block both human and murine VEGF *in vitro* with high potency (Fuh, Wu et al. 2006, Liang, Wu et al. 2006), was administered 5mg/kg, i.p., repeated every 3 days until sacrifice, as per the manufacturer's directions. Angiostatin (kringle domains 1-3) in 1X PBS was administered i.p. 5mg/kg daily until sacrifice.

Bevacizumab (Roche; Mississauga, ON) was obtained by prescription as an intravenous solution for clinical use. B20-4.1.1 was kindly donated for research use by Genentech Inc. (South San Francisco, CA, USA). Angiostatin (human kringle domains 1-3) was obtained from Sigma-Aldrich (Oakville, ON).

2.4 Tissue Processing

Experimental and control animals were sacrificed 7, 14 or 21 days after induction. Just prior to sacrifice, mice were injected with type IV HRP (0.35mg/g dissolved in 100µl saline; Sigma Aldrich; Oakville, ON), which circulated for 15min as part of the protocol for permeability maps. A 200 µl blood sample was collected and anti-coagulated in

heparinized saline for later assessment of plasma HRP concentrations. Mice were then euthanized by one of two methods, depending on subsequent analysis to be conducted.

If the tissue was to be used for histology and permeability analysis, the mouse was placed into surgical plane using sodium pentobarbital (i.p., 50mg/kg in 200µl). The chest cavity of the animal was opened and a needle was placed into the apex of the left ventricle of the heart. The animal was then sacrificed via manual perfusion-fixation using 10ml of heparin saline, followed by 10ml of 10% buffered formalin (Sigma-Aldrich; Oakville, ON). The spinal cord was isolated within the vertebral column, and immersed in 10% buffered formalin for 48h followed by decalcification in Formical-2000 (Decal Chemical Corporation; Tallman, NY, USA) for 72h.

The spinal cords were then paraffin-embedded, cut into 5µm sections using a microtome (model RM2255; Leica; Richmond Hill, ON), and mounted on silinated glass slides for pathological scoring, permeability mapping, and immunohistochemistry. To assess disease severity histologically, lumbar sections were stained with haematoxylin and eosin (H&E) to assess cellular infiltrates and perivascular cuffing, or with luxol fast blue/cresyl violet (LFB/CV) to assess demyelination. Pathological scoring was based upon a 4 point scale (Table 2.1) in each of the following 4 categories: inflammatory cells in the meninges (category 1), perivascular inflammation (category 2), invasion into the spinal cord parenchyma (category 3), and demyelination (category 4).

EAE animals that were to be used for immune cell isolation or PCR were sacrificed by cervical dislocation. The spinal cords were then promptly removed by flushing the vertebral canal with 1X PBS through an 18 gauge needle. Fresh spinal cords were then either immediately processed for lymphocyte extractions, or immersed in 10X

the volume of an RNA stabilization reagent (RNAlater; Qiagen; Toronto, ON) for 24h at 4°C, and then stored at -20°C for future RNA extraction.

Post-mortem formalin-fixed human brain tissue containing MS plaques were paraffin embedded, and cut into 5µm sections using a microtome (model RM2255; Leica; Richmond Hill, ON), and mounted on silinated glass slides for confocal imaging.

2.5 Immunohistochemistry

Paraffin-embedded spinal cord sections were deparaffinized in xylene and graded ethanols. Antigen retrieval was then carried out on deparaffinized sections in a pressure chamber (125°C for 20min) in citrate buffer containing 2.94g/L sodium citrate, 0.5ml/L Tween20, pH 6.0. Slides were allowed to cool to RT and then washed 3 times in TBST (6.1g Trizma base/L dH_20, 9.0 g NaCl /L dH_20, 0.05 ml Tween 20/L dH_20, pH adjusted to 8.4 with HCl). Protein blocking was carried out in 5% horse serum (Cedarlane; Burlington, ON) dissolved in TBST for 2h at RT. Sections were then exposed to primary antibody diluted in TBST for 8h at RT. Table 2.2 details the primary antibodies and dilutions used. Sections were then washed 3 times in TBST and incubated with a prediluted rabbit alkaline phosphatase polymer (Inter Medico; Markham, ON) for 30min at RT. After 3 washes with TBST, alkaline phosphatase was detected with the Vulcan Fast Red chromogen kit 2 (Inter Medico; Markham, ON). One drop of Vulcan Red chromogen was added to 2.5 ml of buffer. This mixture was added to the tissue for 15min at RT. Sections were washed 3 times in dH_20 and counterstained in Meyer's hematoxylin before mounting.

For confocal imaging, slides were incubated for 8h with combinations of 2 primary antibodies, followed by a mix of appropriate secondary antibodies for 1h (all

applications at RT). Secondaries were fluorescently labeled with Dylight 488 or 549, directed against the species-specific IgG portion of the primary antibodies. The 488 and 549 refer to the peak emission wavelength in nanometers (green and red fluorescence, respectively). After mounting, the slides were visualized on a confocal laser-scanning microscope (LSM 510; Zeiss; Toronto, ON). Overlap images were used to detect co-localization of molecules, using ZEN software (Zeiss; Toronto, ON). All stains were validated on positive control tissues. Negative controls were run by omitting the primary antibody.

Tissue was assessed microscopically in a blinded fashion by a minimum of two observers. Vessel counts were performed on the basis of CD31 profiles. VEGF expression was assessed from axon staining in the dorsal columns. Expression of VEGFR-2, Ang-1, Ang-2, Tie-1, and Tie-2 was quantified from numbers of positive cells or processes. Cells were identified as neurons on the basis of nuclear size, the presence of a prominent nucleolus, and a cell body connected to the initial segment of an axon or cell body of similar size when the initial segment could not be seen. Other cells were classified as glia on the basis of smaller nuclear size, absent nucleolus, location in white matter, and/or presence of radiating glial processes. When processes were seen without visible extension from a cell body, they were counted separately. In each case, 2-4 sections of lumbosacral spinal cord were assessed by each observer blinded to the identity of the different groups. Data were then averaged to give a final value per mouse. The mouse values were then averaged to give final data.

2.6 Permeability Mapping

Following tissue processing, 5μm paraffin-embedded sections were analyzed for vascular permeability changes using a previously published protocol (Gauden, Hu et al. 2007, Joice, Mydeen et al. 2009). Sections were deparaffinized in xylene and graded ethanol and then reacted with DAB (8 mg/ml) (Sigma-Aldrich; Oakville, ON), and H_2O_2 (0.006%) to generate a brown reaction product from the enzymatic activity of HRP. During the reaction, the section was transilluminated through a light box containing a uniform flat field light source (3-piece LED; 3M; London, ON). Sequential images were captured every 5sec for 200sec through a stereomicroscope (Leica S6D) via a camera (Hamamatsu C4742-80-12AG; Quorum Technologies; Guelph, ON) and firewire link to a computer under the control of customized image processing software (Image Hopper, Samsara Research; Dorking, UK).

To generate images with an increase in pixel intensity, images of absorption (*A*) were generated: $A = log(Io/It)$; where *Io* is the intensity in the initial image and *I* is the intensity in subsequent images at time *t*. This series of absorption images was further processed to obtain a regression image through the initial sequence of images (0-35sec). This regression image gives pixel values proportional to the initial rate of development of reaction product that are proportional to HRP concentration based on previous calibrations with tissue and plasma [103]. To convert the tissue concentration map into a map of permeability-surface area (PS) product, the image was divided by the plasma concentration derived from the HRP concentration in the blood sample taken at the time of death, multiplied by the circulation time (15min) based on the following: $PS = Qr/X(Cpl)dt$; where *Qr* is the amount of HRP in the tissue and *X(Cpl)dt* is the time integral concentration of HRP in plasma [104]. The image was also multiplied by a volume

term that estimates the interstitial volume per gram of tissue ($0.2cm^3/g$) [105] because HRP during a 15min period is expected to distribute in the interstitial space without significant uptake.

To calculate PS in individual regions of interest, a hand tool was used to outline the region, and its volume calculated from the given pixel number (converted to μm^2) multiplied by the tissue thickness. The PS data from each region were multiplied by its volume to calculate a final PS value in ml/sec/g; 2 spinal cord sections were evaluated for each mouse. Where sections had multiple areas of increased PS, these were averaged to give a PS value per section. The PS values from the 2 sections were averaged to give a PS value per mouse.

2.7 T-Cell Isolation

Mice were sacrificed at day 21 by cervical dislocation. Superficial cervical, axillary, brachial and inguinal lymph nodes were isolated from 2 mice and pooled (n=3, 2 mice pooled per n). Lymph nodes were homogenized and filtered through cell separation columns (Miltenyi Biotec; Auburn, CA, USA) to yield single cell suspensions. Erythrocytes were removed by osmotic shock. Total cell numbers were assessed with trypan blue dye exclusion, and cell viability was typically over 95% with no difference in viability between different groups.

CD4+ T-cells were extracted by negative selection using a CD4+ T-cell isolation kit from Miltenyi Biotec (Auburn, CA, USA). Purity was assessed by two color flow-cytometric analysis using anti-CD4-FITC and anti-TcRβ-PE monoclonal antibodies (mAb) (both from eBioscience, San Diego, CA, USA). Purity of the CD4+ TcRβ+ cell fraction was typically over 90%. For all experiments, T-cells were cultured at 37°C, 5%

CO_2, 95% humidity in RPMI-1640 medium (Invitrogen; Burlington, ON) supplemented with 5% heat-inactivated fetal calf serum,100U/ml penicillin, 100µg/ml streptomycin, 2mM L-glutamine and 5mM HEPES (Sigma-Aldrich; Oakville, ON).

2.8 Spinal Cord Extractions of Mononuclear Cells

Immediately following cervical dislocation, the spinal cord was removed from mice by flushing the vertebral canal with PBS through an 18 gauge needle attached to a syringe. The spinal cord was then cut into small pieces and added to a solution of collagenase D (Roche, 4mg/ml) and DNAse I (SigmaAldrich, 5mg/ml) in RPMI-1640 medium, and incubated for 1h at 37°C, 5% CO_2, 95% humidity. Tissue was then further disrupted by aspiration through an 18 gauge needle and washed by centrifugation (500g, 5min). Red blood cells were removed by osmotic shock, the sample was washed (500g, 5min), filtered, washed again and re-suspended in RPMI-1640 medium. The sample was then centrifuged (1085g, 20min) on a Percoll® gradient composed of 4ml 70% Percoll®, 4ml 30% Percoll® and 5ml of suspension layered sequentially in conical tubes. The mononuclear cell band was removed, washed twice by centrifugation in RPMI-1640 medium and finally re-suspended in RPMI-1640 medium prior to use in experiments.

2.9 Bone-Marrow Derived Dendritic Cell (BMDC) Generation

Murine bone marrow (BM) cells isolated from wild type C57Bl/6J mice were seeded onto 6 well plates (1×10^6 per well) and cultured for 9 days at 37°C, 5% CO_2, 95% humidity in RPMI-1640 medium supplemented with 10% heat inactivated FCS, 0.1% 2-ME (Sigma-Aldrich; Oakville, ON), 20ng/ml GM-CSF (R&D systems), 100U/ml penicillin, 100µg/ml streptomycin, 2mM L-glutamine and 5mM HEPES. On day 9, BM

cell cultures were stimulated with 1μg/ml LPS (Sigma-Aldrich, Oakville, ON) to generate mature BMDC.

2.10 T-Cell Proliferation Assays

Lymph node cells from mice with EAE were labeled with 2μM Oregon Green 488 dye (Invitrogen; Burlington, ON) for 15min at RT and then cultured in 96 well plates (1.5×10^5 cells/well) and stimulated for 72h with 7.5×10^4 anti-CD3/anti-CD28 mAb-coated T-cell expander beads (Invitrogen; Burlington, ON) or restimulated with MOG_{35-55} (25μg/ml). Cells were then labeled with anti-CD4-PE mAb and proliferation analyzed by two color flow-cytometric analysis. Additional experiments were carried out by combining T-cells with bevacizumab, B20-4.1.1 (both 10, 100μg/ml), angiostatin (1, 5μg/ml) or an IgG control (100μg/ml). In these experiments, the lymph node cells were further purified into CD3+ T-cells by passage through cell separation columns (Miltenyi Biotec; Auburn, CA, USA). Cells were either naive T-cells from wild type mice, or T-cells taken from mice with untreated EAE and restimulated by culture with BMDCs (3.2×10^3/well) and MOG_{35-55} (25μg/ml) before labeling with Oregon Green 488 dye to assess proliferation.

2.11 Cytokine Assays

CD4+ T-cells (1×10^5) were cultured in 96 well plates (200μl/well) alone or in the presence of anti-CD3/anti-CD28 mAb-coated T-cell expander beads (5×10^4) or MOG_{35-55} (25μg/ml) for 24h. Following 24h incubation, culture supernatants were harvested and IL-17, IFN-γ and IL-4 concentrations determined by ELISA (BD Biosciences; Mississauga, ON). All assays were performed in quadruplicate. To assess intracellular cytokines, the CD4+ T-cells were activated in the presence of Brefeldin A

(Sigma-Aldrich; Oakville, ON) for 4-6h. Cells were first labeled with anti-CD4-FITC mAb, then fixed, permeabilized and labeled with APC labeled mAb against IL-17, IFN-γ and IL4 (eBioscience; San Diego, CA, USA). Double labeling of CD4 and the appropriate cytokine was then analyzed by two color flow cytometry.

2.12 Quantitative Polymerase Chain Reaction (qPCR)

Fresh spinal cord tissue was immersed in 10X the volume of an RNA stabilization reagent (RNAlater, Qiagen; Toronto, ON) for 24h at 4°C, and then stored at -20°C prior to RNA extraction. Total RNA was extracted with RNeasy Plus Universal kit (Qiagen; Toronto, ON) following manufacturer's instructions. Tissue was lysed in QIAzol Lysis Reagent (Qiagen; 100mg tissue/ml); the tissue lysate was then homogenized using QIAshredder homogenizer spin columns (Qiagen; Toronto, ON), genomic DNA was removed with gDNA Eliminator Solution, and high quality RNA was purified using RNeasy spin columns. Quantification and purity of isolated total RNA was assessed using a NanoDrop2000 spectrophotometer (Thermo Scientific; Asheville, NC, USA). cDNA for each sample was prepared with a cDNA synthesis kit (SuperScript® III First-Strand Synthesis SuperMix for qRT-PCR; Invitrogen; Burlington, ON) according to manufacturer's instructions. The transcript level of each gene was determined using a RotorGene SYBR Green PCR kit (Qiagen; Toronto, ON) and Rotor-Gene 6000 real-time rotary analyzer with the Rotor-Gene 6000 series software version 1.7 (Corbett Research; Concorde, NSW, Australia).

Murine primer sets for genes of interest were selected using qPrimer Depot for mouse (National Institutes of Health) and tested to confirm the specificity of the PCR products. Table 2.3 details forward and reverse primers were utilized. Analysis of the

melting curve showed that each primer amplified a single product. Forward and reverse primers were mixed to give a final concentration of 0.5μM. The PCR reaction profile consisted of an initial denaturation time of 10min at 95°C, followed by 40 cycles of 95°C for 10s, 60°C for 15s, and 72°C for 20s. Reactions lacking cDNA served as a contamination control. Each sample was normalized to GADPH expression. Data is expressed as transcript expression relative to wild type control mice.

2.13 Statistical Analysis

Data from each group are expressed as mean ± standard error of the mean (SEM). Statistical comparisons between treatment groups were made using statistical software (GraphPad Prism; La Jolla, CA). Multiple groups were compared by 1-way analysis of variance followed by the Bonferroni test. In all cases, $p < 0.05$ was taken as significant. Where two groups only were compared an unpaired t test was employed.

Table 2.1. Cumulative pathologic scoring scale.

Category	Grade	Histological observation
Meningeal inflammation	0	No change
	1	Perivascular and/or meningeal infiltration,1-3 vessels involved in any section
	2	4-6 vessels involved
	3	6+ vessels involved
	4	Dense infiltration
Perivascular infiltration	0	No change
	1	1-3 parenchymal vessels infiltrated
	2	4-6 vessels involved
	3	6+ vessels involved
	4	Virtually/nearly all vessels involved
Myelitis	0	No inflammatory cell invasion
	1	A few scattered inflammatory cells
	2	Invasion from several perivascular cuffs
	3	Large area of neural parenchyma involved
	4	Virtually entire section infiltrated
Demyelination	0	No demyelination
	1	Single focus of subpial demyelination
	2	Several small foci of demyelination
	3	One large confluent area of demyelination
	4	Several large confluent areas

Table 2.2. Primary and secondary antibodies used for immunohistochemistry. All antibodies from Abcam (Cambridge, MA, USA), were stored at -20°C and those from Santa Cruz (Santa Cruz, CA, USA) were stored at 4°C, as per suppliers' directions. Dilutions were made in TBST. m.c., monoclonal; p.c., polyclonal.

Primary	Host/Specificity	Order Number/Source	Dilution
Ang-1	rabbit anti-mouse, p.c.	ab8451/Abcam	1:100
Ang-2	rabbit anti-mouse, p.c.	ab65835/Abcam	1:50
Tie-1	rabbit anti-mouse, p.c.	SC-9025/Santa Cruz	1:50
Tie-2	rabbit anti-mouse, p.c.	SC-9026/ Santa Cruz	1:50
VEGF	rabbit anti-mouse, p.c.	ab46154/Abcam	1:100
VEGFR2	rabbit anti-mouse, p.c.	ab39256/Abcam	1:200
CD3	rat anti-mouse, m.c	ab56313/Abcam	1:50
CD68	rat anti-mouse, m.c.	ab53444/Abcam	1:100
Elastase	rat anti-mouse, m.c.	ab2557/Abcam	1:50
Laminin	rat anti-mouse, m.c.	ab79057/Abcam	1:50
GFAP	goat anti-mouse, p.c.	Ab53554/Abcam	1:200
Secondary	**Host/Specificity**	**Order Number/Source**	**Dilution**
Dylight 488	donkey anti-rabbit IgG	ab96891/Abcam	1:100
Dylight 549	donkey anti-goat IgG	ab96937/Abcam	1:100
Dylight 549	rabbit anti-rat IgG	ab102209/Abcam	1:100

Table 2.3. qPCR Primers. Mouse primer sets for genes of interest selected using qPrimer Depot for mouse.

Target	Direction	Sequence
GAPDH	forward	5'CGTCCCGTAGACAAAATGGT-3'
	reverse	5'-TTGATGGCAACAATCTCCAC-3'
CD- 31	forward	5'-CCTCCAGGCTGAGGAAAACT-3'
	reverse	5'GGTGCTGAGACCTGCTTTTC-3'
TNF	forward	5'-CAGCCTCTTCTCATTCCTGC-3'
	reverse	5'-ATGAGAGGGAGGCCATTTG-3'
CD105	forward	5'GTGTAGCTCAGGCTGCCAAT-3'
	reverse	5'-ATGCCTGAAGAGTCAGCTCC-3'
Ang-1	forward	5'-AGCATCTGGAGCATGTGATG-3'
	reverse	5'GTTGTATCTGGGCCATCTCC-3'
Ang-2	forward	5'-GACGACTCAGTGCAAAGGCT-3'
	reverse	5'-TGCACCACATTCTGTTGGAT-3'
VEGF-A	forward	5'AATGCTTTCTCCGCTCTGAA-3'
	reverse	5'-CTCACCAAAGCCAGCACATA-3'

CHAPTER 3: CHARACTERIZATION OF ANGIOGENESIS IN EAE

Portions of this chapter appeared in the following publication:

MacMillan CJ, Starkey RJ, Easton AS. Angiogenesis is regulated by angiopoietins during experimental autoimmune encephalomyelitis and is indirectly related to vascular permeability. J Neuropathol Exp Neurol 2011; 70: 1107-23. *Reprinted with copyright permission.*

Contributions: Disease induction, monitoring, and tissue isolations in all figures of this chapter were completed by CJ MacMillan. RJ Starkey and AS Easton contributed to Figures 3.1 and 3.2 as blinded scorers. Figures 3.3 – 3.11 were completed by CJ MacMillan and observations validated by a blinded observer (AS Easton).

3.1 Summary

The regulation of angiogenesis was studied using immunohistochemistry in the murine model of MS, aEAE. In this model, angiogenesis peaked 21 days following disease induction. Significant increases in vessel density (labelled with the vascular endothelial marker CD31) were apparent in the gray matter and adjacent to the leptomeninges. Angiogenesis correlated with clinical and pathologic scores. Spinal cord expression (assessed from numbers of immunopositive cells) of Ang-1 by neurons and glia was reduced at day 14, but expression levels returned to that of controls, largely through increased numbers of immunopositive inflammatory cells at day 21. Ang-2 expression increased markedly at day 21, again through its expression in infiltrating inflammatory cells. Levels of the angiopoietin receptor Tie-2 in neurons and glia were reduced at day 14, but recovered by day 21. Double labeling demonstrated Ang-1 expression on infiltrating CD3+ T-cells, and Ang-2 was expressed by monocyte/macrophages. The same expression pattern was noted in inflammatory cells in both a chronic inactive and chronic active plaque within a human MS tissue sample. During EAE, expression of VEGF by dorsal column axons peaked at day 14 and began to decrease by day 21. Confocal microscopy was used to show co-localization of Tie-2 and VEGFR-2 with blood vessels at day 21. Vascular permeability increased early in EAE, peaked at day 14 and had returned towards control levels at day 21. Although individual values of PS product did not correlate with angiogenesis, the volume of permeable tissue showed a weak positive correlation with angiogenesis. These temporal changes in angiogenic factors suggest an integral role during EAE-related angiogenesis.

3.2 Introduction

Angiogenesis, the formation of new blood vessels from pre-existing vasculature, has many roles in health and disease. Pathologic angiogenesis has been regarded as a key process in autoimmune inflammatory diseases such as rheumatoid arthritis and psoriasis [106,107], but its involvement in MS and in the animal model EAE has not been fully characterized.

Angiogenesis is controlled by a balance of pro-angiogenic and anti-angiogenic regulators, among which are VEGF and the angiopoietins, Ang-1 and Ang-2. Under normal conditions, angiogenesis is suppressed by an excess of anti-angiogenic factors over pro-angiogenic factors that maintain the vasculature in a quiescent state. In some pathologic conditions, the balance tips in favor of angiogenesis resulting in the activation and proliferation of vascular endothelial cells. These endothelial cells secrete proteases that digest the perivascular basement membrane and interact with each other to grow out as tubes. These tubes establish contact with other vessels to form patent vascular networks and redundant vessels are removed by apoptosis and vessel regression.

In rheumatoid arthritis and psoriasis, inflammatory cells are potent sources of angiogenic factors. Macrophages are described as having a central role, whereas T-cells play an ancillary role [108]. Although the same pro-angiogenic and anti-angiogenic factors regulate both physiological and pathologic angiogenesis, the timing and degree of angiogenesis are thought to have a major impact on these diseases. A rich plexus of new blood vessels can provide enhanced routes by which inflammatory cells enter diseased tissue and provide positive feedback stimuli that perpetuate chronic diseases.

Understanding the precise impact of angiogenesis in disease states may provide rationales for more effective therapies.

MS has been considered to be a T-cell mediated autoimmune disease of the CNS. Because of its metabolic requirements, the CNS is highly vascularized compared with other tissues, and MS lesions have long been recognized to have a relationship to the vasculature, where many inflammatory/demyelinating lesions have been noted to form around blood vessels. As described earlier, there have been reports of angiogenesis occurring in the vicinity of MS plaques [94,109]. Previous reports have documented angiogenesis in EAE as well [110-112], and its molecular regulation has been explored in relation to VEGF. VEGF expression was increased in several studies [93,110-112], and blockade of VEGFR-2 was found to reduce angiogenesis and ameliorate the disease [111]. VEGF is considered to be a pro-angiogenic factor of major importance in pathologic angiogenesis, but its effects are balanced by many other factors. Among these are Ang-1 and Ang-2, whose effects on angiogenesis are mediated by interaction with the Tie-2 receptor. There are indications that Ang-2 is upregulated in EAE based on a tissue microarray study [111], but little else is currently known.

Another aspect of angiogenesis in the CNS is its relationship to vascular permeability across the BBB. Vascular permeability refers to the rate at which transfer of solutes between the blood and CNS tissue occurs, and this is much lower in the CNS than in peripheral microvessels [113]. In both MS and EAE, there are early increases in BBB permeability that precede the onset of clinical signs and occur in the absence of marked inflammation. In MS, an increase in BBB permeability allows the tracer Gd to diffuse into the CNS. This diffusion can be visualized with MRI and is used as a major clinical

indicator of new disease activity in MS patients [27,114-119]. Changes in vascular permeability have been correlated with clinical scores in mice with EAE [119-121], but the relationship between angiogenesis and changes in BBB permeability during EAE has not been explored in detail.

This chapter details published work done to provide insight into the role played by VEGF, Ang-1, and Ang-2 in the regulation of angiogenesis during EAE. Changes in vascular permeability were also explored in relation to disease parameters, as well as to angiogenesis.

3.3 Results

3.3.1 Histological Profile of Inflammatory Progression in EAE

When assessed at day 7, control mice treated with MOG_{35-55} alone showed small foci of inflammatory cells in the leptomeninges; however, other control mice showed no abnormalities. All EAE mice (n=6) developed leptomeningeal inflammatory foci over time. In some cases, this involved multiple meningeal vessels with minor invasion of the underlying parenchyma. Figure 3.1 shows representative H&E histology depicting inflammation in the lumbosacral spinal cord from mice 14 and 21 days following disease induction. The extent of inflammation increased by day 14 with more extensive inflammation in the leptomeninges (Fig. 3.1 A) and tissue invasion in 4 of 6 mice. There was a marked increase in inflammation in the day 21 mice, with all mice showing marked leptomeningeal inflammation with variable parenchymal infiltrates (Fig. 3.1 B). No demyelinated foci were seen in control mice, with only 1 focus in a day 7 mouse and

small foci in 4 of 6 mice at day 14. At day 21, there was extensive demyelination, ranging from multiple discrete foci to several large confluent areas (Fig. 3.1 C).

3.3.2 Inflammation Peaks 21 Days Post-Induction in EAE

In control mice (n = 6), clinical scores did not increase, with the exception of 1 mouse treated with ovalbumin and pertussis toxin that had a score of 0.5 on day 7. Control mice were scored daily for 21 days before death, with no significant weight loss observed in this group. In mice immunized for EAE, clinical scores began to increase at day 9 (in 2/12 mice), and by day 12, all mice had scores ranging from 0.5 to 1. The scores progressively increased; between days 17 and 21 they ranged between 2 and 4. Mean scores were significantly increased over control between days 11 and 21, reaching a plateau between days 18 and 21 (Fig. 3.1 D). This worsening of clinical score was accompanied by weight loss; average weight at day 7 was 17.72 ± 0.18g (n = 18), reaching a low of 16.73 ± 0.35g (n = 6) at day 15, but recovering by day 21 (17.42 ± 0.20g, n = 5).There was progressive increase in both degree and extent of inflammation, accompanied by demyelination, which peaked at day 21 (Fig. 3.1 E). Pathologic scores were increased over controls at days 14 and 21.

3.3.3 Blood Vessel Density Increases in the Leptomeninges and Gray Matter 21 Days Post-Induction and Correlates with Pathologic and Clinical Scores

CD31 immunohistochemistry was used to assess angiogenesis (Fig. 3.2 A). Vessels were identified as dot-like or tubular structures and were quantified separately in gray matter, white matter, and the leptomeninges. Vessel counts were not significantly different between EAE and control mice at days 7 or 14. There was a significant increase in vessel count at day 21 compared with controls ($p < 0.001$) for gray matter and total counts. Controls were separated based on day and treatment and compared to each other

with no statistical difference between the different controls. White matter counts showed an upward trend that was not significant (Fig. 3.2 B). In the leptomeninges vessels, there was a small but significant increase in vessel numbers at day 21 ($p< 0.001$). Total counts at day 21 increased from 207.1 ± 11.87 (n = 6) in controls to 331.7 ± 19.37 (n = 5), an increase of 160%. Gray matter counts increased to a similar extent, from 162.0 ± 7.6 (n = 6) in controls to 258.3 ± 12.5 (n = 5). Leptomeningeal counts almost doubled, increasing from 19.2 ± 1.1(n = 6) in controls to 36.8 ± 5.0 in EAE (n = 5, $p< 0.001$). Leptomeningeal vessels were also classified into subgroups as inflamed or non-inflamed based on perivascular inflammation. Day 21 counts increased over controls in both subgroups: from no vessels (n = 6) to 10.0 ± 2.0 (n = 5, $p< 0.001$) in the inflamed subgroup and 19.2 ± 1.1 (n = 6) to 26.8 ± 2.2 (n = 5, $p< 0.01$) for the non-inflamed subgroup. Vessel counts in each section (4 per mouse) showed a positive correlation with clinical and pathologic scores (Figs. 3.2 C, D). At higher scores, the vessel count was significantly increased compared to animals with a score of 0. The regression coefficient relating vessel counts to each parameter were 0.62 and 0.80 for clinical and pathologic scores, respectively.

3.3.4 VEGF Expression Increases 14 Days Following Disease Induction Then Reduces to Levels Below Control After Peak Angiogenesis

Control animals showed immunostaining for VEGF at the periphery of the dorsal columns, with a central area of pallor (Fig. 3.3 A). VEGF expression was estimated by subtracting this pale zone from the total area of the dorsal column (Fig. 3.3 G). Compared with controls, staining increased significantly at day 14 (Fig. 3.3 B). At day 21, there was a significant reduction in staining in 3 of 5 mice (Fig. 3.3 D). Staining was preserved in the other 2 mice examined (Fig. 3.3 E). VEGF expression in the 3 mice with reduced

staining was significantly lower than controls (Fig. 3.3 G). The staining in the dorsal columns was not associated with inflammatory infiltrates, as shown in adjacent H&E-stained sections (Figs. 3.3 C, F). To determine whether VEGF expression reduced consistently with further disease progression, an additional 5 mice were evaluated with EAE at day 35. All of these mice showed significant reductions in dorsal column staining for VEGF, comparable to the reduction seen in the low staining subgroup at day 21; staining levels were significantly lower than controls (Fig. 3.3 G). In all groups in which dorsal root ganglia (DRG) were present in the sections, the ganglion cells (the axons of which project to the dorsal columns) were immunopositive. There was also expression of VEGF by anterior horn cells in control mice (4/6), at day 7 (3/6), and at day 14 (4/6), but not at day 21. The anterior columns were positive in 3 of 6 mice at day 14 but not in the other groups. Nerve roots were positive in all mice. Expression was always present in the dorsal roots, with expression in anterior roots (into which axons from the anterior horn cells project) in 2 of 6 mice only at day 14. The mean percentage of positive dorsal roots was approximately 70% in control animals but fell to around 50% in the 3 immunized groups (control expression, 67.50% ± 6.62% (n = 6) vs 46.62% ± 5.55% (n = 6) at day 7, 48.97% ± 11.31% (n = 6) at day 14 and 49.14% ± 7.86% (n = 5) at day 21). DRG cells also expressed VEGFR-2. Receptor expression was in a dot-like pattern on the soma of ganglion cells. VEGFR-2 was also evaluated in neurons and glia. There was no significant difference in expression between the 4 groups (Fig. 3.3 H).

Confocal imaging was used to evaluate VEGF expression in astrocytes (using GFAP) as well as inflammatory cells in EAE mice at day 21. In these mice, there was no

detectable expression of VEGF in astrocytes (Figs. 3.4 A-C) or in T-cells, macrophages or neutrophils (data not shown).

3.3.5 Ang-1 Expression is Reduced Preceding Peak Inflammation and Angiogenesis, Followed by an Increase in Ang-2 Expression at Day 21

Control sections showed basal expression of Ang-1 and Ang-2 in both neurons and glial cells (Figs. 3.5 A, D). Neurons were identified morphologically by their size, and the presence of prominent nucleolus, while glial cells lacked extensive cytoplasm or a nucleolus, and in some cases showed fibrillary processes. Ang-1 expression was reduced in immunized mice at days 7 and 14 (Fig. 3.5 B) but was expressed by scattered inflammatory cells at day 14 (Fig. 3.5 B) and by larger numbers at day 21 (Fig. 3.5 C, G). Ang-1 was detected in more glial cells than neurons in all groups. There was a reduction in Ang-1 expression when compared to controls at both days 7 and 14. By day 21, its expression had increased back to control levels, due largely to expression by inflammatory cells (Fig. 3.5 G).

Ang-2 expression in neurons and glia remained constant at days 7 and 14 (Fig. 3.5 E) but was expressed by scattered inflammatory cells at days 7 and 14, and in large numbers at day 21 (Figs. 3.5 F, G). The number of cells expressing Ang-2 in control tissue was approximately 25% of those expressing Ang-1. At days 7 and 14, the expression was not significantly different from that in control, whereas at day 21, there was a striking increase in Ang-2 expression, mostly due to the expression by inflammatory cells. At day 21, the number of cells expressing Ang-2 was greater than those expressing Ang-1. The ratio of inflammatory cells expressing Ang-2 compared with Ang-1 was 1.81, based on the averages, and the ratio of all cells expressing Ang-2 compared with Ang-1 was 1.55.

To evaluate the types of inflammatory cells expressing Ang-1 and Ang-2, sections of lumbosacral spinal cord from mice with EAE at day 21 were double labeled and examined by confocal microscopy. Ang-1 co-localized with CD3+ T-cells (Figs. 3.6 A-C) but was absent in CD68+ macrophages and elastase+ neutrophils (Figs. 3.6 D-I). Ang-2 co-localized with macrophages (Figs. 3.7 D-F) but was absent in T-cells (Figs. 3.7 A-C) and neutrophils (Figs. 3.7 G-I).

3.3.6 Ang-1 Expression can be Attributed to Perivenous T-cells, and Ang-2 Expression to Infiltrating Macrophages in Human MS Tissue

Expression of Ang-1 and Ang-2 was explored in MS autopsy material from two cases (Fig. 3. 8). Similar to that observed in EAE tissue, Ang-1 was found to co-localize with perivenous T-cells in a chronic inactive plaque from a human MS tissue sample (Fig. 3.8 A-C, G). Ang-2 expression was found to localize with infiltrating CD68-postive macrophages in a chronic active plaque (Fig 3.8 D-F, H).

3.3.7 Angiopoietin Receptor Tie-2 Expression is Reduced at Day 14 in EAE

Tie-1 expression was found in neurons, glia, and in glial processes running perpendicular to the pial surface in control and EAE mice (Figs. 3.9 A, B). There was a non-significant trend to a reduction in Tie-1 expression at day 21 compared with control (Fig. 3.9 E). Tie-2 was also expressed by neurons and glia in both controls and mice with EAE (Figs. 3.9 C, D). There was a significant reduction ($p< 0.01$) in positive cells at day 14 with a rebound in expression noted at day 21 (Fig. 3.9 E). Scattered inflammatory cells also expressed Tie-2 at day 14 and 21 but far fewer than those expressing Ang-1 or Ang-2.

3.3.8 Expression of Tie-2 and VEGFR-2 but not Ang-2 is Localized in Blood Vessels

Spinal cord sections from mice with EAE at day 21 were examined by confocal microscopy to determine expression profiles of Ang-2, Tie-2, and VEGFR-2 in blood vessels. Ang-2 was present in inflammatory cells but did not co-localize with adjacent blood vessels (labelled with laminin) (Figs. 3.10 A-C). Tie-2 was present as dot-like immunoreactivity in blood vessel lumens (Figs. 3.10 D, F), which was evident both by immunohistochemistry (Fig. 3.10 D) and confocal microscopy (Fig. 3.10 F). Dot-like reactivity for Tie-2 was also noted on adjacent neurons in the anterior horns (Fig. 3.10 E). VEGFR-2 was detected as areas of luminal reactivity in blood vessels (Figs. 3.10 G-I).

3.3.9 Changes in Vascular Permeability

Permeability maps were used to assess vascular permeability in sections of lumbosacral spinal cord, based on HRP extravasation. A representative H&E-stained section with its corresponding permeability map is shown (Figs. 3.11 A, B). Discrete areas of increased signal are circled on the images and were used to calculate PS product values (Fig. 3.11 C). Average PS was 8.02×10^{-6} ml/s/g in controls. One of 6 EAE mice had no detectable increase, whereas the remaining 5 mice had values between 0.5 and 24 $\times 10^{-6}$ ml/s/g. The PS value can be converted to an estimate of HRP permeability (P) when divided by 142, which estimates the vessel surface area (S) in cm^2/g in CNS tissue [122]. A more useful figure is an estimate of Lucifer Yellow permeability ($Pest_{LY}$), because Lucifer Yellow (LY) was previously used to estimate changes in permeability across the BBB during inflammation [123]. $Pest_{LY}$ is obtained by multiplying HRP permeability by 9.82, the ratio of diffusion coefficients for LY and HRP. This assumes that they both diffuse freely through the same permeable pathway. P_{LY} across the intact BBB is 0.2 x

10^{-7} cm/s or less. $Pest_{LY}$ in controls were below this value in 3 of 6 mice, whereas 3 of 6 had values of 5.63x 10^{-7} cm/s (MOG_{35-55} immunized) and 9.49 x 10^{-7} and 1.66 x 10^{-6} cm/s (2 mice treated with ovalbumin and Pertussis toxin). Thus, 3 of 6 mice showed an intact blood-spinal cord barrier, whereas the remaining 3 showed focal areas of increased permeability.

Compared with controls, there was a significant increase in PS at day 7 (to 27.06 ± 6.79 x 10^{-6} ml/s per gram, n = 6, $p< 0.05$) equivalent to $Pest_{LY}$ of 1.87 ± 0.47 x 10^{-6} cm/s. There was a further increase at day 14 (to 41.30 ± 8.53 x 10^{-6} ml/s per gram, n = 6, $p< 0.001$) equal to $Pest_{LY}$ of 2.86 ± 0.59 x 10^{-6} cm/s. PS declined sharply at day 21, reaching 16.56 ± 4.04 x 10^{-6} ml/s per gram (n = 5) equivalent to $Pest_{LY}$ of 1.15 ± 0.28 x 10^{-6} cm/s and not significantly different from control. In keeping with the increase in PS at day 7 (before the onset of clinical signs), there was a range of PS values for animals with a clinical score of zero (control and day 7 groups), ranging from 0 to 59.1 x 10^{-6}ml/s per gram, with a mean of 17.54 ± 4.70 x 10^{-6}ml/s per gram (n = 12) equivalent to $Pest_{LY}$ of 1.21 ± 0.32 x 10^{-6} cm/s.

The PS values per mouse are plotted as a function of vessel count and clinical score (Fig. 3.11 D). Regression lines through the data show no correlation between PS values and each parameter, with r^2 of approximately 0.005. A similar regression comparing PS to pathologic score also showed no correlation ($r^2 = 0.0071$). The mean volume of tissue showing permeability increases regardless of the magnitude of PS (calculated from regions of increased signal on the permeability maps) was also plotted against vessel count for each mouse and showed a weak positive correlation ($r^2 = 0.36$;

Fig. 3.11 E). A similar correlation was seen when mean volume was plotted against clinical score ($r^2 = 0.32$) or pathologic score ($r^2 = 0.33$).

The permeable regions were further evaluated by location in the spinal cord. In 98 regions displaying permeability changes, 87 were at or adjacent to the leptomeninges on the surface of the cord, 6 were confined to white matter, and 5 were confined to gray matter. There was no significant difference in PS between the different regions. Mean PS was $28.59 \pm 4.13 \times 10^{-6}$ml/s/g in the leptomeninges, $41.83 \pm 25.72 \times 10^{-6}$ ml/s/g in white matter and, $20.91 \pm 7.30 \times 10^{-6}$ml/s/g in gray matter. There was no correlation between PS in either white matter or gray matter when plotted against blood vessel counts (data not shown).

3.4 Discussion

Our results indicate that angiogenesis occurs at day 21 of aEAE in mice and correlates with clinical and pathologic markers of disease severity. At earlier phases of the disease, there is upregulation of VEGF, and reductions in Ang-1 and Tie-2 (Figs. 3.3, 3.5, and 3.9, respectively). These changes precede the angiogenesis that becomes apparent at day 21. At day 21, several changes were observed: VEGF was markedly reduced in 3 of the 5 mice examined (Fig. 3.3), levels of Ang-1 were augmented by the infiltration of T-cells into the involved spinal cord (Fig. 3.6), and levels of Ang-2 were augmented by monocytes/macrophages (Fig. 3.7). Blood vessels at this stage expressed Tie-2 and VEGFR-2 but not Ang-2 (Fig. 3.10).

Despite the strong correlation between angiogenesis and disease activity, we did not demonstrate a direct relationship between angiogenesis and increased vascular

permeability (Fig. 3.11). There were early increases in vascular permeability (at day 7, before the onset of clinical signs), but absolute values did not correlate with disease activity and angiogenesis. However, the volume of tissue affected by permeability increases showed a correlation with angiogenesis (Fig. 3.11 D). Angiogenesis may, therefore, increase dye leakage as a simple function of increased vessel density without affecting absolute values of permeability that reflect the rate of dye leakage across individual vessels. New vessels are likely to be capillaries, while permeability changes across the BBB tend to affect larger venules (Prof. Paul Fraser, personal communication).

3.4.1 Comparisons to Previous Studies

Angiogenesis has previously been documented in rodent EAE [110-112]. One of the only other mouse studies to explore angiogenesis in EAE documented angiogenesis at day 21, whereas in guinea pigs, vessel density increased 15 days after inoculation and coincided with peak clinical scores and VEGF expression. In rats, angiogenesis did not occur in the acute phase of EAE (days 13 and 16) but vessel density increased at day 27 [112].

There are several differences between the present study and the previous mouse study [111]. We found an increase in vessel counts in the leptomeninges and gray matter, at some apparent distance from inflammatory infiltrates, although some but not all of the leptomeningeal vessels were inflamed. The previous study found that vessels only increased in regions of active inflammation in spinal cord white matter. We localized VEGF exclusively in neurons or their processes (Fig. 3.3), but Roscoe et al [111] detected VEGF only as extracellular deposits. We found a striking reduction in VEGF expression that begins at day 21 and becomes established in all EAE mice at day 35. This

corresponds to the finding that mRNA levels for VEGF were not increased in the day 21 mice [111] and another study that documented a reduction in VEGF expression during EAE [124]. The finding that VEGF expression precedes angiogenesis implicates VEGF in its initiation. This is also implied by reduced angiogenesis when animals were treated with the VEGFR-2 antagonist SU5416 [111]. Increases in angiogenesis in gray matter during EAE were also noted in a rat study [112]. These increases may be more easily detected in gray matter because of its greater baseline capillary density versus that in white matter.

3.4.2 VEGF and Angiopoietins in EAE

Our findings of VEGF expression in neurons in mouse spinal cord (Fig. 3.3) is in keeping with previous reports. For instance, control Lewis rats expressed VEGF (mRNA and protein) in spinal cord motor neurons [124], although control rats did not express VEGF in another study [93]. Neurons in the adult rat brain and cultured mouse DRG cells [125] have also been shown to express VEGF [126], as have neurons in human control brain [127]. In contrast to other reports [93,124], we did not detect VEGF in reactive GFAP+ astrocytes in later stages of EAE (Fig. 3.4), perhaps because VEGF is down regulated in astrocytes at this stage. Other studies have reported VEGF associated with inflammatory infiltrates during EAE [112] and in activated T-cells used to induce pEAE [128], but we did not detect this in our model. We also found that mouse DRG cells express multiple angiogenic factors (VEGF, VEGFR-2, Ang-1, Ang-2, Tie-1, and Tie-2), but only VEGF was expressed by axons in the dorsal columns. We speculate that VEGF may be transported to the synaptic terminals of these axons and released locally to mediate its effects.

VEGFR-2 has been previously demonstrated to be expressed by brain vessels as a marker of angiogenesis during development in mice but to generally be absent in adults

[129,130]. During ischemia, however, levels of mRNA and protein are markedly increased, promoting VEGF-induced angiogenesis [129]. VEGFR-2 has also been reported in cultured mouse DRG cells [125]. During EAE in rats, mRNA levels for VEGFR-2 were described as ‘‘generally weak,’’ and upregulation was not detected during disease progression [93]. We find that VEGFR-2 expression is restricted to neurons, glia (Fig, 3.3 H), and blood vessel lumens (Fig. 3.10 G-I) in EAE, and expression levels remain constant throughout the disease course (Fig. 3.3 H).

Ang-1 expression has been reported in cortical neurons, cerebellar Purkinje cells and blood vessels in normal human brain [131], as well as in Purkinje cells and astrocytes but not blood vessels in normal rat brain [130,132]. Control vessels from rat expressed Ang-1 but not Ang-2 in another study [133]. Ang-2 was shown to be expressed by Purkinje cells in human brain [131] but was not detected in control rats [132]. Vessels and astrocytes are known to express Ang-2 after ischemic injury [132]. Ang-2 was found in vessels, macrophages, and neutrophils in adult rat brain after cold injury [133]. The present study adds additional information on the Angiopoietins during disease, specifically by documenting the expression of Ang-1 by T-cells and Ang-2 by macrophages in EAE (Figs. 3.6, 3.7).

Tie-2 has been shown to be widely expressed in vessels in both control rats and rats subjected to ischemia [132]. Tie-2 expression has been reported in mouse cortical neurons *in situ* [134] and in rat cortical neurons in culture [135] although not without controversy [136]. Tie-2 has also been reported in human autonomic neurons and rat DRG [137,138]. We noted co-localization of Tie-2 expression with scattered inflammatory cells, and interestingly, previous studies have shown that the infiltration of Tie-2-expressing macrophages into tumors is controlled by Ang-2 [82] raising a potential mechanism for

macrophage recruitment in EAE. We find that blood vessels express Tie-2 (as well as VEGFR-2) but not Ang-2 in mouse spinal cord during the peak stages of EAE (day 21; Fig. 3.10).

Neuronal expression of VEGF, Ang-1, and their respective receptors may mediate neuroprotective effects of VEGF and Ang-1 and stimulate proliferation of neural progenitor cells [139]. This may have implications for neuroprotection during EAE and MS. The role of the Ang/Tie system during inflammation is likely to be complex. In general, Ang-1 is thought to promote vessel stability and to have anti-inflammatory, anti-apoptotic effects. Ang-2 either induces angiogenesis in concert with VEGF or, when present with low VEGF levels, will induce vessel regression through apoptosis. Ang-2 has other proinflammatory effects and is able to increase vascular permeability and promote leukocyte recruitment [140,141]. We found the highest expression of Ang-2 at day 21 when permeability was decreasing (Figs. 3.5), indicating complex regulation.

Our data suggest that, during EAE, the stage is set for angiogenesis by a reduction in Ang-1 at days 7 and 14 after EAE induction and a reduction in Tie-2 at day 14. We speculate that the increased neuronal expression of VEGF at day 14 might initiate angiogenesis so that the vessel numbers increase by day 21. Indeed, neuronal expression of VEGF can be induced by growth factors and cytokines released by inflammatory cells at sites of injury [142,143]. T-cells may promote the stability of newly formed vessels through Ang-1 expression, which could also play a role in neuroprotection. Macrophages express Ang-2 after new vessels have formed and VEGF levels have started to decline. This might prune newly formed vascular networks and have additional pro-inflammatory effects such as the promotion of further leukocyte infiltration. If angiogenesis is assumed

to worsen EAE, our results suggest that during angiogenesis, functional blockade of Ang-1 would worsen EAE, whereas blockade of Ang-2 would improve it.

3.4.3 Vascular Permeability Changes in EAE

The BBB restricts permeability to water- soluble solutes to the CNS. BBB permeability increases early in EAE and MS, before the onset of clinical manifestations [27,114-119]. The subsequent role of BBB dysfunction is not well understood, but changes in permeability may act as a marker of endothelial activation in which the endothelium is primed (through exposure to inflammatory cytokines) for entry of leukocytes and the diffusion of pathogenic mediators into the CNS [144]. Indirect measurements suggest a correlation between permeability and clinical severity, including alterations in the endothelial cell tight junction protein ZO-1[119] and accumulation of sodium fluorescein in spinal cord [121]. BBB permeability often responds alongside EAE severity and inflammation when treatments are administered, suggesting a close linkage to these variables [144-149].Our data also shows early increases in vascular permeability, but the values for PS product did not correlate with clinical score, pathologic score, or angiogenesis. Indeed, angiogenesis became apparent at day 21, and inflammatory changes peaked as permeability was reducing, perhaps because new vessels are less reactive or less permeable than other vessels. Ang-1 is recognized to reduce vascular permeability [150], and its increased expression at day 21 provides an alternative explanation for the reduction in permeability.

We did, however, find a weak correlation between the volume of tissue affected by permeability increases and clinical score, pathologic score, and vessel counts (r^2 values of 0.32-0.36). This may imply that greater volumes of tissue show permeability

increases when affected by inflammation or a higher vessel density but that the exact permeability values (reflecting the rate of solute movement into the tissues) in these permeable areas is unpredictable. Permeability can be reduced by high doses of histamine, calcitonin gene- related peptide and neutrophils, among many other factors [151-153]. Angiogenesis may generate less permeable vessels, but because vessel density is increased, the total volume of tissue showing increases will also increase. In a clinical context, where Gd is used to detect lesions, this suggests that lesion burden (ie. the location and size of lesions) would be a more significant clinical variable than signal intensity in individual lesions.

During inflammation, we have previously described two stages of permeability increase [123]. The earlier stage (first phase) produced relatively stable increases in permeability of 10 to 50-fold. The later stage (second phase) produced yet further increases of 10 to 100-fold, in which there was significant protein leakage into the CNS associated with frank edema. For purposes of comparison, the PS values in this study were converted to estimates of P_{LY}, which were between 0.30 and 4.91 x 10^{-6} cm/s, and which are equivalent to first phase values [123]. This corresponds to the lack of significant edema and mass effect in most EAE lesions. Most of the permeable regions in the spinal cord were identified on the periphery, at or adjacent to the leptomeninges, suggesting that the pial vessels may be more reactive to inflammatory stimuli than parenchymal vessels. Few permeable regions were identified in gray matter despite the angiogenesis noted here. Therefore, the correlation between volumes and angiogenesis (rather than PS product and angiogenesis) may reflect the lesser degree of angiogenesis occurring in leptomeningeal vessels.

3.4.4 Conclusions

This study provides temporal information on key regulators of angiogenesis during EAE and is the first to describe angiopoietin expression in detail in this animal model of disease. Angiogenesis coincides with peak disease during EAE and may provide a positive feedback mechanism that amplifies the disease. We suggest that Ang-1 and Ang-2 cooperate with VEGF in the regulation of angiogenesis in EAE. Key to this process is the expression of Ang-1 by T-cells and expression of Ang-2 by macrophages. We also confirm that increases in BBB permeability occur early in EAE, but vessel counts, clinical score, and pathologic score are only indirectly related to permeability. Whereas absolute permeability values did not correlate with these variables, a correlation was found between the volume of permeable tissue and each variable. To the extent that EAE replicates changes occurring in MS, the modulation of angiogenesis may represent a promising strategy in its management, as we go on to explore in the next chapter of this thesis.

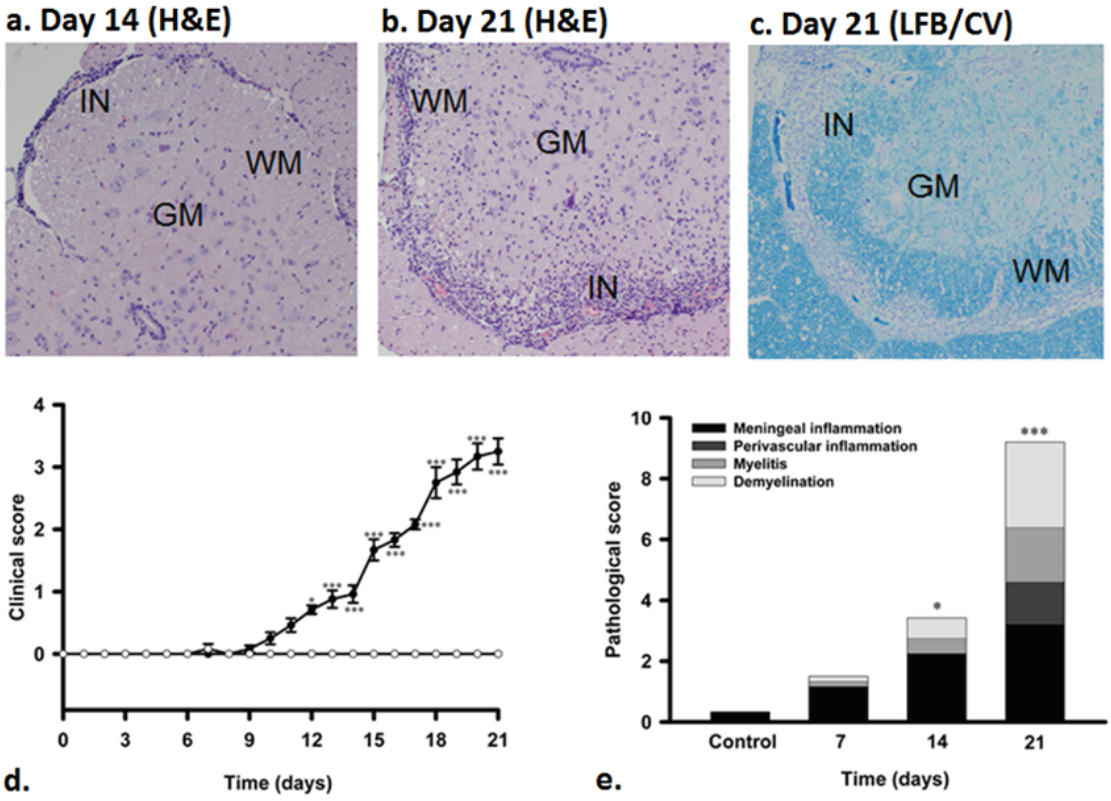

Figure 3.1. Pathological changes in murine EAE. a-c. Images of lumbosacral spinal cord (a, day 7 (H&E), b, day 14, H&E, c, day 21, LFB-CV). Key is GM = grey matter, WM = white matter, IN = inflammation. Scale bar, 200µm. d. Changes in clinical score, and e. pathological score in control mice and mice with EAE (days 7, 14, and 21 post-immunization). Clinical score data is shown as mean ± SEM. Open circles, controls (n = 6); filled circles, EAE mice (n = 18 at day 7, 12 at day 14 and 5 at day 21). Pathological score data is shown as stacked bars with averages from each category (calculated per mouse: n = 6, except day 21 where n = 5). Significance is relative to control, * = $p < 0.05$, ** = $p < 0.01$, *** = $p < 0.001$. *In collaboration with RJ Starkey and AS Easton.*

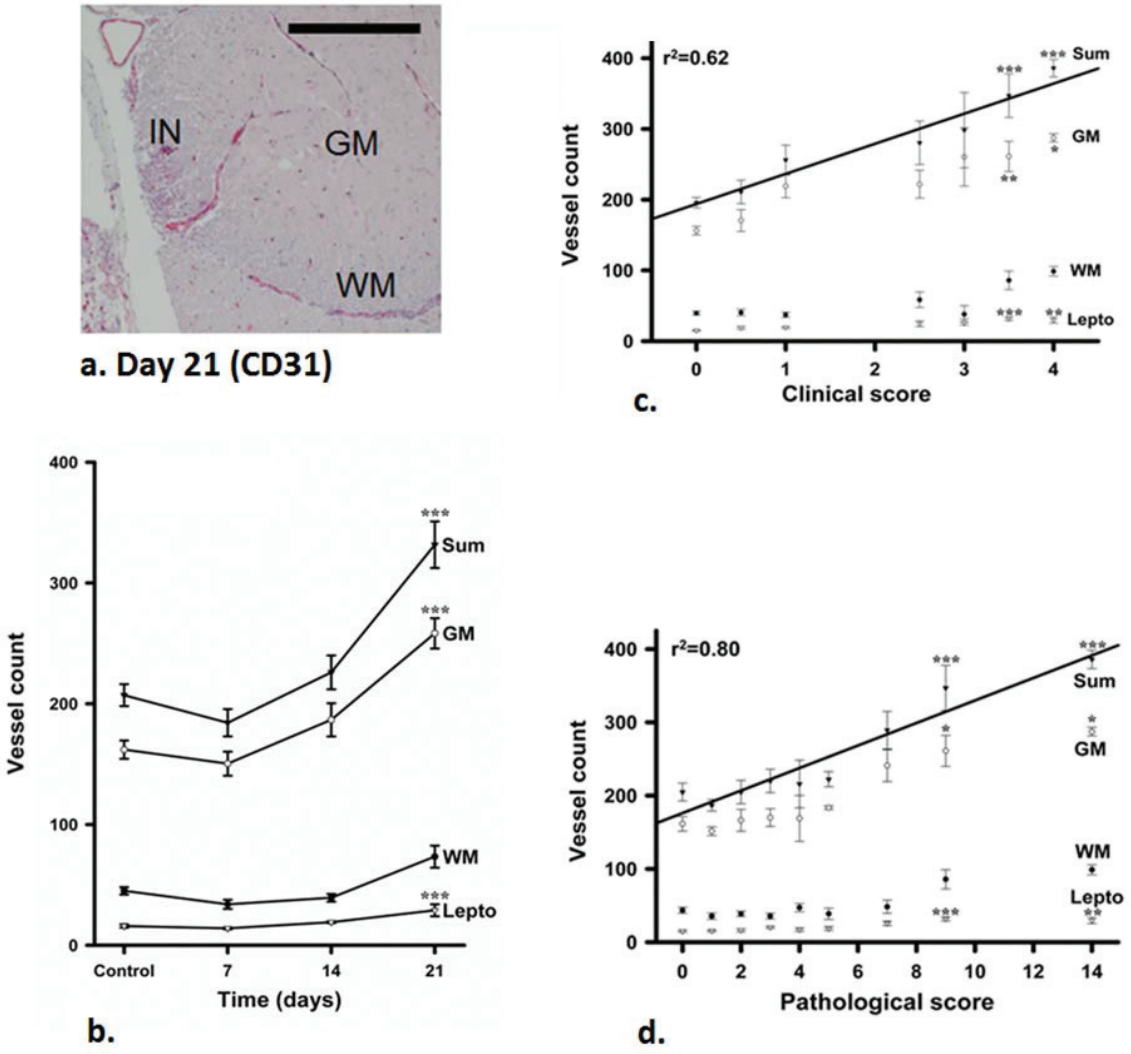

Figure 3.2. Blood vessel counts to determine angiogenesis. a. immunohistochemistry depicting CD31 profile. Key is GM = grey matter, WM = white matter, IN = inflammation. Scale bar, 200μm. b. Vessel counts for control mice and mice with EAE at days 7, 14 and 21. c, d. Vessel counts in each tissue section (4 per mouse) as a function of clinical score (c) or pathological score (d). A regression line is inserted and r^2 value indicated. Data is shown as mean ± SEM for WM, GM and the two in combination (Sum). Significance is relative to control (b) or data with zero scores (c, d), * = $p < 0.05$, ** = $p < 0.01$, *** = $p < 0.001$. *In collaboration with RJ Starkey and AS Easton.*

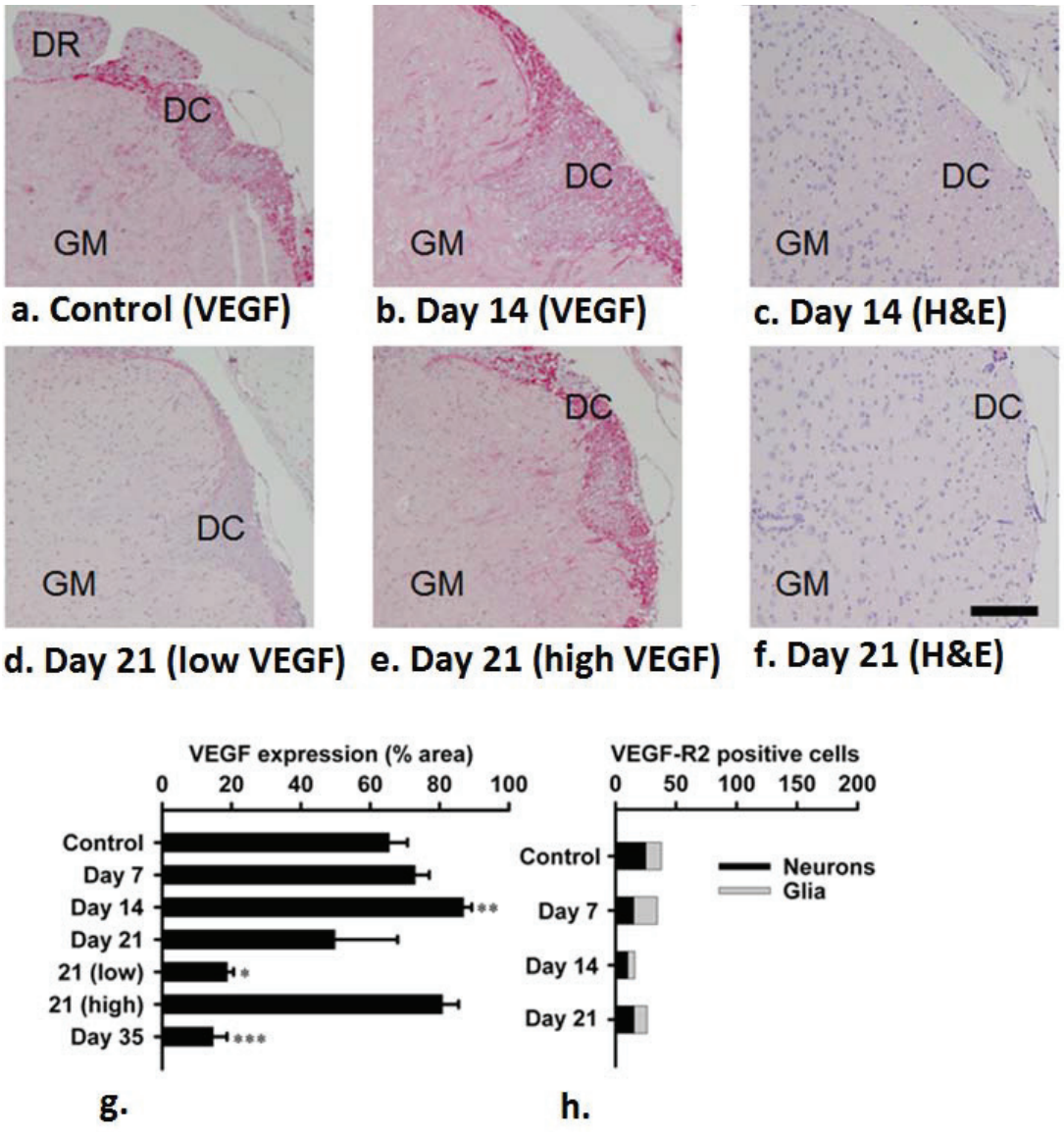

Figure 3.3. Expression of VEGF and VEGFR-2. a-f. Selected images of VEGF immunohistochemistry and corresponding H&Es (c, f) in control mice and mice with EAE. Key is DC = dorsal columns, DR = dorsal roots, GM = grey matter. Scale bar, 200µm. g. Bar chart of VEGF expression based on positive staining in the dorsal columns (% area). Data is mean ± SEM, per mouse (n = 6, except n = 5 at day 21). Day 21 is subdivided into low (n = 3) and high staining (n = 2) animals. Significance is compared to control, * = $p < 0.05$, ** = $p < 0.01$. h. VEGFR-2 expression as stacked bars for average number of positive cells (neurons or glia), based on counts per mouse.

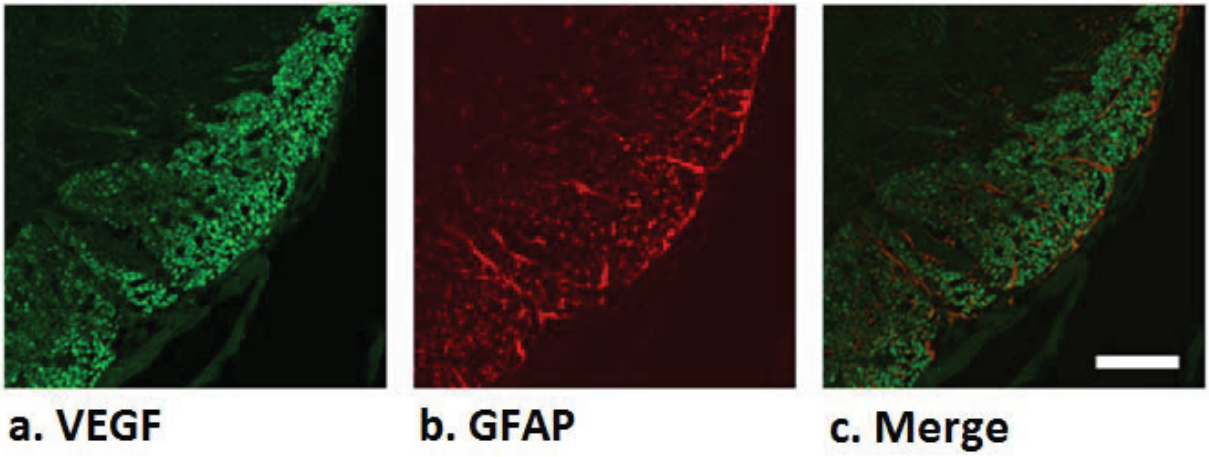

Figure 3.4. Confocal expression of VEGF. a-c. VEGF expression by astrocytes was assessed with double labeled sections of the dorsal columns in mice with EAE at day 21. Confocal imaging compares VEGF expression (green, a) with the astrocyte marker GFAP (red, b). There is no co-localization on the overlap image (c). Scale bar, 100µm.

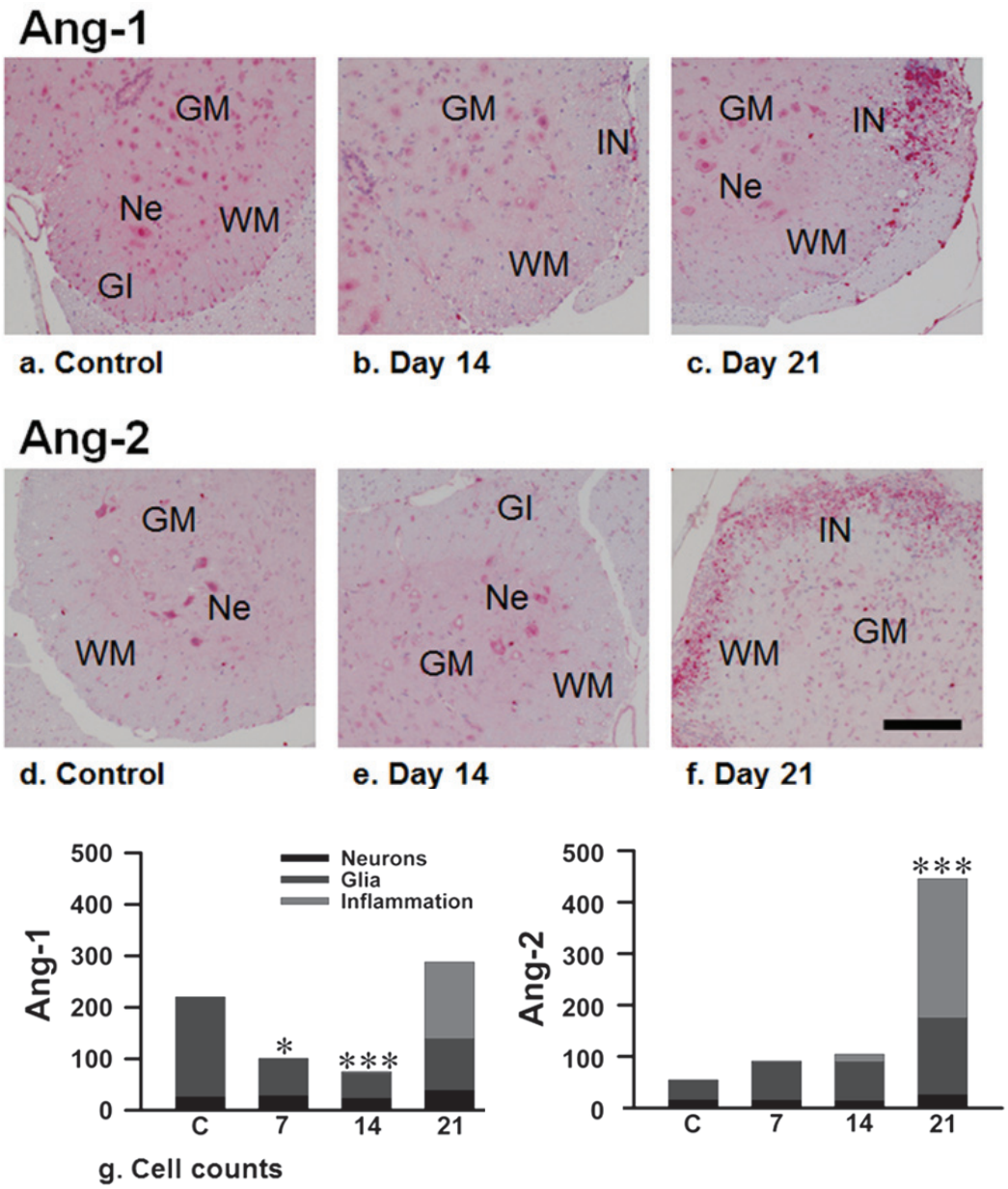

Figure 3.5. Angiopoietin expression during EAE. a-f. Selected images of lumbosacral spinal cord in control mice and mice at different stages of EAE, with immunohistochemistry for Ang-1 (a-c) or Ang-2 (d-f). Key is Gl = glia, GM = grey matter, IN = inflammation, Ne = neuron, WM = white matter. Scale bar, 200µm. g. Cell counts quantify expression of Ang-1 and Ang-2 in control mice (C) and mice with EAE at day 7, 14 and 21 as indicated. Data is shown as stacked bars for the average counts for indicated cell types per mouse (n = 6, except n = 5 at day 21). Significance is relative to control, * = $p < 0.05$,** = $p < 0.01$,*** = $p < 0.001$.

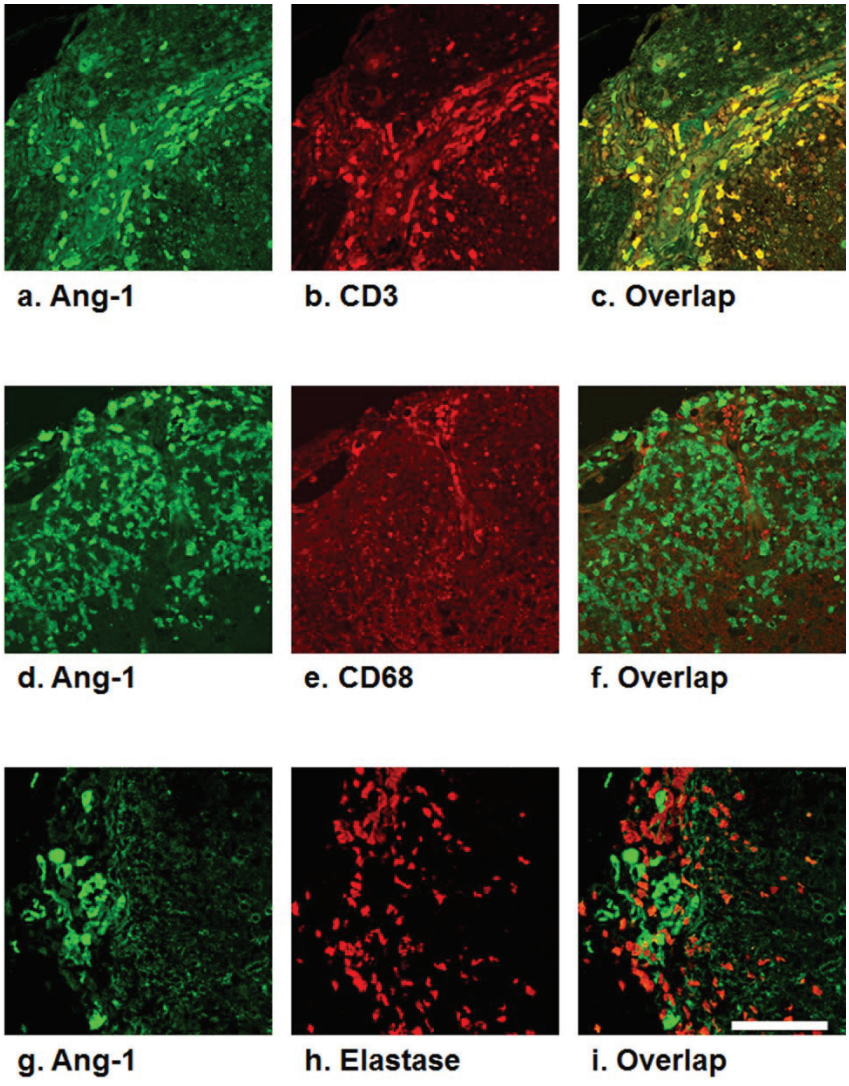

Figure 73.6. Images of spinal inflammatory infiltrate in EAE.

Figure 3.6. Images of spinal inflammatory infiltrates in mice with EAE. Sections examined by confocal microscopy. Green images (a,d,g) show Ang-1 labeling. Red images show inflammatory cell subtypes labeled for CD3 (T-cells, b), CD68 (macrophages, e) and elastase (neutrophils, h). Overlap images show co-localization of Ang-1 with CD3 positive T-cells (c), but no overlap with CD68 (f) or elastase (i). Scale bar, 50μm.

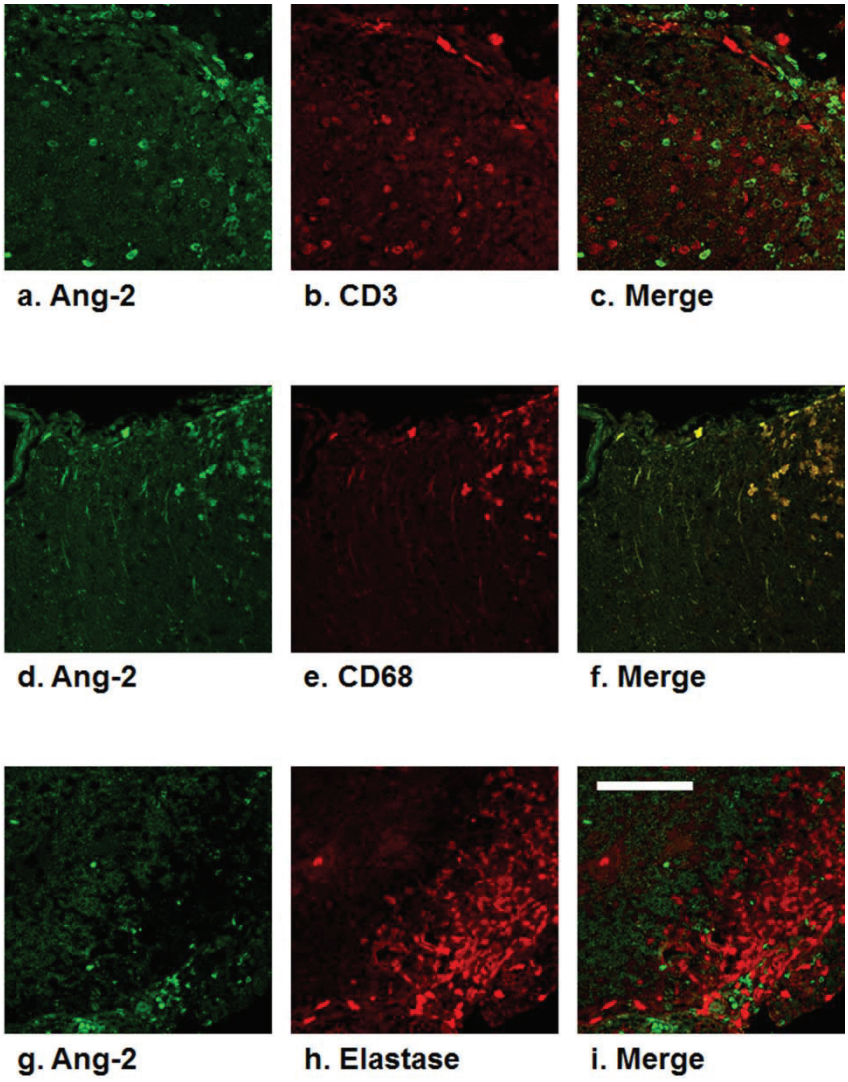

Figure 3.7. Images of spinal inflammation in mice with EAE. Sections examined by double labeling and confocal microscopy. Green images (a,d,g) show Ang-2 labeling. Red images show inflammatory cell subtypes labeled for CD3 (T-cells, b), CD68 (macrophages, e) and elastase (neutrophils, h). Overlap images show co-localization of Ang-2 with CD68 positive macrophages (f), but no overlap with CD3 (c) or elastase (i). Scale bar, 50μm.

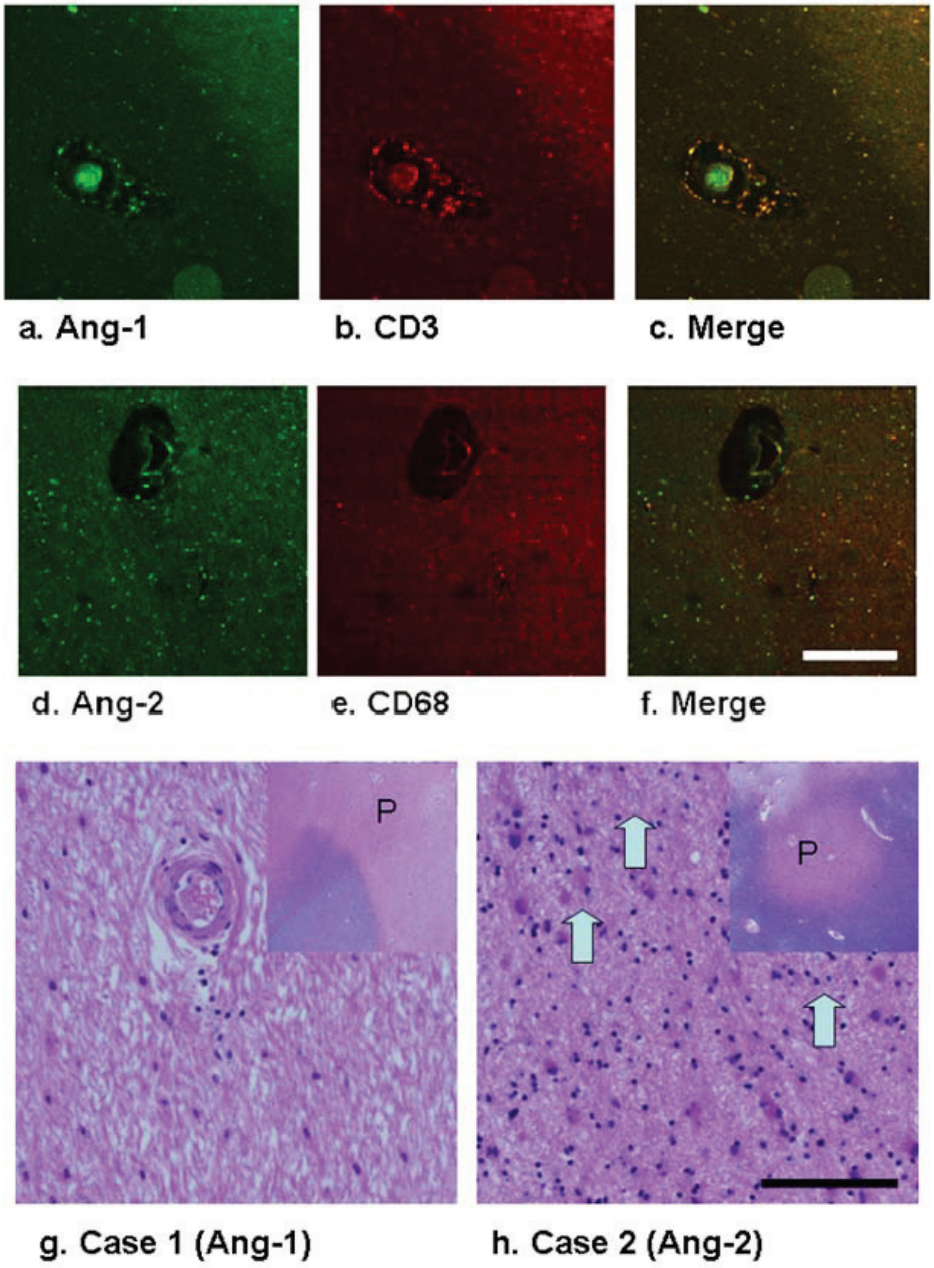

Figure 3.8. Inflammatory cells express Ang-1 and Ang-2 in MS. a-f. Double-labeled sections examined by confocal microscopy. Images of Ang-1 labeling (green, a) and CD3 (red, b) showing co-localization of Ang-1 with perivenous T-cells (c) in a chronic inactive plaque from case 1 (g). Images of Ang-2 labeling (green, d) and CD68 (red, e) showing co-localization with infiltrating macrophages (f) in a chronic active plaque from case 2 (h). Scale bar, 200µm. g,h. H&E-LFB stained sections from case 1 (g) and case 2 (h) showing the regions assessed by double labeling. Inset shows plaques as discrete areas of demyelination. Higher power shows perivenous lymphocytes (g) or infiltrating macrophages (h). Scale bar, 100µm.

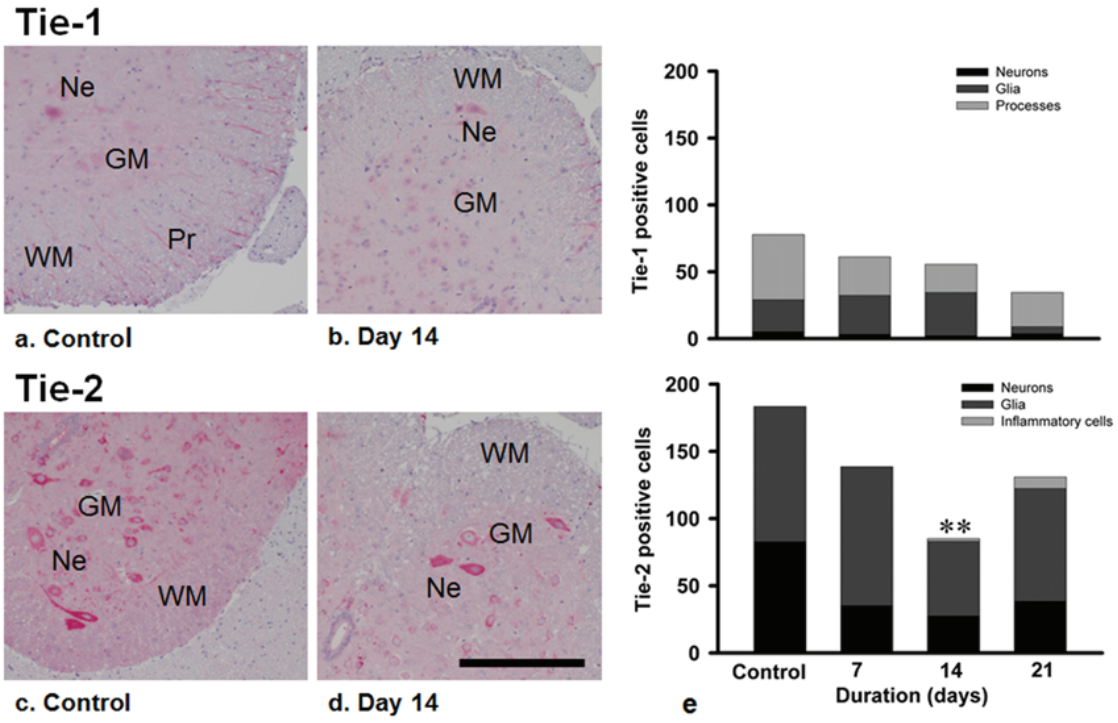

Figure 3.9. Tie receptor expression during EAE. a-d. Selected images of lumbosacral spinal cord in control mice, and mice with EAE at day 14. Key is GM = grey matter, Ne = neuron, Pr = glial processes, WM = white matter. Scale bar, 200µm. e. Stacked bars showing average counts for positive cells as indicated for Tie-1 (upper panel) or Tie-2 (lower panel). Data is per mouse (n=6, except n=5 at day 21). Significance is relative to control, * = $p < 0.05$, ** = $p < 0.01$, *** = $p < 0.001$.

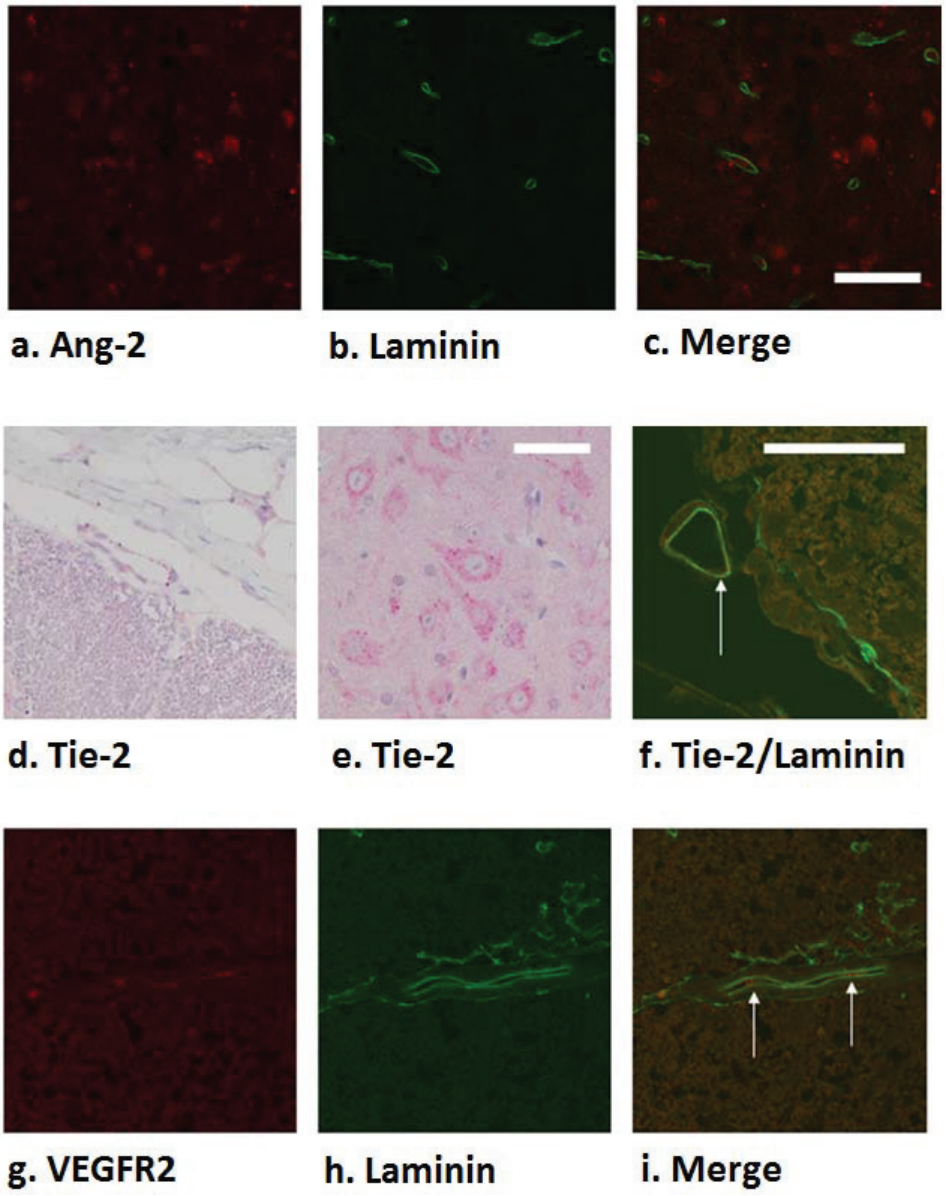

Figure 3.10. Ang-2, Tie-2, and VEGFR-2 co-expression in spinal cord blood vessels. a, c. staining for Ang-2 (red,a.) in inflammatory cells but no co-localization in adjacent blood vessels (green, b, c.). d, e. Tie-2 immunohistochemistry. f. dot-like labeling for Tie-2 in blood vessels (white arrow), e. shows similar reactivity in neurons in the anterior horn. g-i. areas of positivity for VEGFR-2 in a blood vessel. Scale bars = 50μm.

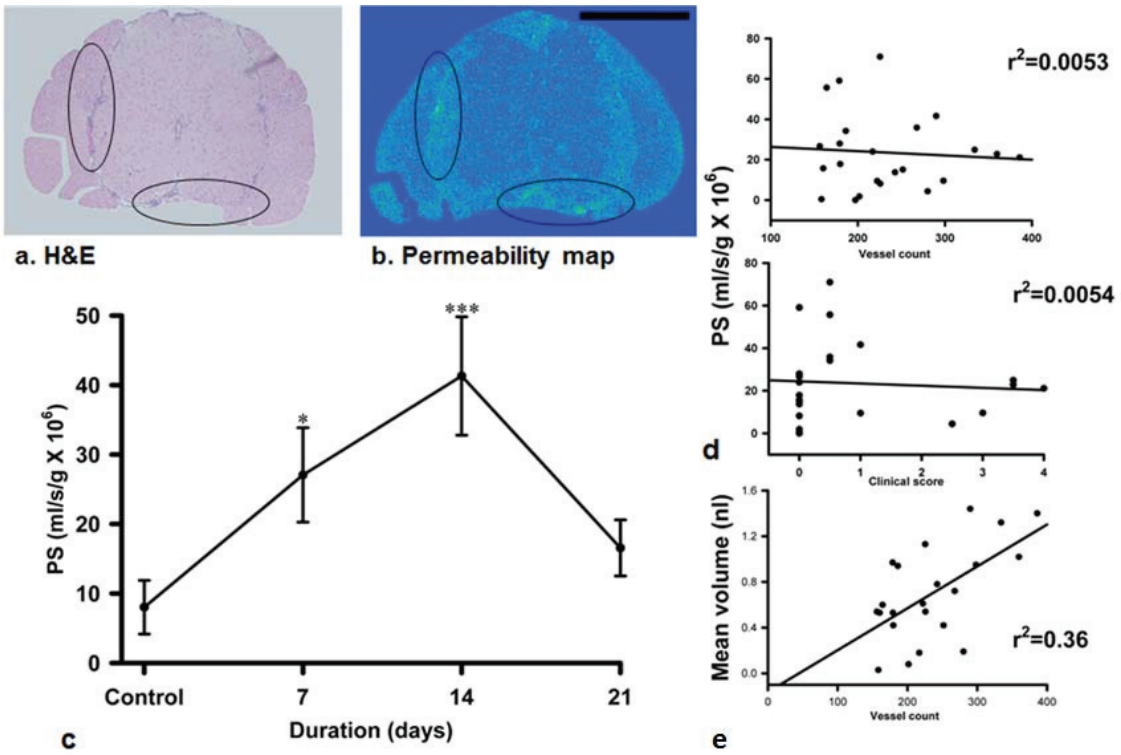

Figure 3.11. Permeability-surface area (PS) changes during EAE. a,b. Sections from the lumbosacral spinal cord of a mouse with EAE at day 21, clinical score 2.5. H&E image (a) is compared with a permeability map of the adjacent section (b). Pixel intensity has been pseudocolored, with lighter areas indicating regions of increased permeability. Two regions of increased permeability are encircled. Scale bar, 200µm. c. Per mouse PS values in each experimental group. Data is mean ± SEM, significance compared to control, * = $p < 0.05$, *** = $p < 0.001$. d. per mouse PS values as a function of that animal's vessel count and clinical score. E. mean volume of permeable tissue in sections from each mouse as a function of that animal's vessel count, with regression lines fitted to all the data.).

CHAPTER 4: BEVACIZUMAB DIMISHES EAE BY INHIBITING ANGIOGENESIS AND REDUCING PERIPHERAL T-CELL RESPONSES

Portions of this chapter appeared in the following publication:

MacMillan CJ, Furlong SJ, Chen P-L, Doucette C, Hoskin DW, Easton AS. Bevacizumab diminishes experimental autoimmune encephalomyelitis by inhibiting spinal cord angiogenesis and reducing peripheral T cell responses. J Neuropathol Exp Neurol 2012; 71(11): 983-99. *Reprinted with copyright permission.*

Contributions: Disease induction, monitoring, and tissue isolations in all figures of this chapter were completed by CJ MacMillan. AS Easton contributed to Figures 4.1 and 4.2 as a blinded scorer. Figures 4.4 data was obtained by P-L Chen. Figures 4.6, 4.8, 4.9 and 4.10 were completed by SJ Furlong. Figure 4.7 was done in collaboration between CJ MacMillan and SJ Furlong. Figures 4.3, and 4.5 were completed by CJ MacMillan.

4.1 Summary

In chapter 3, my work adds to the literature showing that angiogenesis plays a role in EAE and is regulated by VEGF, Ang-1 and Ang-2. However, the therapeutic potential of interfering with angiogenesis by blocking VEGF activity during EAE remains to be explored in detail. This study determines whether VEGF blockade with the monoclonal antibody bevacizumab (a humanized mouse antibody that binds to VEGF and used clinically as the drug Avastin®) can inhibit angiogenesis and reduce disease. Mice were treated with bevacizumab from symptom onset (5mg/kg, every 3 days), which resulted in reduced clinical and pathologic scores. Bevacizumab completely suppressed angiogenesis during EAE, and also reduced the number of Ang-2 expressing cells in spinal cord at day 21, with no effect on VEGF upregulation at day 14. Messenger RNA levels for CD105 were increased at day 14. Bevacizumab significantly reduced vascular permeability in the spinal cord at day 14 and 21. In peripheral lymph nodes, bevacizumab induced retention of CD4+ T-cells, and inhibited T-cell proliferation. In addition, bevacizumab reduced mononuclear cell infiltration into spinal cord together with the relative proportion of CD4+ and CD4- T-cells. Isolated CD4+ T-cells showed reduced expression of the T helper-17 (T_h-17) cell cytokine interleukin (IL)-17 and the T_h-1 cytokine interferon (IFN)-γ. We conclude that bevacizumab ameliorates CNS and lymphoid responses during EAE, and may hold promise as a therapy in MS.

4.2 Introduction

There are now several reports that document angiogenesis in the CNS of animals with EAE [110-112,154]. Its presence has been shown to correlate with clinical and pathologic criteria of disease in EAE [110,111,154], which implicates angiogenesis in disease progression.

However, direct evidence requires that several additional criteria be met. These include a reversal of disease parameters when angiogenesis is inhibited using pharmacologic approaches, as well as an exacerbation when angiogenesis is induced or exaggerated. Angiogenesis should also precede or coincide with disease; if angiogenesis occurs after peak disease then its role assumes less importance.

The regulation of angiogenesis in the CNS during murine EAE implicates several molecular factors. Among these are VEGF, as well as Ang-1 and Ang-2. As described in chapter 3, we demonstrated temporal changes in these three moieties that implicate them in the regulation of angiogenesis during EAE [154]. VEGF expression increased 14 days after disease onset, which preceded the increase in blood vessel counts at 21 days. Ang-1 is envisioned to play a role in stabilizing blood vessels, and countering angiogenesis. Therefore, the reduction in levels of Ang-1 we observed at days 7 and 14 appears to set the stage for angiogenesis. A sharp increase in levels of Ang-2 at day 21, which acts in concert with VEGF to promote angiogenesis, suggests that this molecule plays an additive role during angiogenesis [140,141]. Of these three factors, VEGF is generally considered to play a key role, but this is modulated by changes in the other factors.

While EAE is widely acknowledged to be an imperfect model of the human disease MS, one of its most useful functions has been to screen potentially useful pharmacologic compounds as therapies for MS. As a result, the immune component of MS has been successfully treated with drugs that reduce the immune activation seen in EAE [155,156]. However, an additional benefit may be conferred by using drugs that target other aspects of the pathogenesis of MS. Ideally, one would combine current therapies with other agents that have already received clinical approval. To this end, we have

investigated the utility of treating EAE with bevacizumab, a humanized monoclonal antibody that binds to VEGF [157-159].

Bevacizumab (trade name Avastin®) is currently approved for use in advanced cancers, as an adjunct therapy. Although bevacizumab is specifically engineered to bind to the human 165 amino acid isoform of VEGF-A, it effectively inhibits angiogenesis in rodents and rabbits [160-170]. There is evidence of a weaker binding affinity of bevacizumab for murine VEGF (164 amino acid isoform of VEGF-A) [160], although some investigators consider the degree of binding to be too weak to be effective [171,172].

The aim of this work was to carry out a detailed investigation on the impact of bevacizumab as a treatment for murine EAE. Since VEGF regulates angiogenesis in our model of EAE, we studied the impact of bevacizumab on CNS angiogenesis, and related this to disease parameters. We also studied the collateral effects of bevacizumab treatment on Ang-2 expression, in view of the cooperative role of Ang-2 in promoting angiogenesis. Further studies were aimed at characterizing the effects of bevacizumab on vascular permeability in the CNS, and on the activation of peripheral T-cells, and their transit into the CNS. This work has been published [173].

4.3 Results

4.3.1 Bevacizumab Reduces Clinical Scores in EAE

Bevacizumab was given to mice on the day of symptom onset (day 9 from disease induction) and administered every 3 days until sacrifice. Fig 4.1 A shows the effect of bevacizumab treatment on clinical scores. While clinical scores continued to climb for mice with untreated EAE, reaching a peak of 2.85 ± 0.27 at day 21 (n = 10 mice), mice

treated with bevacizumab exhibited a markedly slowed increase in scores that reached a plateau between days 15-21. Peak scores in the bevacizumab treated mice were 0.84 ± 0.16 at day 14 (n = 16 mice). The clinical score was significantly reduced in comparison to untreated EAE between days 13-21 ($p< 0.05$-0.001). Disease-free mice treated with bevacizumab showed no increase in clinical scores (n = 18 mice).

To determine whether the effect of bevacizumab can be attributed to the administration of immunoglobulin which can improve the course of inflammatory disease when given intravenously [174], mice were given IgG (by the same dose and intraperitoneal route of administration as bevacizumab) from the onset of EAE symptoms (Fig. 4.1 B). While bevacizumab reduced clinical scores in these animals, IgG had no significant effect (n = 6 mice for the IgG-treated group, n = 4 mice in the bevacizumab-treated group).

4.3.2 Bevacizumab Reduces Pathologic Scores

Pathologic score was assessed from histological features in the lumbar spinal cord. Overall scores were based on the degree of mononuclear inflammation (on H&E stained sections, Fig 4.1 D) as well as demyelination (using LFB/CV stained sections). Fig 4.1 C illustrates the data as stacked means for each category. The pathologic score increased significantly over control at day 21 in mice with untreated EAE. The score was significantly reduced at day 21 in EAE mice treated with bevacizumab. Of the 8 mice in this cohort at day 21, two had scores of 7 and one a score of 8. The remaining 5 mice scored between 0-1. This disparity in scores is shown in Fig. 4.1 D. In the upper panel, a mononuclear infiltrate is seen in the surface leptomeninges (score 1). However, in the lower panel the infiltrates are diffuse and invade the underlying parenchyma (score 8).

4.3.3 Bevacizumab Suppresses Spinal Cord Angiogenesis

Angiogenesis was assessed from blood vessel counts in sections stained for the endothelial marker CD31. Separate counts were performed in the leptomeninges, white matter, and gray matter and added to give a total count. In mice with untreated EAE, there was a significant increase in vessel count on day 21 for total count and counts in the gray matter ($p < 0.001$), with no increase in counts in the white matter or leptomeninges (Fig. 4.2 A, filled circles). Total counts were then related to clinical or pathologic score, taking each spinal cord section (2 per mouse) as an individual data point. The overall count in mice with untreated EAE showed a robust positive correlation to both clinical score ($r^2 = 0.96$; Fig. 4.2 B, filled circles) and pathologic score ($r^2 = 0.83$; Fig. 4.2 C, filled circles). The count at higher scores was significantly increased above counts in animals with a zero score.

By contrast, mice treated with bevacizumab during EAE did not show an increase in vessel counts on day 21 (Fig. 4.2 A, open circles). On day 21, the total and gray matter counts were not significantly increased over controls and were significantly lower than counts in mice with untreated EAE ($p < 0.001$). In the bevacizumab group, the total counts at higher clinical or pathologic scores were not significantly greater than counts at a zero score (Fig. 4.2 B, C, open circles). The correlation coefficient relating vessel count to clinical score ($r^2 = 0.27$) and pathologic score ($r^2 = 0.36$) was also reduced in comparison with that in untreated EAE.

4.3.4 Increased VEGF Expression is Unaltered and Ang-2 Expression Reduced Following Bevacizumab Treatment

VEGF was only expressed in neurons and axons in the lumbosacral spinal cord of mice with EAE, with predominant expression in the dorsal columns (Fig. 4.3 A). To

quantify VEGF expression, we calculated the % area containing positively stained axons within the dorsal columns (see chapter 3). The data showed a significant increase in VEGF expression at day 14 in mice with EAE that were either untreated or treated with bevacizumab. There was no difference between the two groups (Fig. 4.3 D). Both groups showed a decline in VEGF expression at day 21; however, VEGF expression remained elevated in a subset of the mice, while others showed significant reductions below control levels. In the bevacizumab-treated group, 3 of 9 mice showed expression levels under 60% (14.0, 36.2 and 53.7%).

Additional sections were examined for Ang-2 expression in neurons, glial and inflammatory cells (Fig 4.3 B, C). There was a significant increase over control at day 21 in untreated EAE due largely to Ang-2 expression by inflammatory cells (average count 270.6, n=5 mice). In bevacizumab-treated mice, the number of Ang-2 immunopositive inflammatory cells was markedly reduced (average count 49.6, n = 7 mice) which reflects the reduced inflammation seen in these animals (see pathologic score data, Fig.4.1 C), and overall expression was not increased above control (Fig. 4.3 E).

4.3.5 Bevacizumab Reduces CD105 mRNA Expression in EAE

To further evaluate the effects of bevacizumab, quantitative PCR (qPCR) was used to evaluate mRNA expression using samples of lumbosacral spinal cord taken from mice with EAE at day 14 and 21, either untreated or treated with bevacizumab. Comparison was also made to mice treated with bevacizumab in the absence of disease. Data are normalized to expression in tissue from disease free, untreated control mice (expressed as relative units, Fig. 4.4).

The data showed a significant increase in mRNA expression for CD105 at day 14 ($p< 0.01$) in untreated EAE mice, which is selectively expressed by blood vessels formed during angiogenesis [175,176]. This increase in CD105 was blocked by treatment with bevacizumab. By contrast, CD31, which is a marker of vascular endothelial cells in general, showed no selective increase in mRNA expression. There was a non-significant trend to increased mRNA expression for TNF, which is a general marker of inflammation; the average mRNA increased to 5.19 times the expression in untreated controls. Although local expression of VEGF increases at day 14, and Ang-2 increases at day 21 (Fig. 4.3), mRNA levels in whole tissue for Ang-2 alone tended to increase at day 14, while mRNA for VEGF was generally unaltered during EAE. The average mRNA expression for Ang-2 at day 14 in mice with EAE was 2.73 times the expression in untreated control mice. Ang-1 levels showed little change at either day 14 or day 21.

4.3.6 Vascular Permeability in EAE is Reduced Following Bevacizumab Treatment

PS values were calculated from permeability maps of the spinal cord in mice with EAE, either untreated or treated with bevacizumab. In the untreated EAE group there was a significant increase in PS over controls at day 14 that had sharply reduced at day 21 (Fig. 4.5 A, filled circles). In the bevacizumab-treated mice, the increase in PS at day 14 and day 21 was significantly reduced relative to EAE alone (Fig. 4.5 A, open circles; $p < 0.001$ at day 14, $p < 0.05$ at day 21).

In bevacizumab treated mice at day 14, the estimated LY permeability, $Pest_{LY} = 1.00 \pm 0.30 \times 10^{-6}$ cm/s ($n = 8$) compared to $2.86 \pm 0.59 \times 10^{-6}$ cm/s ($n = 6$) in mice with untreated EAE. At day 21, the $Pest_{LY} = 0.02 \pm 0.01 \times 10^{-6}$ cm/s ($n = 8$) for bevacizumab treatment compared to $1.15 \pm 0.28 \times 10^{-6}$ cm/s in untreated EAE ($n = 5$). In the EAE only

group, there was no relationship between PS values and clinical score (Fig. 4.5 B, filled circles) or vessel count (Fig. 4.5 C, filled circles). For the bevacizumab treated group, there was also no relationship between PS and clinical score (Fig. 4.5 B, open circles). However, a weak positive correlation (r^2=0.13) was found for PS relative to vessel count in these animals (Fig 4.5 C, open circles), suggesting a relationship between vessel density and permeability when angiogenesis is suppressed by bevacizumab. In both groups, there was a weak correlation between vessel counts and the volume of tissue affected by permeability increases (Fig. 4.5 D). This was more marked for untreated EAE (r^2=0.36) by comparison to EAE treated with bevacizumab (r^2=0.13).

4.3.7 Bevacizumab Reduces the Proliferative Response of Peripheral CD4+ T-cells to the Inciting Antigen in EAE

To assess the effect of bevacizumab treatment on immune responses, lymph nodes were harvested from treated and untreated EAE animals at day 21 to coincide with peak clinical and pathologic scores. Controls were taken from untreated disease-free (wild type) mice. Both treated and untreated EAE mice showed a significant increase in total cell numbers in the harvested nodes (Fig. 4.6 A).

Cells were then sorted into different groups based on the presence of surface markers. During EAE in both treated and untreated groups, there was a significant reduction ($p< 0.001$) in the proportion of CD4+ TcRβ+ cells in the lymph nodes compared to disease-free controls (Fig. 4.6 B), consistent with a significant egress from lymphoid tissue towards the CNS. However, the reduction was significantly less for mice treated with bevacizumab when compared to mice with EAE alone ($p< 0.01$), suggesting that bevacizumab may lead to retention or trapping of CD4+ TcRβ+ cells in the lymph nodes. Compared to controls, EAE mice treated with bevacizumab showed a significant

reduction ($p < 0.05$) in the proportion of non-CD4+ T-cells (CD4- TcRβ+, Fig. 4.6 C) and both EAE groups showed significant compensatory increases ($p < 0.001$) in the proportion of non-T-cells (TcRβ-, Fig. 4.6 D).

CD4+ T-cells were then isolated and stimulated to determine their proliferative response. T cells from mice with EAE showed increased proliferation over controls when exposed to the inciting antigen (MOG_{35-55}), but this was significantly blunted ($p < 0.01$) in bevacizumab-treated mice. Lymphocytes from all groups responded to stimulation with T-cell expander beads, but no differences were detected between the groups (Fig. 4.6 E).

4.3.8 Bevacizumab Inhibits CD4+ T-cell Recruitment in EAE

The preceding data suggested that bevacizumab may cause retention of CD4+ T-cells in peripheral lymph nodes. This would result in a reduction in trafficking from lymphoid tissue to the inflamed spinal cord during EAE. To confirm this, mononuclear cells were isolated from spinal cord tissue in mice with EAE sacrificed at day 21, and total numbers as well as receptor specific subtypes were quantified in different groups of mice. Mononuclear cells were not detected in wild type mice (Fig. 4.7 A), so further comparisons were restricted to mice with EAE, either untreated or treated with bevacizumab.

There was a significant ($p < 0.05$) increase in the number of spinal cord mononuclear cells during EAE that was significantly reduced by bevacizumab treatment (Fig. 4.7 A, $p < 0.05$). The proportion of spinal cord mononuclear cells co-expressing CD4 and TcRβ was approximately 5% during EAE, but this fell following treatment with bevacizumab to approximately 0.5% (Fig. 4.7 B, $p < 0.05$). A similar pattern was noted for T-cells (TcRβ positive) that did not express CD4 (from about 5% to about 1%, Fig.

4.7 C, $p < 0.05$). There was a compensatory increase in the proportion of non-TcRβ-expressing cells in the bevacizumab-treated group (Fig. 4.7 D, $p < 0.05$).

4.3.9 Bevacizumab Inhibits T_h-1 and T_h-17 Cytokines

CD4+ T-cells were isolated and stimulated *in vitro* with MOG_{35-55} and T-cell expander beads, and supernatants were collected to measure levels of cytokines characteristic of T_h-17 cells (IL-17), T_h-1 cells (IFN-γ) and T_h-2 cells (IL-4). Bevacizumab treatment during EAE resulted in a reduced secretion of IL-17 and IFN-γ, while IL-4 secretion was unaffected (Fig. 4.8).

To further define the subpopulations of T-helper cells, they were stained for intracellular cytokines after treatment with the Golgi inhibitor Brefeldin-A to inhibit cytokine secretion. Representative flow cytometry scatter plots are shown for co-staining with CD4 and each of the marker cytokines (Fig. 4.9 A). Within the CD4+ population, there is a subgroup (% of the total population) that shows high co-expression of each cytokine. The percentage of cells with increased co-expression of IFN-γ, defining the T_h-1 subgroup, was significantly reduced in mice treated with bevacizumab during EAE. Cells co-expressing IL-17, defining the T_h-17 subgroup, showed a non-significant downward trend, while the IL-4-containing subgroup (defining T_h2 cells) was unaffected (Fig. 4.9 B).

To assess direct effects of bevacizumab on T-cell responses, additional experiments were carried out with T-cells isolated from wild type mice and mice with untreated EAE, that is, they were not exposed to bevacizumab *in vivo*. The former was stimulated with CD3/CD28-coated microbeads, whereas the latter was restimulated with MOG_{35-55} added to BMDCs. Cells were assessed for proliferation fraction or secretion of

IL-17 and IFN- γ. Addition of bevacizumab (10, 100 μg/mL) to the cultures had no effect on proliferation fraction or the secretion of IL-17 and IFN- γ (Fig. 4.10).

4.4 Discussion

4.4.1 Impact of Bevacizumab During EAE

Angiogenesis is regulated by different molecules during EAE, but previous work from our group as described in Chapter 3 [154] indicates that VEGF and Ang-2 are both likely to stimulate angiogenesis, based on their temporal expression, and putative roles during pathological angiogenesis [140,141]. Treatment with bevacizumab reversed the increase in blood vessel counts seen 21 days from the onset of EAE, with significant reductions in gray matter and total vessel counts (Fig. 4.2 A). The positive correlation between vessel count and clinical and pathologic score during untreated EAE was significantly blunted in the bevacizumab-treated cohort (Fig. 4.2 B, C).

During untreated EAE, there is a significant early increase in VEGF expression within dorsal column axons (Fig. 4.3 A, D) that reverses in a proportion of mice by day 21, after angiogenesis is established. This pattern of expression was not altered in the bevacizumab-treated EAE group (Fig. 4.3 D). Ang-2 is also expressed at higher levels in mice with EAE by day 21, largely attributed to infiltrating macrophages [154]. This increase in Ang-2 was reversed in the bevacizumab treated animals through a reduction in the numbers of infiltrating immune cells (Fig. 4.3 B, C, E).

The expression data was then compared to mRNA expression (Fig. 4.4) for VEGF, Ang-1, and Ang-2, as well as the inflammatory marker TNF, and two markers of angiogenesis: CD105, which is specifically expressed in newly formed blood vessels

[175,176], and CD31, which is present on all blood vessels. This technique proved to be considerably less sensitive than protein detection by immunohistochemistry on tissue sections. There was a trend towards reduced Ang-1 expression, and increased Ang-2 expression, during EAE. The increase in Ang-2 mRNA levels was slightly inhibited in the bevacizumab-treated group. VEGF appeared to be reduced by day 14 in the EAE group compared to controls, which may reflect the subsequent fall in protein levels observed previously at day 21. Interestingly, the only significant increase was seen in mRNA levels for CD105 at day 14, which is a further confirmation of angiogenesis (Fig. 4.4 A).

Vascular permeability is another variable that is of interest during EAE. Our previous work showed an increase in permeability from day 7 and day 14, with a sharp reduction by day 21 during EAE [154]. Bevacizumab treatment during EAE caused a significant reduction in PS product at day 14 and 21 compared to EAE alone (Fig. 4.5 A). The relationship between PS, clinical score and angiogenesis (as measured by vessel counts) was also assessed. During untreated EAE there was no correlation between PS and either clinical score (Fig. 4.5 B, filled circles) or vessel count (Fig. 4.5 C, filled circles). Bevacizumab-treated mice also showed no relation to clinical score (Fig. 4.5 B, open circles) but there was a weak positive correlation between PS and vessel count (Fig. 4.5 C, open circles). Since angiogenesis is blocked in this group (Fig. 4.2 A) the data suggest that permeability is related to the density of resident vessels, before angiogenesis occurs. The data conversion to estimates of LY permeability allows comparison to data obtained on LY permeability in rat pial microvessels [123]. In general, permeability values at or around 0.2×10^{-6} cm/s reflect the normally very low permeability across CNS

microvessels. Values up to 5 x 10^{-6} cm/s are relatively modest in size, such that significant extravasation of protein and fluid leading to edema do not occur [177]. The values in this study are in this range. At day 21, bevacizumab essentially returned permeability to normal, or that seen in controls (Fig. 4.5 A). Bevacizumab could act by reducing the direct effect of VEGF, which is known to induce increases in vascular permeability in the CNS [178]. However, bevacizumab's actions could also be indirect, through reduced expression of permeability factors by invading immune cells.

4.4.2 Impact of Bevacizumab on Peripheral T-cell Responses

The effect of bevacizumab on EAE and angiogenesis can be attributed to a combination of central effects (such as reduced Ang-2 expression, and decreased infiltration of immune effector cells), as well as effects on the peripheral immune system. Bevacizumab treatment had no effect on overall cell numbers within peripheral lymph nodes (Fig. 4.6 A). However, when the cells were defined by their expression of surface markers, the peripheral nodes in bevacizumab-treated mice with EAE contained a higher proportion of CD4+ T-cells (TcRβ+) than the mice with untreated EAE (Fig. 4.6 B). Other populations (CD4- T-cells, and non-T-cells) were unaffected by bevacizumab treatment (Fig. 4.6 C, D). Fewer CD4+ T-cells responded to stimulation with MOG_{35-55} in the bevacizumab-treated mice, showing an inhibitory action on antigen-specific T-cell clones (Fig. 4.6 E).

The increase in CD4+ T-cells in peripheral lymph nodes after bevacizumab treatment implies that there is reduced trafficking of these cells from lymphatic tissue to the CNS. To confirm this, mononuclear cells were extracted from spinal cord samples. As implied by the reduction in pathologic score (Fig. 4.1 C), there was a marked reduction in

total cell counts in the bevacizumab-treated group at day 21 (Fig. 4.7 A). The proportion of mononuclear cells expressing CD4 was sharply reduced in these mice (Fig. 4.7 B), as well as CD4 negative T-cells (Fig. 4.7 C) with a compensatory increase in non-T-cells (Fig. 4.7 D).

CD4+ cells were then further defined in terms of their cytokine secretion profiles. T_h-17 and T_h-1 cells both contribute to the evolution of EAE [179], and are defined by secretion of IL-17 and IFN-γ, respectively. CD4+ cells that were subsequently stimulated with MOG_{35-55} and T-cell expander beads showed reduced secretion of IL-17, while MOG_{35-55} stimulated cells showed reduced IFN-γ secretion (Fig. 4.8 A, B). T_h-2 secretion of IL-4 was unaffected (Fig. 4.8 C). Lymphoid cells were also stained to detect those CD4+ cells with high levels of each intracellular cytokine. The bevacizumab-treated mice showed a significant reduction in IFN-γ-expressing cells (T_h-1 cells) with a trend to reduction of IL-17-expressing cells (T_h-17 cells, Fig. 4.9). Taken together, these data indicate that bevacizumab has a significant impact on the differentiation of CD4+ cells towards the T_h-1 and T_h-17 phenotypes that drive EAE.

4.4.3 Mechanism of Action of Bevacizumab

Bevacizumab is currently used in a clinical context to treat advanced cancers that depend on angiogenesis for tumor progression, and its mechanism of action through binding of the human VEGF-A isoform has been extensively studied and reviewed [157-159]. However, the ability of bevacizumab to inhibit processes linked to the murine VEGF-A isoform is a subject for debate in the literature. There is less binding of murine VEGF by bevacizumab in studies that have compared this to the binding of human VEGF. In one study, the authors reported detectable binding of murine VEGF by bevacizumab,

although in an ELISA-based assay, they found that 1000 times as much bevacizumab was required to detect the binding of murine VEGF, in comparison to the human protein [160]. This study was reappraised in a study that found an 'extremely weak' interaction between bevacizumab and murine VEGF by Western blot analysis, but failed to detect its interaction using other methods [172].

Despite this, bevacizumab has been shown to ameliorate a number of processes linked to VEGF expression in animal models. Application of bevacizumab in mice inhibited corneal neovascularization induced by inserting nylon sutures [160] or by acute chemical injury [161] and did not induce injury to the normal mouse cornea after topical application [162]. By inhibiting angiogenesis, subconjunctival bevacizumab also inhibited rejection of mouse corneal allografts [163]with high penetration [164]. These effects extended to proliferation of lymphatic vessels in the mouse [162]. Bevacizumab also inhibited corneal angiogenesis in rabbit models [165]. In another rabbit study, bevacizumab reduced the adhesions induced by injecting chemicals into the pleural space, and resulted in reduced vascular density at this site [166]. Bevacizumab also inhibited angiogenesis in the dorsal skinfold chamber model of ischemic injury in mice [167]. Bevacizumab reduced the secretion of VEGF by murine melanoma B16LS9 cells co-cultured with mouse vascular endothelial cells, although the effect was more pronounced when human melanoma lines were used [168]. Bevacizumab inhibited endothelial functions (specifically, cell adhesion and proliferation) linked to angiogenesis when applied to a cell line derived from murine coronary artery endothelial cells [169]. In another study, bevacizumab reduced the ability of exogenously applied murine VEGF to increase the proliferation of human umbilical vein endothelial cells (HUVEC) by 17%, although bevacizumab inhibited HUVEC

proliferation in response to human VEGF to a greater extent (by 35%) [170]. This contrasts with other reports, one in bovine retinal capillary endothelial cells [172] and another in HUVEC [171] in which bevacizumab did not inhibit the proliferation induced by murine VEGF.

Glycine-88 is one of three residues at the periphery of the VEGFR-1 binding epitope that differ in the sequence between murine and human VEGF. In the mouse, it is substituted with a serine residue, which adds a side chain that weakens its binding to bevacizumab. The binding sequence used to bind B20-4.1.1 is, however, conserved between mouse and human VEGF, so this antibody retains the capacity for high affinity binding to both proteins [171,180]. In chapter 5, we explore the ability of B20-4.1.1 to replicate the effects of bevacizumab in EAE, however as a preliminary comment, it was also shown to be effective in reducing the impact of EAE. It seems likely that bevacizumab is acting through specific binding rather than the non-specific effects of immunoglobulin since control administration of IgG did not reduce clinical scores in EAE (Fig. 4.1 B). However, if bevacizumab does not directly bind to murine VEGF, then it might act by binding to an intermediary molecule in the mouse, which then alters the secretion of VEGF by target cells. Alternatively, as reported in patients treated with bevacizumab [181], it might lead to paradoxical increases in serum VEGF that mediate its peripheral inhibitory effects on CD4+ T-cells. However, this seems unlikely, since VEGF augmented the differentiation of pro-inflammatory T-cells with a T_h-1 phenotype [182]. Nevertheless, these effects resulted in a reduced infiltration of the CNS by mononuclear cells in general, and those that do infiltrate contained a smaller proportion of CD4+ T-cells (Fig. 4.7).

In the periphery there was reduced differentiation into both T_h-1 and T_h-17 phenotypes (Figs. 4.8, 4.9), which is consistent with a reduction in VEGF activity. There is evidence that bevacizumab inhibits infiltration of tumor xenografts by macrophages [128]. A reduction in macrophage infiltration into the spinal cord could have resulted in the observed reduction in Ang-2 expression in this study (Fig. 4.3 D). Although bevacizumab can circulate freely in the blood, it may have limited penetration into the CNS, owing to its molecular weight, and the problem of crossing the BBB barrier. If bevacizumab binds weakly, if at all, to VEGF in the CNS, then the concurrent reduction in Ang-2 expression by inflammatory cells could account for much of the inhibitory action of bevacizumab on EAE-associated angiogenesis (Fig. 4.3). Alternatively, its effects might be mediated exclusively through VEGF binding in blood, serving as a trap or sink for VEGF expressed within the CNS.

4.4.4 Conclusion

This study demonstrates that EAE can be effectively treated with bevacizumab. The effect is potent, and results in significant reductions in CNS inflammation, Ang-2 expression, and infiltration by mononuclear and CD4+ T-cells. There is evidence of trapping of CD4+ T-cells in peripheral lymph nodes, as well as a reduced differentiation into T_h-1 and T_h-17 subtypes, both of which regulate the initiation and maintenance of EAE. The precise mechanism of action may be through direct binding of murine VEGF, or through indirect effects on the processing or downstream actions of VEGF and other regulators. To the extent that EAE models aspects of the human disease MS, this study suggests that bevacizumab, and other therapies that target angiogenesis could be useful adjuncts in its treatment. We will explore the role of binding to murine VEGF with B20-

4.1.1 as well as the impact of angiostatin as therapies directed against angiogenesis during EAE in chapter 5.

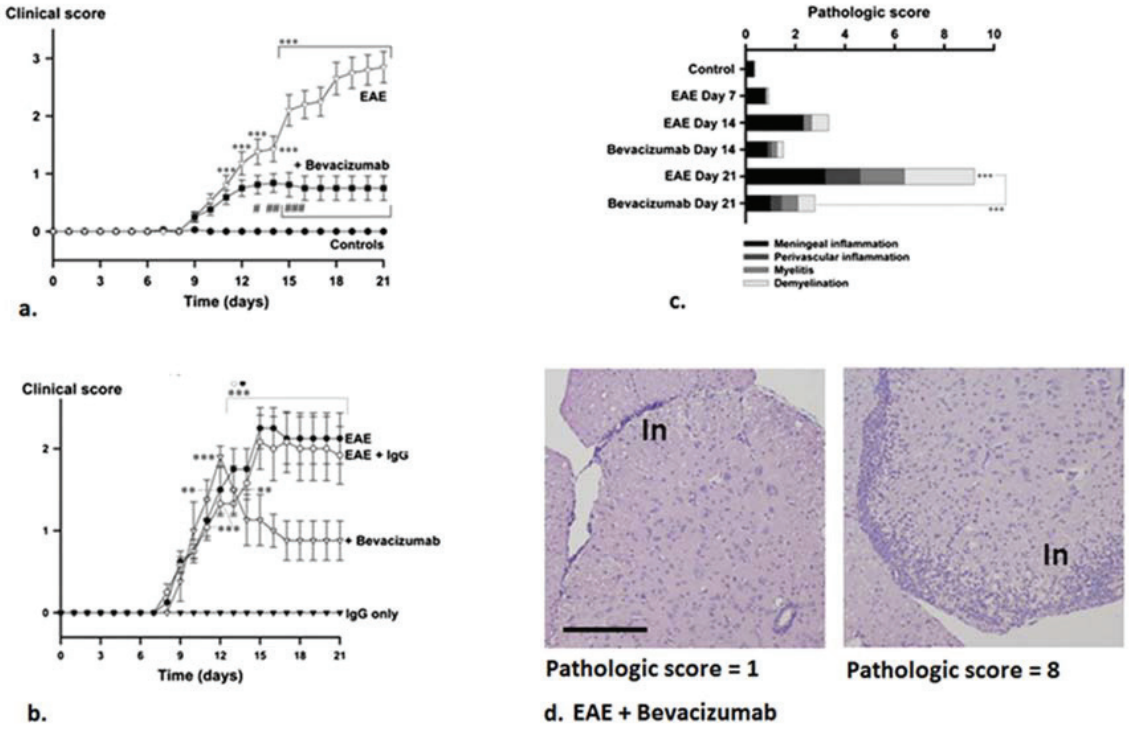

Figure 4.1. Bevacizumab reduces clinical and pathologic scores in EAE. a. Clinical scores in bevacizumab-treated and untreated control mice with EAE. Disease-free mice treated with bevacizumab (controls) showed no increase in clinical scores. b. Treatment with IgG. c. Pathologic score data for bevacizumab versus control during EAE. d. H&E-stained sections of lumbar spinal cord in mice with EAE treated with bevacizumab on day 21, illustrating different degrees of inflammation (In = inflammatory infiltrates). Data are shown as mean ± SEM (a,b). Significance (*, **, *** $p < 0.05–0.001$) at each time point is relative to control, except when comparing bevacizumab-treated EAE with EAE alone (a, #, ##, ### $p < 0.05–0.001$) or comparing data points linked by connecting lines (c). Scale bar, 200 μm. *In collaboration with AS Easton.*

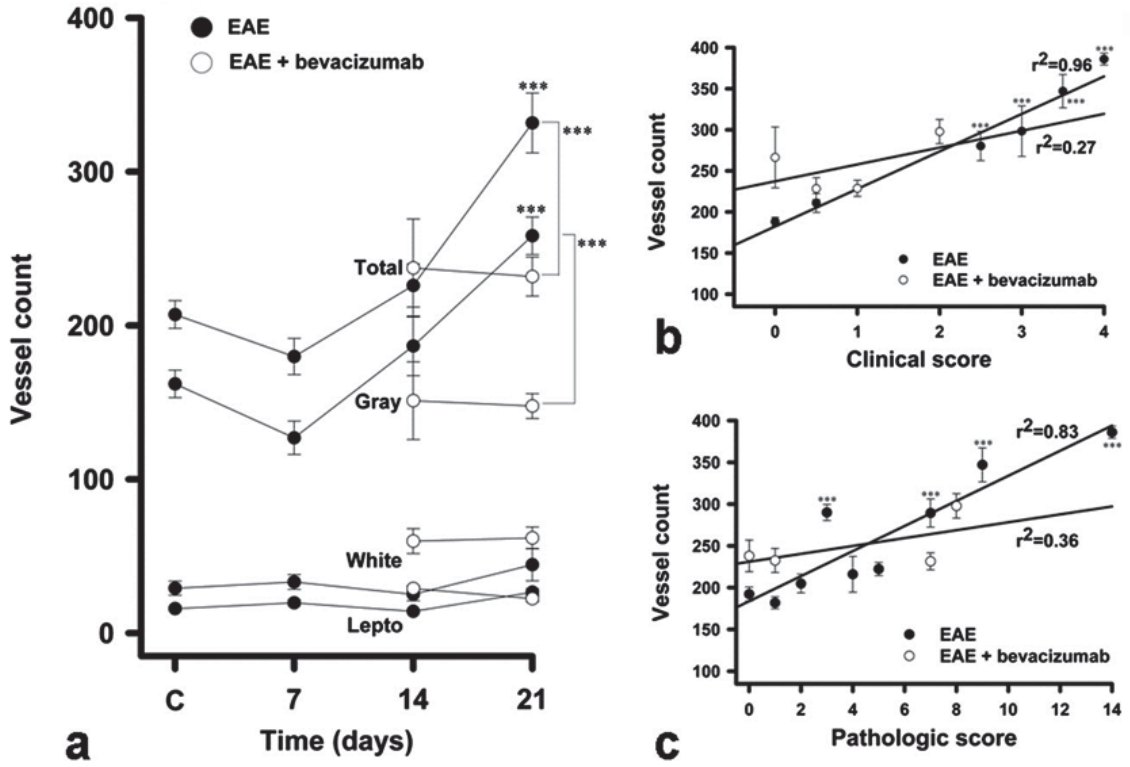

Figure 4.2. Bevacizumab inhibits spinal cord angiogenesis during EAE. a. Vessel counts as a function of days post-immunization. b. Vessel count versus clinical score for individual mice. c. Vessel count versus pathologic score for individual mice (filled circles, EAE; open circles, EAE treated with bevacizumab). Data are shown as mean ± sem. In a., each data point is derived from n = 5–13 mice. In b., n = 4–73 (EAE) and 6–28 (EAE + bevacizumab). In c., n = 4–38 (EAE) and 6–22 (EAE + bevacizumab). Significance (*** $p < 0.001$) is versus control mice without EAE (a) or versus animals with a clinical or pathologic score of 0 (b, c). *In collaboration with AS Easton.*

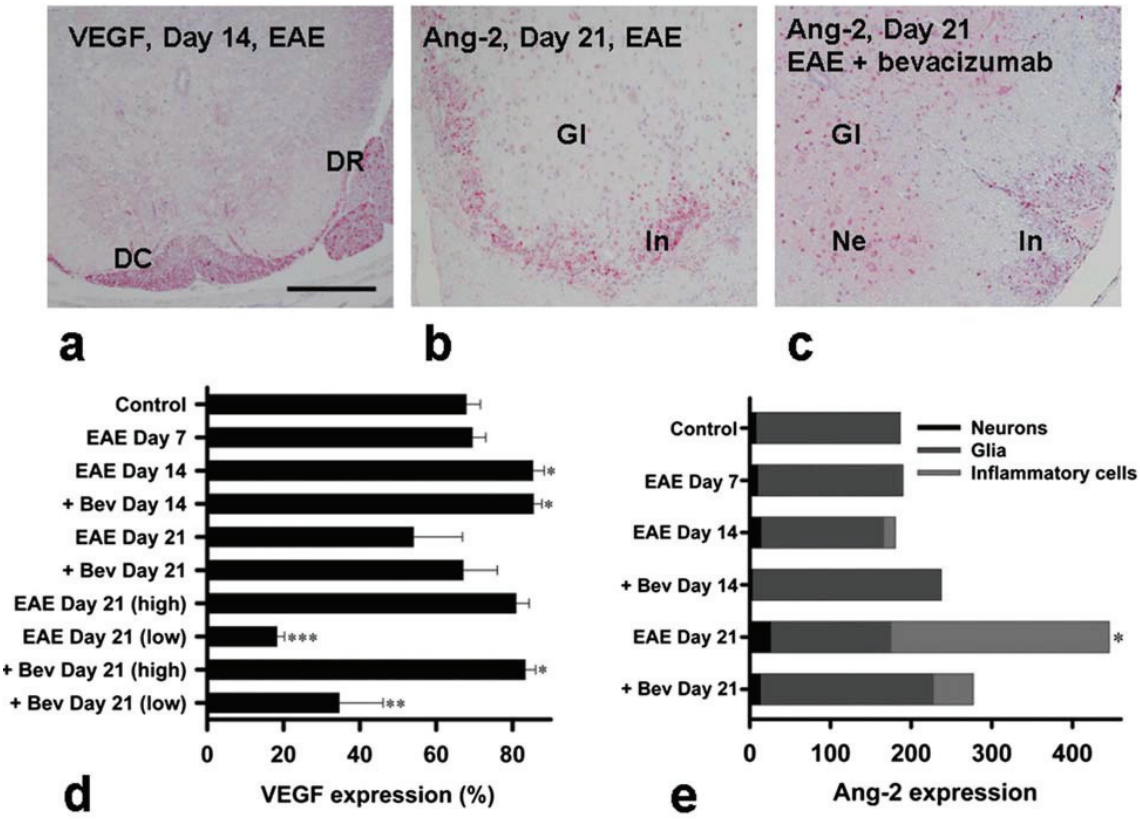

Figure 4.3. Bevacizumab has no effect on VEGF expression during EAE but reduces the expression of Ang-2. a. Staining for VEGF by immunohistochemistry was detected in the dorsal column (DC) and dorsal roots (DR) (EAE, day 21). b., c. Expression of Ang-2 was detected by immunohistochemistry in different types (Ne = neurons; Gl = glial cells; In = inflammatory cells) on day 21 untreated EAE (b) or EAE treated with bevacizumab (c). Scale bars, 100 μm. d. Per mouse data on VEGF expression using the percentage area of positive staining in DC. Control mice were disease free. Mice with EAE alone or treated with bevacizumab (+Bev) are shown at different times. Day 21 data are further subdivided into high and low expression (n = 6 mice in EAE alone, n = 5 on day 21; high-expression group, n = 3 of 5; low, n = 2 of 5; n = 9 mice for +Bev-treated mice, n = 6 of 9 for high-expression group; low, n = 3 of 9). Data are mean ± SEM. Significance versus untreated controls: *, ** $p < 0.05$–0.01). e. Expression of Ang-2 is shown as stacked means of the number of immunopositive cells (subtypes indicated). Significance is versus disease-free controls (* $p < 0.05$).

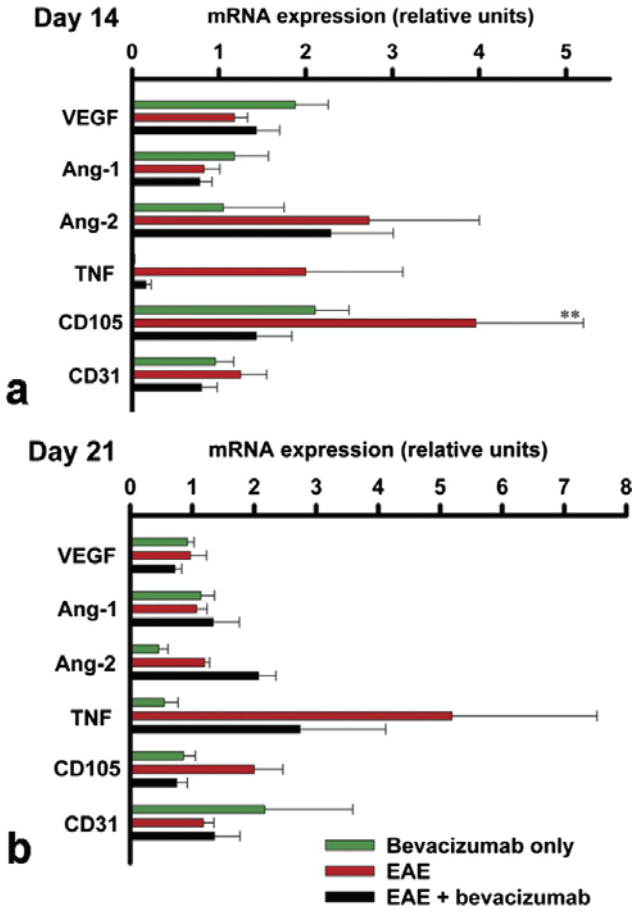

Figure 4.4. Messenger RNA expression in lumbosacral spinal cord on day 14 (a) or day 21 (b), comparing mice with untreated EAE and bevacizumab-treated EAE mice. Disease-free control mice were treated with bevacizumab for the same duration as mice with EAE. Quantitative PCR was used to evaluate mRNA expression for each of VEGF, Ang-2, Ang-1, TNF, CD105, and CD31 normalized to the housekeeping gene GAPDH. Data are expressed relative to mRNA expression in tissue from disease-free untreated controls (relative units). Data are shown as mean ± SEM, n = 8–12 per data point. Significance versus control (** $p < 0.01$). *Data obtained by Dr. P-L Chen.*

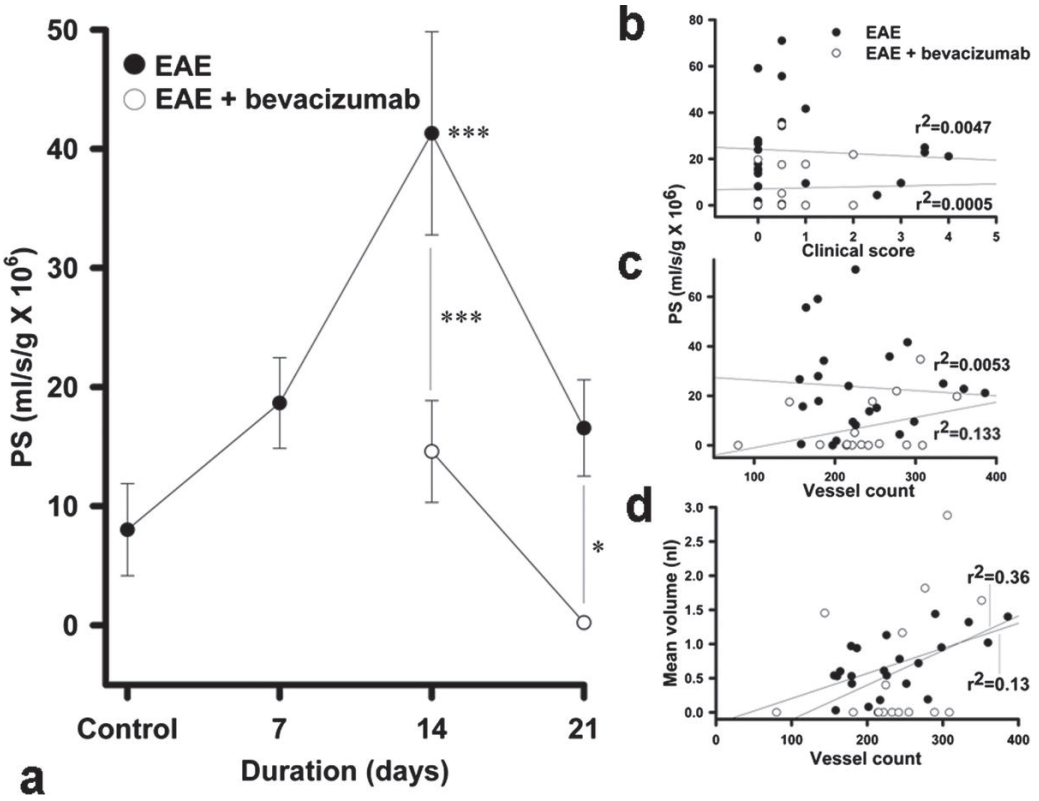

Figure 4.5. Bevacizumab suppresses permeability increases during EAE. a. PS in control mice (without disease, n = 6) and in animals with untreated EAE is shown on day 7 (n = 14), day 14 (n = 6), and day 21 (n = 5, filled circles). Comparative values are shown for EAE treated with bevacizumab on day 14 (n = 8) and day 21 (n = 8, open circles). The PS values per mouse in each group are shown as mean ± SEM; significance versus control or between linked groups (*, **, *** $p < 0.05, 0.001$). b - d. Regression plots for values from individual mice, comparing PS with clinical score (b) or vessel count (c). d. Plot compares the mean volume of tissue showing increased permeability to vessel count. Regression lines through each data set (untreated EAE, filled circles; EAE + bevacizumab, open circles) are shown with the regression coefficient.

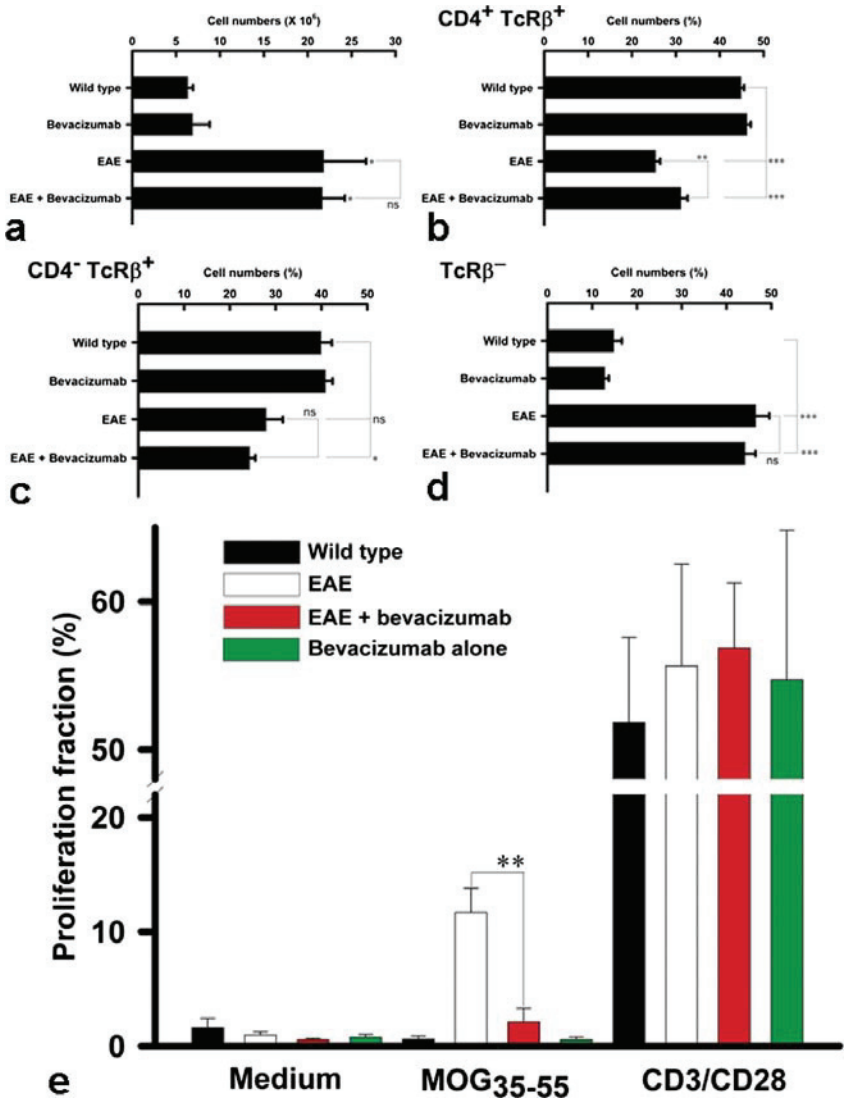

Figure 4.6. Bevacizumab treatment during EAE causes retention of CD4+ T-cells in peripheral lymph nodes. Data are shown as mean ± SEM for wild-type control mice, wild-type mice given bevacizumab, EAE only, and EAE treated with bevacizumab. Significance is versus untreated control without EAE or as indicated by cross bars (ns, not significant; *, **, *** $p < 0.05–0.001$). a. Effect on total numbers of lymph node cells (n = 6–12 for each group; each data point was obtained by pooling lymph nodes from 2 mice). b. Percentage of lymph node cells co-expressing CD4 and TcRβ (n = 7–13). c. Percentage of CD4-negative, TcRβ+ cells (n = 7–15). d. Percentage of cells lacking TcRβ (n = 7–15). e. Proliferation assay *in vitro* for culture medium (negative control), the inciting antigen $MOG_{35–55}$, and costimulation with T-cell expander beads (CD3/CD28). *Data obtained by Dr. SJ Furlong.*

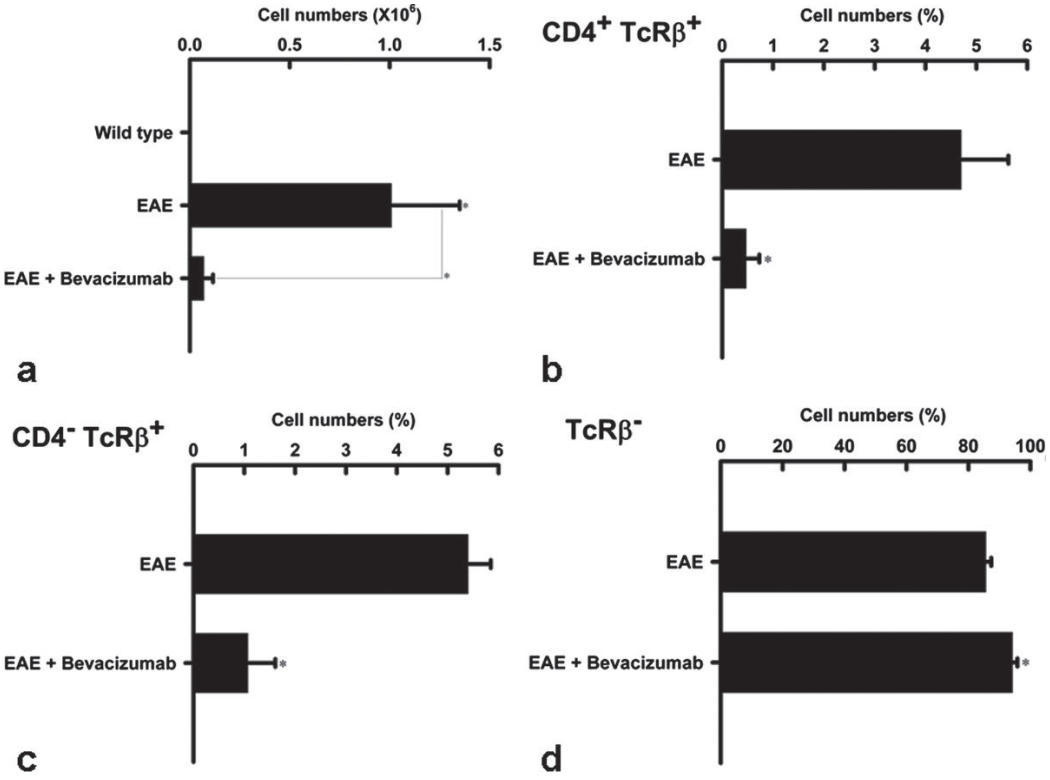

Figure 4.7. Bevacizumab treatment during EAE reduces spinal cord infiltration of T-cells. a. Effect on total number of mononuclear cells isolated from spinal cord at day 21 post disease induction (samples pooled from 2 mice, n = 3 samples for wild type, n = 5 samples for EAE groups). b-d. Proportion of surface marker–defined cell populations in samples from untreated EAE and EAE treated with bevacizumab. CD4 and TcRβ status are indicated in each panel (each sample pooled from 2 mice, n = 3 samples for each data set). Data are shown as mean ± SEM; significance versus wild type (a) or between groups as indicated by cross bars (* $p < 0.05$). *In collaboration with Dr. SJ Furlong.*

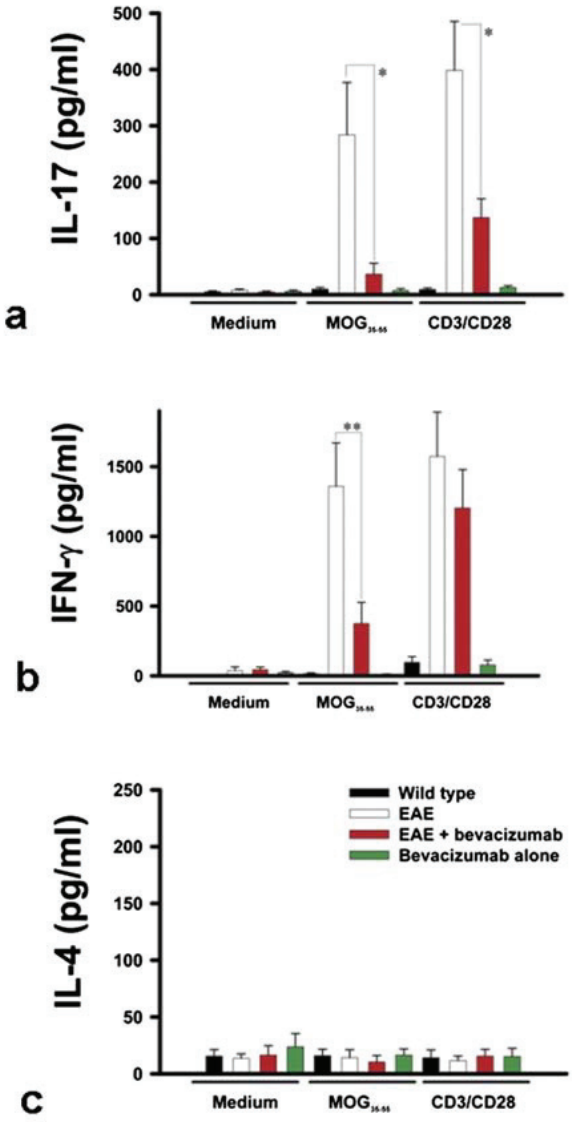

Figure 4.8. Isolated T-cells from mice with EAE that were treated with bevacizumab show reduced IL-17 and IFN-γ release after stimulation with antigen ($MOG_{35–55}$) or T-cell expander beads (CD3/CD28). Supernatants were analyzed by ELISA. The individual bars compare untreated disease-free mice to mice with untreated EAE, EAE treated with bevacizumab, and disease-free mice treated with bevacizumab. Data are shown as mean ± SEM; each sample was pooled from 2 mice, n = 4–12 samples for each bar; significance between groups is indicated by cross bars (*, ** $p < 0.05–0.01$). a. IL-17 release. b. IFN- γ release. c. IL-4 release. *Data obtained by Dr. SJ Furlong.*

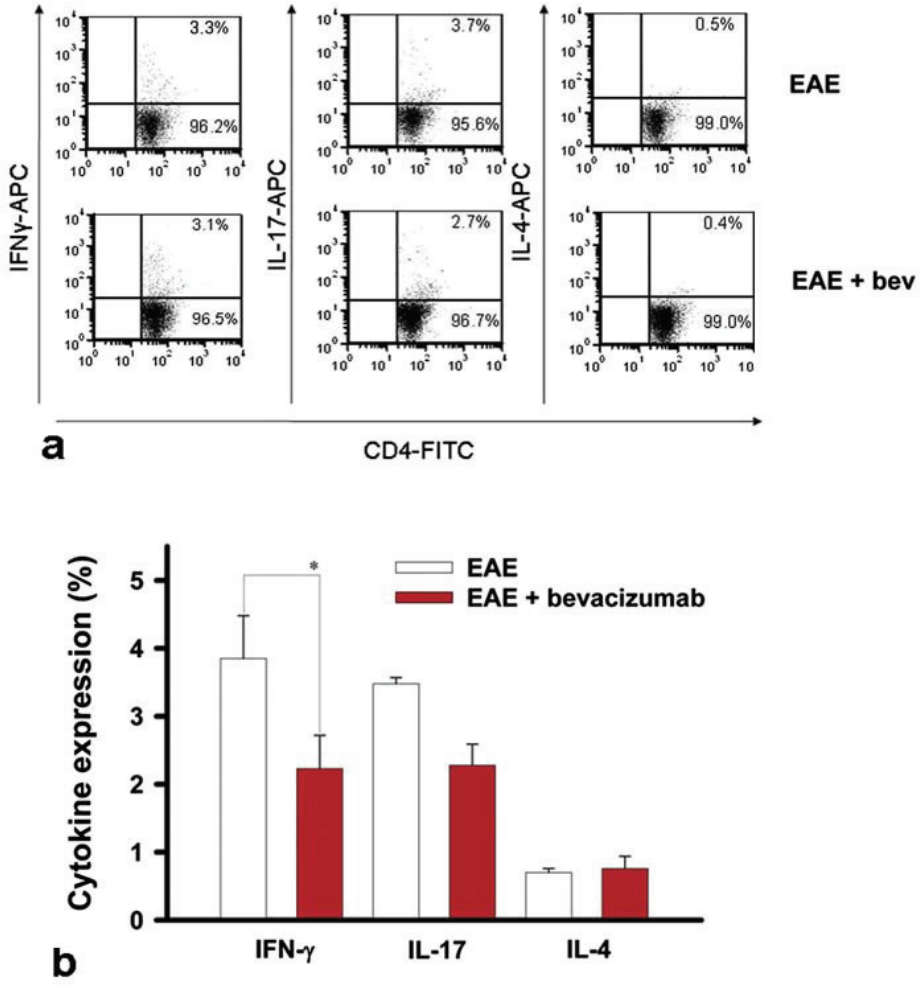

Figure 4.9. Bevacizumab treatment during EAE reduces the proportion of T_h-1 CD4+ cells showing intracellular expression of IFN- γ and results in a non-significant trend to reduced expression of IL-17 by T_h-17 cells following MOG stimulation. a. Representative scatter plots gated to selecT-cells with a high expression of both CD4 and the respective intracellular cytokine defining T_h-1 cells (IFN γ) T_h-17 cells (IL-17), and T_h-2 cells (IL-4). b. Combined data for each intracellular cytokine are as indicated. Data are shown as mean ± SEM; each sample was pooled from 2 mice, n = 4–7 samples for each bar, significance between groups is indicated by cross bars (* $p < 0.05$). *Data obtained by Dr. SJ Furlong.*

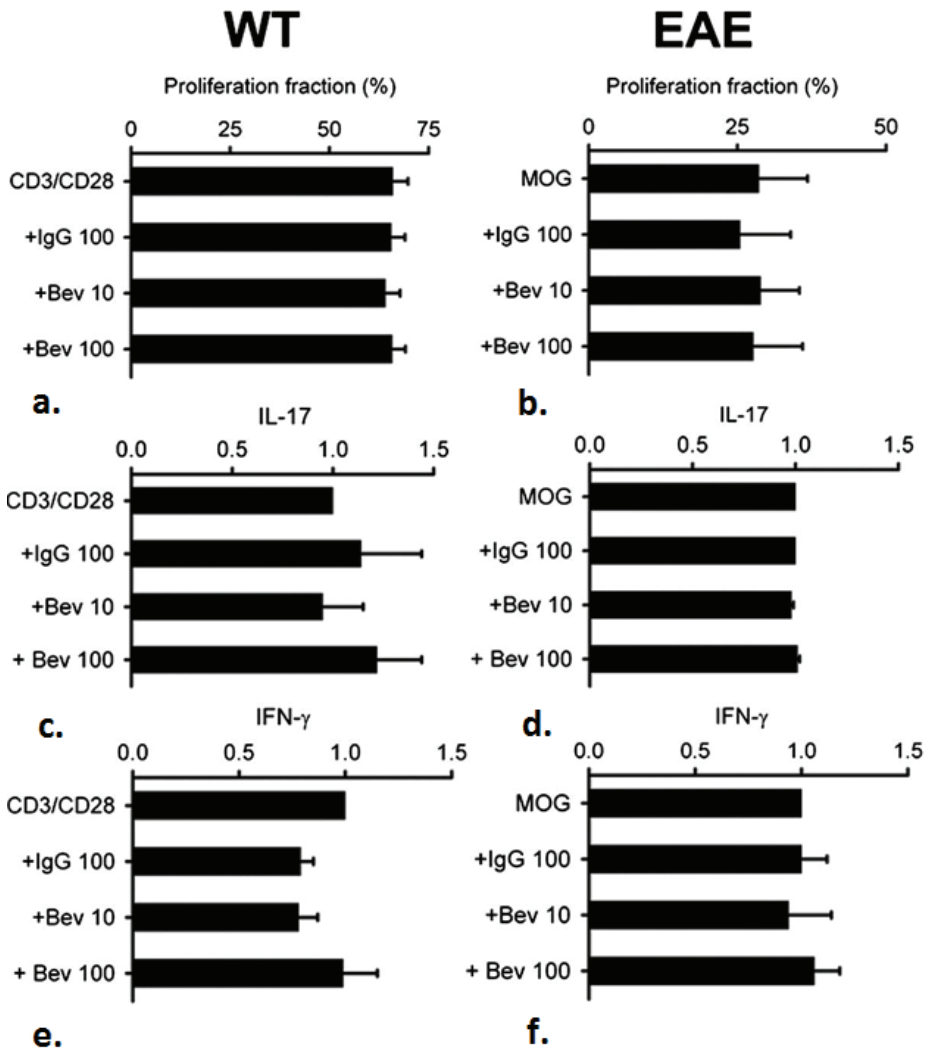

Figure 4.10. Bevacizumab has no effect on proliferation or cytokine secretion by isolated T-cells. a, c, e. Naive CD4+ T-cells stimulated with CD3/CD28-coated microbeads. b, d, f. T-cells from mice with untreated EAE restimulated with antigen ($MOG_{35–55}$) added to BMDCs. Data are normalized to untreated CD3/CD28- or $MOG_{35–55}$-stimulated cells and are shown as mean ± SEM; each data point pooled from 2 mice; n = 4 for a, c, e.; 2 for b, d, f. Key is: Bev = bevacizumab; IgG = immunoglobulin G. *Data obtained by Dr. SJ Furlong.*

CHAPTER 5: EAE IS REDUCED BY TREATMENT WITH DIRECT AND INDIRECT INHIBITORS OF ANGIOGENESIS

Contributions: Disease induction, monitoring, and tissue isolations in all figures of this chapter were completed by CJ MacMillan. Figures 5.1, 5.2 and 5.4 were completed by CJ MacMillan. Figure 5.3 was done in collaboration with AS Easton. Figures 5.5, 5.6 and 5.7 were completed by CD Doucette.

5.1 Summary

Angiogenesis may represent a therapeutic target in EAE, as suggested in chapter 4 where bevacizumab was shown to suppress angiogenesis and result in reduced clinical and pathologic scores. However, there remains a controversy over the target of bevacizumab, since it may not be able to bind with sufficient avidity to murine VEGF. Therefore we explored the impact of additional inhibitors of angiogenesis on EAE. First, we used B20-4.1.1, a monoclonal antibody that binds with high affinity to murine VEGF. Secondly, we used angiostatin, which targets angiogenesis by a different mechanism of action, i.e. by directly inhibiting endothelial vascular processes such as proliferation that result in angiogenesis. Mice treated with B20-4.1.1 and angiostatin beginning at clinical presentation of EAE showed a delayed reduction in clinical scores during the phase of peak disease (days 19-21). Both agents suppressed angiogenesis in the spinal cord at day 21, but had no effect on the normal increase in VEGF expression seen at day 14 in the course of EAE. B20-4.1.1 reduced vascular permeability in the spinal cord while angiostatin had no effect. In peripheral lymph nodes, B20-4.1.1 tended to induce retention of CD4+ T-cells, and inhibited T-cell proliferation, while angiostatin had no effect. Isolated lymphoid cells from mice treated with both agents showed reduced secretion of the T_h-17 cytokine IL-17 with no effect on the T_h-1 cytokine IFN- γ, or T_h-2 cytokine IL-4. However, when both drugs were added *in vitro* to naive T-cells or to antigen stimulated T-cells from mice with untreated EAE they had no effect on proliferation or secretion of IL-17 or IFN-γ. We conclude that these angiogenesis inhibitors are effective during peak disease in EAE and act by suppressing angiogenesis

with a secondary effect on peripheral T-cell activation. This data compliments that described in chapter 4 for the effects of bevacizumab.

5.2 Introduction

During inflammatory diseases of the CNS a number of adaptive responses occur, some of which are related to the processes described in wound healing. As previous described, angiogenesis is among these responses. We have demonstrated that there is a significant role for VEGF in angiogenesis that occurs during EAE, and that it acts in concert with other mediators including Ang-1 and Ang-2 [154]. VEGF is regarded as a key orchestrator of angiogenesis in inflammatory settings. In light of this, strategies to inhibit its actions may hold promise for the treatment of diseases with a significant inflammatory component, such as MS.

EAE serves as a useful model for studying the impact of therapeutics on the inflammatory component of MS. With increasing confidence that angiogenesis occurs in both MS and EAE, and evidence that angiogenesis coincides with peak disease during EAE, there is a rationale for robust studies investigating the therapeutic potential of angiogenesis inhibitors. Angiogenesis can be inhibited by binding key mediators such as VEGF, or by using drugs that directly target the vasculature to inhibit angiogenesis. Drugs that bind key factors have been described as indirect inhibitors of angiogenesis, while those that target endothelial cells are classed as direct inhibitors of angiogenesis [183]. VEGF itself has been targeted in previous studies of EAE including our own [173]. In one study, angiogenesis was inhibited when mice were treated with the VEGFR-2 antagonist SU5416 and mice responded with a significant improvement in disease scores. In chapter 4 we describe the impact of bevacizumab on EAE in mice [173]. Bevacizumab binds with

high affinity to human VEGF; however, its ability to bind to murine VEGF is more controversial. Despite this uncertainty over its precise target, bevacizumab produced a significant reduction in clinical and pathologic scores in EAE, as well as the complete arrest of angiogenesis in the spinal cord. Bevacizumab also resulted in a reduction in peripheral T-cell responses linked to the development of EAE at both the T_h-1 and T_h-17 levels.

Because of the uncertainty about the ability of bevacizumab to bind to murine VEGF, this study examined the impact of B20-4.1.1, a monoclonal antibody that binds with high affinity to both murine and human VEGF. We also explored inhibition of angiogenesis in EAE through an additional theurapeutic agent (angiostatin) that directly targets the vasculature. Angiostatin is formed from the kringle domains of plasminogen and has been shown to inhibit angiogenesis in a variety of contexts through direct targeting of vascular endothelial cells. We describe the effect of these drugs on clinical and pathologic scores during EAE, downstream effects on angiogenesis, permeability and VEGF expression in the spinal cord, and their impact on peripheral T-cell responses. This work is in the final stages of preparation to be submitted for publication.

5.3 Results

5.3.1 B20-4.1.1 and Angiostatin Reduce Clinical Scores in EAE

B20-4.1.1 treatments were given to mice on the day of clinical presentation (around day 9) and administered every 3 days until sacrifice. Angiostatin was administered daily beginning on the day of clinical presentation. Fig. 5.1 A shows the effect of B20-4.1.1 on clinical scores. In contrast to the rapid onset of action seen with

bevacizumab treatment, a reduction in clinical scores (compared to untreated EAE mice) only became apparent at approximately day 16 in B20-4.1.1 treated mice, with the most significant reduction occurring between days 18-21 ($p< 0.001$). This period was associated with peak clinical scores during untreated EAE with means between 2.85 ± 0.27 and 2.85 ± 0.27 (n = 12 mice). The effect of B20-4.1.1 could not be attributed to non-specific effects of infusing immunoglobulin, as IgG had no effect (Fig. 5.1 B). B20-4.1.1 treatment resulted in significant reductions in clinical score compared to EAE alone between days 18-21 ($p< 0.001$); however, the effect was not as profound as bevacizumab (Fig. 5.1 C). Scores were significantly lower in bevacizumab-treated mice by comparison to B20-4.1.1-treated mice at days 15-17, 19 and 20 ($p< 0.05$-0.001).

Angiostatin treatment was also started around day 9 shortly after symptom onset during EAE. Like B20-4.1.1 it resulted in a delayed reduction in clinical scores compared to matched animals with untreated EAE (Fig. 5.1 D). Like B20-4.1.1 the clinical scores began to reduce at day 16 with significant reductions between days 18-21 ($p< 0.05$-0.001). Once again, this coincided with peak disease scores during untreated EAE with means between 2.85 ± 0.27 and 2.85 ± 0.27 (n = 16 mice). Disease-free mice treated with either B20-4.1.1 (n = 6 mice) or angiostatin (n = 6 mice) showed no increase in clinical scores.

5.3.2 B20-4.1.1 and Angiostatin Suppress Spinal Cord Angiogenesis

Angiogenesis was assessed from blood vessel counts in sections stained for the endothelial marker CD31. Separate counts were performed in the leptomeninges, white matter and gray matter, and then added to give a total count. In mice with untreated EAE, there was a significant increase in vessel count at day 21 for total count as well as

counts in gray matter ($p < 0.001$), with no increase in white matter or leptomeninges (Fig. 5.2 A, filled circles). By contrast, mice treated with B20-4.1.1 during EAE did not show an increase in vessel counts at day 21 (open circles, Fig. 5.2 A). In the angiostatin group, at day 14 there was a transient increase in vessel counts of the white matter (Fig. 5.2 B, open circles). The total and gray matter counts in both groups were not significantly increased over controls at day 21, and significantly lower than counts in mice with untreated EAE ($p < 0.001$).

5.3.3 Reduction in EAE Severity Can Not Be Attributed to Altered VEGF Expression Following B20-4.1.1 or Angiostatin Treatment During EAE

VEGF was only expressed in neurons and axons in the lumbosacral spinal cord of mice with EAE, with predominant expression in the dorsal columns. To quantify VEGF expression, we calculated the % area containing positively stained axons within the dorsal columns. The data show a significant increase in expression compared to untreated controls at day 14. This is similar when EAE was untreated or treated with B20-4.1.1 (Fig. 5.3 A) or Angiostatin (Fig. 5.3 B). Mice with untreated EAE and each of the treatment groups showed a decline in VEGF expression at day 21; however, VEGF expression remained elevated in a subset of the mice, while others showed significant reductions below control levels. The pattern of VEGF expression during EAE showed no significant differences when mice were treated with either agent.

5.3.4 Vascular Permeability is Reduced by B20-4.1.1 But Not By Angiostatin Treatment

Permeability-surface area (PS) values were calculated from permeability maps of the spinal cord in mice with EAE, either untreated or treated with B20-4.1.1 or angiostatin. PS values during untreated EAE were assessed at day 14 and day 21 in order

to draw comparisons to drug treated mice (Fig. 5.4). PS values were similar at day 14 and 21 in untreated mice with EAE, and significantly greater than disease free controls. B20-4.1.1 treated mice showed a significant reduction in PS at day 21 compared to untreated EAE ($p < 0.001$) but no reduction was apparent at day 14. Angiostatin treatment had no effect on PS either at day 14 or day 21 (Fig. 5.4).

5.3.5 B20-4.1.1 Reduces Proliferation in Peripheral $CD4^+$ T-cells, However this Phenomenon is Not Apparent with Angiostatin Treatment

To assess the effect of B20-4.1.1 and angiostatin on peripheral immune responses, lymph nodes were harvested from EAE animals at day 21 to coincide with peak disease scores. We used flow cytometry to assess the proportions of different cell types based on surface markers. During EAE, there was a significant reduction ($p < 0.05$) in the proportion of $CD4^+$ $TcR\beta^+$ cells in the lymph nodes compared to disease-free (wild type) controls, consistent with a significant egress towards the CNS. However, there was no significant reduction in mice treated with either inhibitor. The mean % is closer to the disease free control in the B20-4.1.1 treated group consistent with retention of $CD4^+$ $TcR\beta^+$ cells in the lymph nodes (Fig. 5.5 A). Compared to wild type controls, all groups of mice with EAE (untreated or treated) showed a significant reduction ($p < 0.001$) in the proportion of non-$CD4^+$ T-cells ($CD4^-$ $TcR\beta^+$, Fig. 5.5 B) and all EAE groups showed significant compensatory increases ($p < 0.01$-0.001) in the proportion of non-T-cells ($TcR\beta^-$, Fig. 5.5 C).

Lymph node cells were then isolated and stimulated to determine their proliferative response. In order to estimate T-cell responses, cells from mice with EAE were stimulated with MOG_{35-55} or CD3/CD28 coated microbeads. Oregon Green labeled CD4+ T-cells showed increased proliferation over controls when exposed to the inciting

antigen (MOG_{35-55}), that was significantly blunted ($p < 0.001$) in mice treated with B20-4.1.1. However, proliferation was unaffected by B20-4.1.1 when mice were co-treated with angiostatin, or treated with angiostatin alone. Lymphocytes from all groups responded to stimulation with CD3/CD28 coated microbeads, but no differences were detected between the groups (Fig. 5.5 D).

5.3.6 B20-4.1.1 and Angiostatin Both Inhibit T_h-17 Cytokines

Lymph node cells were isolated and stimulated *in vitro* with MOG_{35-55} or CD3/CD28 coated microbeads, and supernatants collected to measure cytokines characteristic of T_h-17 cells (IL-17), T_h-1 cells (IFN-γ) and T_h-2 cells (IL-4). Treatment with B20-4.1.1 or with angiostatin during EAE resulted in a reduced secretion of IL-17 ($p < 0.05$ for angiostatin, $p < 0.01$ for B20-4.1.1, Fig. 5.6 A) while IFN-γ and IL-4 secretion was unaffected (Fig. 5.6 B, C). There was a trend to a reduction in IFN-γ secretion in animals treated with B20-4.1.1 that did not reach statistical significance (Fig. 5.6 B). Statistically significant reductions were not found in cells treated with CD3/CD28 coated microbeads (Fig. 5.6).

To assess direct effects of these agents on T-cell responses, additional experiments were carried out with T-cells isolated from wild type mice and mice with untreated EAE, and neither was exposed to either agent *in vivo*. The former were stimulated with CD3/CD28 coated microbeads, while the latter were restimulated with MOG_{35-55} added to BMDC. Cells were assessed for proliferation fraction or secretion of IL-17 and IFN-γ. Addition of B20-4.1.1 (10, 100μg/ml) or angiostatin (5 μg/ml) to the cultures had no effect on proliferation fraction or the secretion of IL-17 and IFN-γ (Fig. 5.7).

5.4 Discussion

Both B20-4.11 and angiostatin reduce clinical scores in EAE. The effect for both inhibitors only became significant at the time that angiogenesis occurs in this particular model of EAE, between days 18-21 after induction (Fig. 5.1). As expected, both inhibitors suppressed angiogenesis in the spinal cord of mice with EAE, assessed from blood vessel counts in spinal cord cross sections at day 21 (Fig. 5.2). Since angiogenesis is vascular in origin, we also explored the impact of the agents on permeability in the spinal cord. Although angiogenesis was suppressed by both agents, only B20-4.1.1 reduced permeability at day 21 while angiostatin had no effect (Fig. 5.3). This strongly implicated VEGF in the changes in permeability seen during EAE.

VEGF is expressed by axons in the dorsal columns of the spinal cord, up regulated at day 14 before angiogenesis occurs, and down regulated in a proportion of cases at day 21 when angiogenesis is established. This process, which we reported previously [154], was unaffected by treating the mice with either B20-4.1.1 or angiostatin (Fig. 5.4). Our previous work also suggested that VEGF blockade results in a reduction in peripheral T-cell responses during EAE. To investigate this in the context of these newly tested agents, we measured the impact of treatment on peripheral lymph node cells. We found a suggestion that B20-4.1.1 in particular leads to retention of $CD4^+$ T-cells in peripheral lymph nodes (Fig. 5.5 A). This agent also resulted in reduced T-cell proliferation in cells subsequently restimulated with the inciting antigen MOG_{35-55} (Fig. 5.5 D). *In vivo* treatment with both B20-4.1.1 and angiostatin reduced the release of the proinflammatory T_h17 cytokine, IL-17, from peripheral lymph node cells stimulated *ex vivo* with MOG_{35-55} but not anti-CD3/CD28 coated microbeads, implicating reduced

activation of MOG specific T_h17 cell clones (Fig 5.6). However, *ex vivo* treatment of $CD3^+$ T-cells taken from mice with EAE that were not exposed to the drugs *in vivo* showed that neither B20-4.1.1 nor angiostatin affect IL-17 or IFN-γ release, or proliferation in response to MOG_{35-55}. Similar results were obtained in T-cells from naive mice restimulated with anti-CD3/CD28 coated microbeads (Fig. 5.7). This data shows that both drugs only affect peripheral immune function in the context of suppressed angiogenesis, and in the context of the work described in chapter 4 as well as this chapter, strongly implicate angiogenesis in peripheral immune activation during EAE, since effects on T-cell function only occur in the whole animal and not *ex vivo*.

5.4.1 Impact of B20-4.1.1 and Angiostatin During EAE

We report for the first time a study on the effects of the two angiogenesis inhibitors B20-4.1.1 and angiostatin in EAE. B20-4.1.1 belongs to the group of indirect angiogenesis inhibitors that inhibit angiogenesis through binding to exogenous pro-angiogenic factors. In this case, it acts by binding the pathogenic isoform (164 amino acids in mice, 165 in humans) of VEGF. Angiostatin is representative of direct angiogenesis inhibitors that function through multiple direct effects on vascular endothelial cells to inhibit new blood vessel formation. If angiogenesis is inhibited by different classes of inhibitor with similar effects on disease, then this adds to mounting evidence for a pathogenic role for angiogenesis during EAE and by extension, perhaps to the inflammatory phase of MS.

Previous studies have explored the role of VEGF in EAE. VEGF expression has been reported in EAE, and was found to increase before the onset of angiogenesis in some studies. In chapter 4, we describe the effects of bevacizumab in EAE, showing that

bevacizumab induces a rapid stabilization in clinical scores early after the onset of treatment [173]. Bevacizumab also reduces peripheral T-cell proliferation, release of IL-17 and IFN-γ and, like the agents reported here, does not affect T-cell responses in isolation. The use of B20-4.1.1 lays to rest the suggestion that direct binding to VEGF cannot reduce angiogenesis in EAE and have an impact on disease parameters. Bevacizumab was specifically engineered to bind with far greater affinity to the 165 amino acid isoform of human VEGF, and although effective in several animal models, may not bind animal isoforms of VEGF with enough avidity to explain its effects during murine EAE. By using B20-4.1.1 we can affirm that direct binding to the 164 amino acid murine isoform of VEGF is effective in suppressing angiogenesis and impacting the disease.

However, bevacizumab and B20-4.1.1 did not have identical effects in murine EAE. Bevacizumab had an earlier impact on clinical scores, reaching significance 13 days after disease onset. By contrast, B20-4.1.1 was only effective from day 18. This 5 day gap suggests that the effect of B20-4.1.1 on clinical scores closely parallels its inhibitory action on angiogenesis, and allows the contribution of angiogenesis on disease scores to be assessed with greater accuracy. Bevacizumab also had a more profound effect on permeability (reducing permeability at day 14 and day 21 while B20-4.1.1 was ineffective at day 14) and on peripheral T-cell responses (where bevacizumab also reduced pro-inflammatory IFN-γ secretion). The data suggest that bevacizumab may act through targets additional to VEGF in murine EAE, since it reduced clinical scores before angiogenesis occurs.

In contrast to indirect inhibition of angiogenesis through VEGF blockade, we are the first to explore the effect of direct angiogenesis inhibitors on EAE. Angiostatin is a

prototype of these inhibitors that derives from the first four kringle domains of circulating plasminogen. Kringle domains in plasminogen are loop structures containing approximately 80 amino acids. Angiostatin has been shown to inhibit angiogenesis by direct targeting of vascular endothelial cells, although the precise mechanism varies depending on the study. Mechanisms include binding to putative endothelial receptors (ATPase, angiomoietin [184-186]), cell cycle arrest at the G2/M transition [187] and induction of endothelial apoptosis [188-190]. Previous studies have reported that angiostatin reduces angiogenesis in models of cancer-related angiogenesis [191]. In our hands, angiostatin also reduced peripheral T-cell activation, since antigen stimulated lymph node cells from mice treated with angiostatin during EAE released lower levels of the T_h17 cytokine IL-17 (Fig. 5.6). However, compared to B20-4.1.1 it had no effect on MOG specific T-cell proliferation (Fig 5.5 D).

The lack of impact of both agents on the activation of isolated T-cells (Fig. 5.7) is further evidence that these agents reduce peripheral T-cell responses by suppressing spinal cord angiogenesis, since this is the effect they have in common. How angiogenesis affects peripheral T-cell responses is speculative, but one possibility is that new blood vessels allow increased trafficking of APCs from the CNS to peripheral lymph nodes. This may simply be a field effect as the result of enhanced vascular surface area, so that more cells transmigrate between CNS and blood. Another possibility is that CNS antigens are transported directly along perivascular spaces to peripheral lymphatics, and that antigen delivery is enhanced by a greater density of blood vessels.

The different impact of these agents on permeability is also of interest. Permeability is generally modulated at the level of postcapillary venules in the CNS.

VEGF has multiple effects apart from being pro-angiogenic, and is known to cause increases in vascular permeability in the CNS. It is therefore not surprising that permeability is reduced when VEGF is blocked with B20-4.1.1 (and bevacizumab). The lack of effect of angiostatin on permeability is also not surprising if one considers that angiogenesis mostly increases the number of capillaries rather than postcapillary venules in the CNS, and so is likely to have little impact on permeability. This suggests that the impact both of bevacizumab and B20-4.1.1 on permeability is unrelated to the suppression of angiogenesis, but the direct result of reducing the binding of VEGF to postcapillary venules.

Finally, angiostatin may also have clinical advantages over VEGF blocking agents. Long term blockade of VEGF reduces downstream levels of NO leading to cardiovascular complications such as hypertension, among other side effects that have been reported [192]. However angiostatin appears to be relatively well tolerated when administered in clinical trials, perhaps because it acts principally by targeting activated vascular endothelial cells. The current arsenal of agents in use during MS act by general suppression of peripheral T-cell responses or by preventing all T-cells from entering the CNS. A side effect of treatment includes general immune suppression. Perhaps angiogenesis inhibitors such as angiostatin that are well tolerated would result in reduced stimulation of antigen specific clones in peripheral lymph nodes, without the unwanted effects produced by general immune suppression. This implies that the suppression of angiogenesis during MS has a direct effect on peripheral immune activation perhaps, as previously mentioned, because new blood vessels serve as conduits for antigen delivery from the CNS to the periphery.

5.4.2 Conclusion

This study demonstrates that EAE can be effectively treated with both a direct and an indirect inhibitor of angiogenesis. Clinical scores reduce in parallel to the suppression of angiogenesis by both agents in the spinal cord. This shared effect from two agents with different mechanisms of action (VEGF binding by B20-4.1.1 and vascular endothelial inhibition by angiostatin) is likely to produce secondary effects on peripheral immune activation. Both agents affected aspects of peripheral T-cell activation such as T_h17 cytokine expression however neither agent affected these responses when applied to T-cells in isolation, indicating a possible line between the suppression of angiogenesis and reduced T-cell responses *in vivo*.

This study adds to the evidence that angiogenesis plays a pathogenic role in EAE and by extension MS. Angiogenesis inhibitors like angiostatin with minimal side effects (in contrast to bevacizumab, the drug most closely related to B20-4.1.1) may represent a novel therapeutic option for the more effective treatment of MS, since immune responses against CNS antigens may be targeted through the suppression of angiogenesis without general immune suppression.

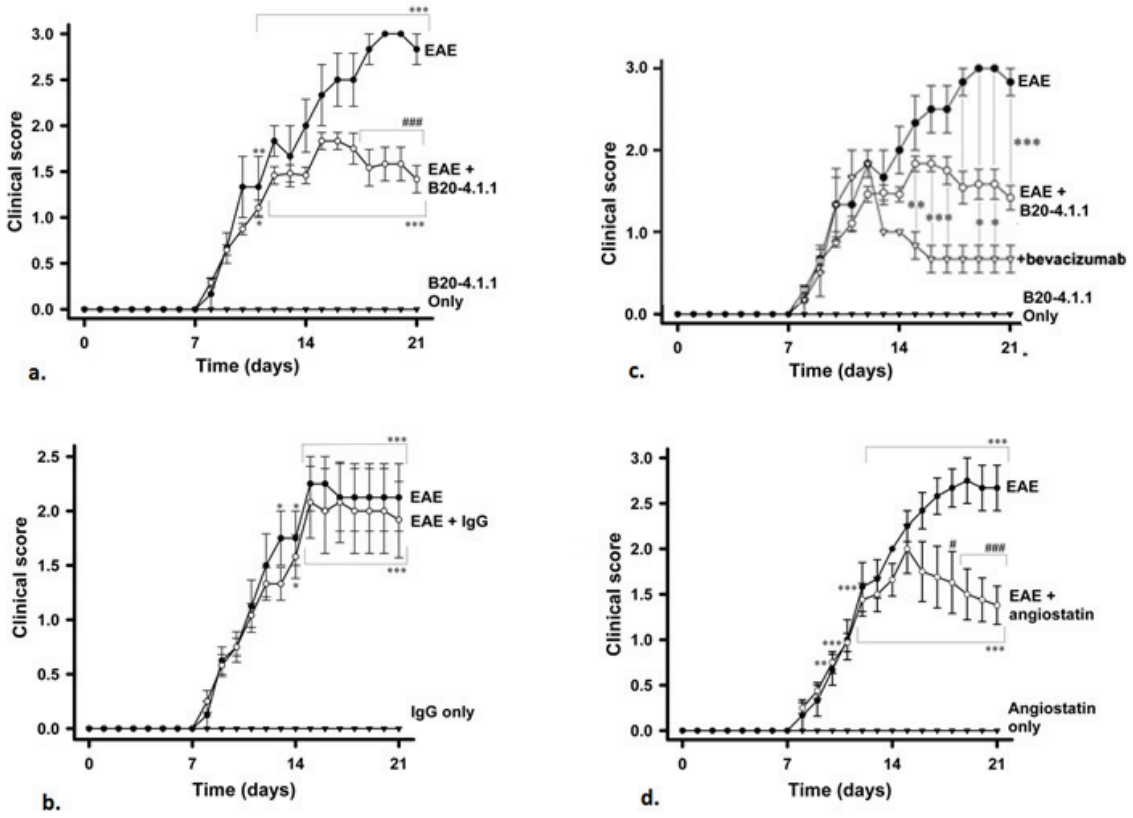

Figure 5.1. B20-4.1.1 and angiostatin reduces clinical scores in EAE. a. Clinical score data for treatment of EAE with B20-4.1.1. b. Treatment with IgG. c. Effect of treatment with B20-4.1.1 as compared to bevacizumab treatment. d. Treatment with angiostatin. Data are shown as mean ± SEM. Indicated significance (*-***, p <0.05-0.001) is relative to control, except when comparing treatment effects during EAE (#-###, p <0.05-0.001).

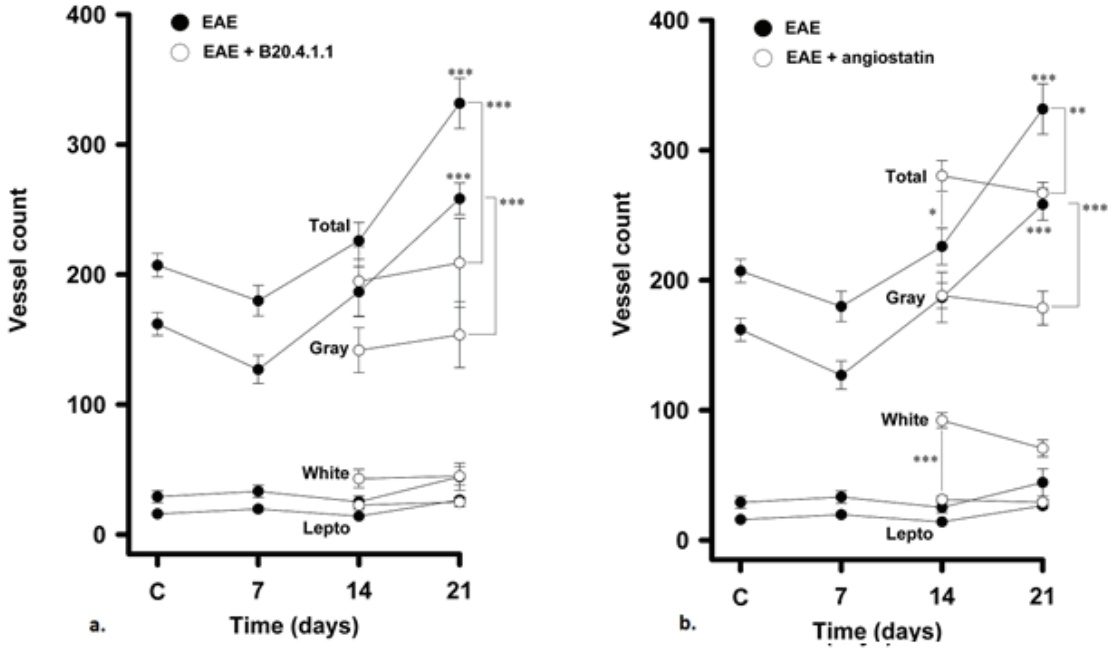

Figure 5.2. B20-4.1.1 and angiostatin inhibit spinal cord angiogenesis during EAE. a. Vessel counts as a function of disease duration following B20-4.1.1 treatment (filled circles, EAE; open circles, EAE treated with B20-4.1.1). b. Vessel counts as a function of disease duration following angiostatin treatment (filled circles, EAE; open circles, EAE treated with angiostatin). Data are shown as mean ± SEM. In a, each data point is derived from n = 5 - 16 mice. *In collaboration with AS Easton.*

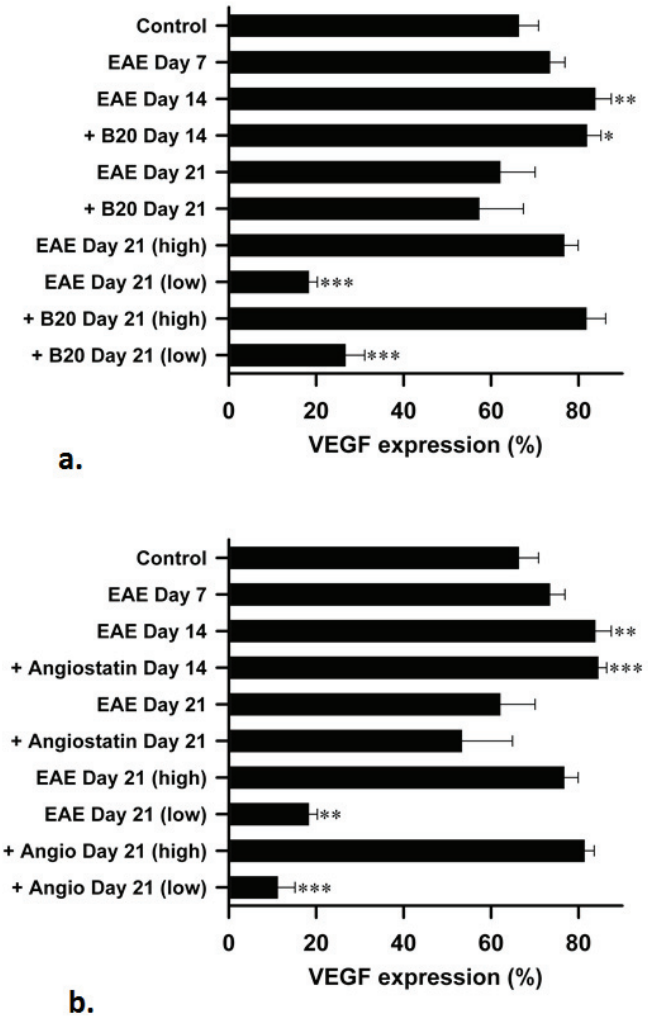

Figure 5.3. B20-4.1.1 and angiostatin have no effect on VEGF expression during EAE. a,b. Per mouse data on VEGF expression, using the % area of positive staining in the dorsal columns. Control mice were disease-free. EAE alone is compared to mice treated during EAE with B20-4.1.1 (a) or angiostatin (b). Day 21 data is further subdivided into high and low expression (n = 6 mice in EAE alone, n = 5 at day 21, high expression group n = 3/5, low n = 2/5; n = 9 mice for B20-4.1.1 treated mice, n = 6/9 for high expression group, low n = 3/9; n = 10 mice for angiostatin treated mice, n = 6/10 for high expression group, low n = 4/10; data is mean ± SEM, significance relative to untreated controls (*-**, p <0.05-0.01). *In collaboration with AS Easton.*

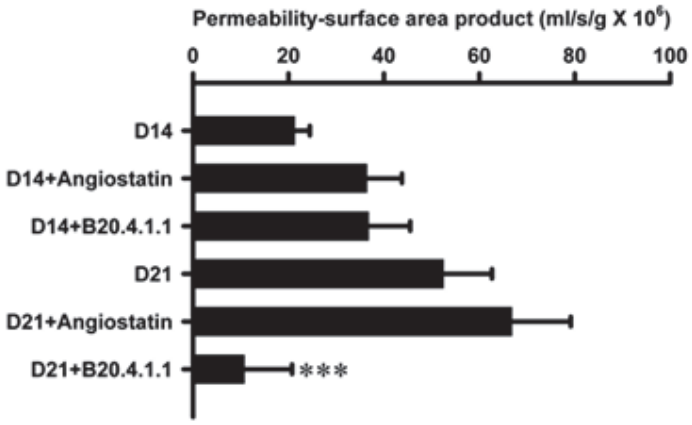

Figure 5.4. B20-4.1.1 but not angiostatin reduces permeability-surface area product (PS) values during EAE. PS values at day 14 and 21 are shown for EAE, EAE + B20-4.1.1 and EAE + angiostatin. PS values per mouse in each group; data are shown as mean ± SEM, significance compares EAE with each treatment (***; $p < 0.001$).

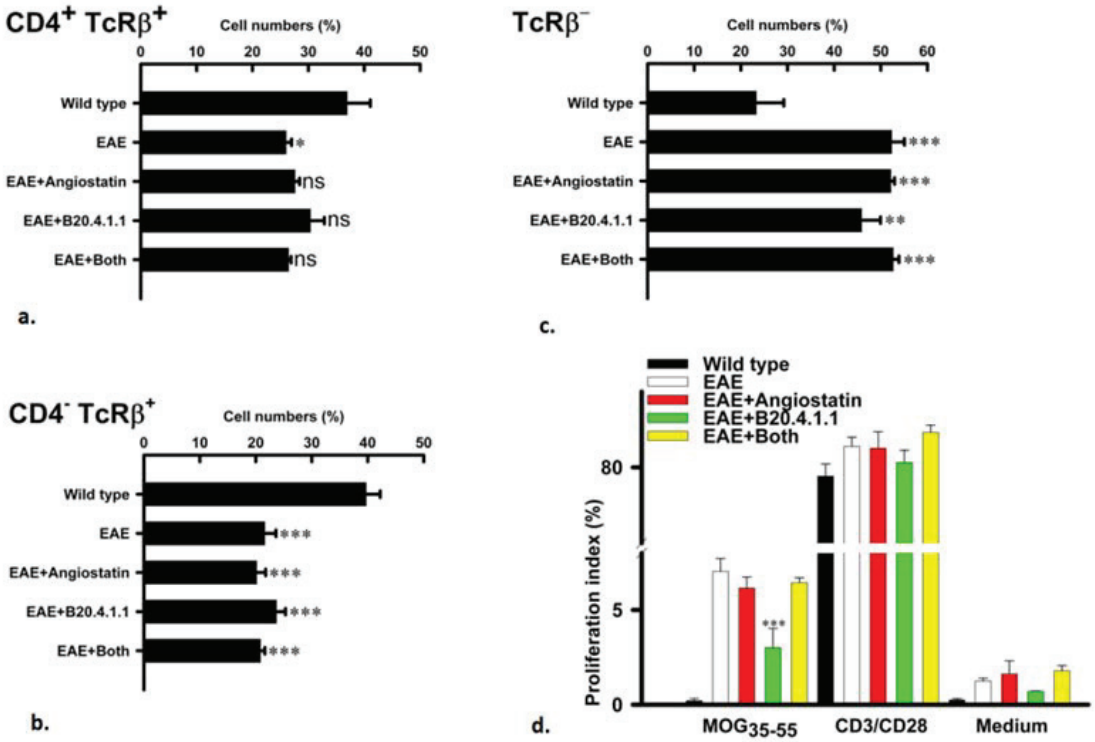

Figure 5.5. B20-4.1.1 treatment during EAE reduces proliferation in peripheral lymph node cells and tends to mitigate a reduction in $CD4^+$ T-cells in peripheral lymph nodes. Data are shown as mean ± SEM for wild type controls, untreated EAE, EAE + B20-4.1.1, EAE + angiostatin and EAE + agents combined. Significance is relative to untreated EAE (ns = not significant, ***, p <0.05-0.001). a. % of lymph node cells co-expressing CD4 and TcRβ (n = 7-13). b. % $CD4^-TcR\beta^+$ cells (n = 7-15). c. % cells lacking TcRβ (n = 7-15). d. Proliferation assay in vitro for culture medium (negative control), the inciting antigen (MOG_{35-55}) and co-stimulation with T-cell expander beads (CD3/CD28). *Data obtained by Dr. CD Doucette.*

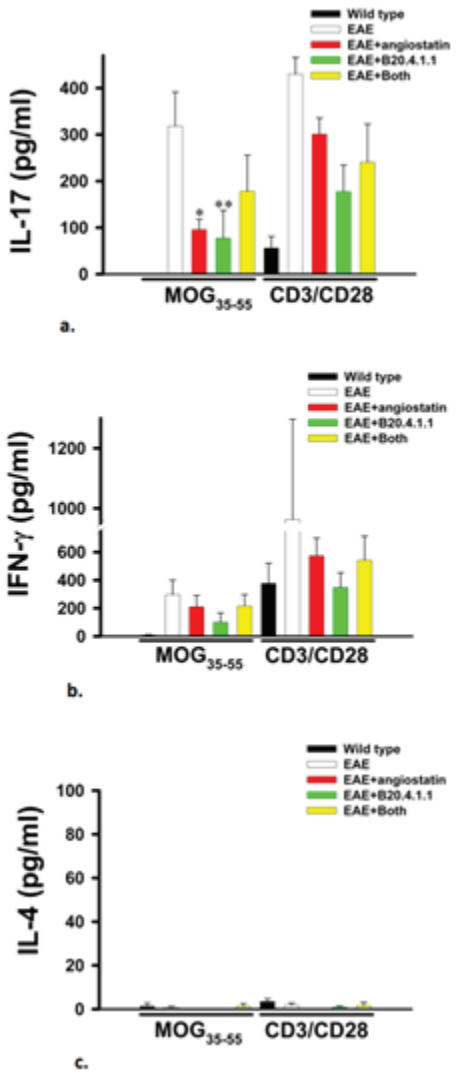

Figure 5.6. Isolated lymph node cells in EAE mice treated with B20-4.1.1 and angiostatin show reduced IL-17 release following stimulation with antigen (MOG_{35-55}). Data is also shown for co-stimulation with T-cell expander beads (CD3/CD28). Supernatants were analyzed by ELISA. Bars indicate release for wild type controls, untreated EAE, EAE + B20-4.1.1, EAE + angiostatin and EAE + treatments combined. Data are shown as mean ± SEM, each sample was pooled from 2 mice, n = 4-12 samples for each bar, significance compares untreated EAE to treated groups (*-**, $p < 0.05$-0.01). a. IL-17 release. b. IFN-γ release. c. IL-4 release. *Data obtained by Dr. CD Doucette*

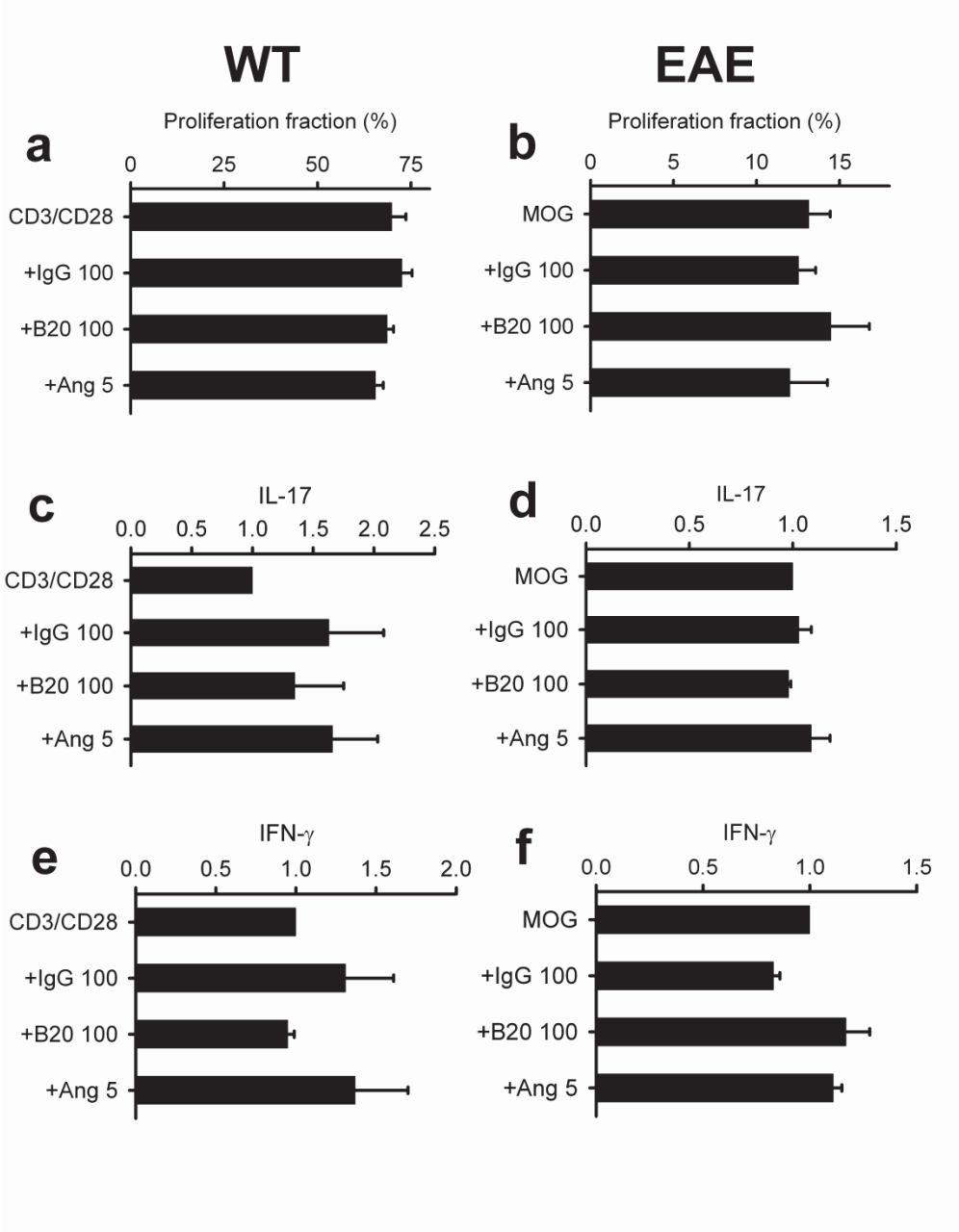

Figure 5.7. B20-4.1.1 and angiostatin have no effect on proliferation and cytokine secretion by isolated T-cells. a, b. naive $CD4^+$ T-cells co-stimulated with T-cell expander beads (CD3/CD28). c, d.. T-cells from mice with untreated EAE restimulated with MOG_{35-55} added to BMDCs. Data is shown as mean ± SEM, each data point pooled from 2 mice, n = 4 for panels a,b, 2 for panels b,d. Control, Ab = IgG; Anti-VEGF = B20-4.1.1. *Data obtained by Dr. CD Doucette*

CHAPTER 6: CONCLUSIONS

6.1 Significance of Experimental Findings

This study is among the first to explore the regulation of angiogenesis in MS pathogenesis using EAE, and to determine its potential as a therapeutic target. We demonstrate that angiogenesis coincides with peak inflammation and clinical markers of disease severity and that this process can be linked to alterations in the VEGF and Ang/Tie pathways – both of which have been previously implicated as pathogenic mechanisms in other disease models. In addition, we provide novel evidence for immune regulation of angiogenesis in EAE and MS tissue by demonstrating that infiltrating immune populations contribute to the expression of angiogenic regulators. Using several anti-angiogenic strategies, the use of two indirect inhibitors that modulate VEGF, and one direct inhibitor that inhibits vascular endothelial processes, angiostatin, we provide evidence to suggest a direct link between angiogenesis and disease parameters in EAE. In addition, we find that anti-angiogenic therapy produces secondary effects on peripheral immune activation during EAE, reducing the proliferative capacity of the effector pathogenic immune population in EAE and reducing the recruitment of these cells into the CNS, suggesting close links between angiogenesis and immune activation in autoimmune diseases like MS. By showing that different classes of angiogenesis inhibitor have similar effects on EAE, this work adds to the mounting evidence for a pathogenic role for angiogenesis in this animal model, and by extension, perhaps to MS.

6.2 VEGF and Angiopoietins in EAE

As previously described, during angiogenesis the vasculature of the CNS is established by endothelial cells, and in the case of small capillaries, this process is facilitated by pericytes [193]. Physiological angiogenesis, such as occurs during embryonic

development or wound healing, progresses through degradation of the vessel ECM, proliferation and migration of the vascular endothelial cells and sprouting of the vessel, followed by a resolution phase where endothelial cell proliferation is reduced and the new blood vessel is stabilized by recruitment of pericytes [193]. Pathologic angiogenesis shares many processes and regulators with physiological angiogenesis, but is characterized by disruption of the resolution and/or restabilization phase [193].

VEGF has been identified to be a key regulator of physiological angiogenesis [194,195]; however, it has also been implicated in several autoimmune and CNS diseases [195]. In MS specifically, VEGF expression has been shown to be consistently upregulated in both acute and chronic lesions [93]. In addition, MRI studies have demonstrated that VEGF levels positively correlate with the length of spinal cord lesions [196]. Elevated levels of VEGF have also been shown in animal models of MS as presented in this thesis, among other studies [111,154] and induced expression of VEGF leads to worsening of disease progression [111]. Taken together, this data suggests that expression of VEGF in MS may exacerbate the inflammatory response, making this a potential therapeutic target.

While VEGF has been shown to be vital for induction of endothelial activation, proliferation and survival, its effects are complimented by the Ang/Tie pathway in pathologic angiogenesis [193], making this another interesting pathway to explore in EAE and MS. Our studies provide the first evidence that this pathway becomes altered in EAE in concert with changes in VEGF expression [154]. Ang-1/Tie-2 signalling has been shown to be important for vascular maintenance and in allowing the endothelium to respond to pro-angiogenic stimuli. Ang-2 release from endothelial cells interferes with Ang-1 signalling by binding to Tie-2 resulting in destabilization of the endothelium, and

promotion of angiogenesis in the presence of VEGF [197]. The ratio of Ang-2 to Ang-1 is therefore critical in balancing homeostasis and endothelial responsiveness to angiogenic cues [193].

We propose that the reduced expression of Ang-1 and the elevated expression of VEGF that we observed to precede angiogenesis during EAE results in a permissive environment for angiogenesis. This environment is further promoted by upregulation of Ang-2 in the model, the expression of which coincides with peak inflammation. This lends evidence to the notion that the VEGF and Ang/Tie pathways may be beneficial targets in EAE.

6.3 Angiogenesis and Inflammation

We hypothesize that angiogenesis in MS results in the formation of new vessels which ultimately facilitate the destruction of CNS tissue by serving as a conduit for pathogenic immune cell recruitment, and through the pro-inflammatory properties of some angiogenic regulators. The sprouting of new blood vessels and the recruitment of inflammatory populations are hallmarks of both acute and chronic inflammation, suggesting a potential link between inflammation and angiogenesis. In light of this, it is reasonable to suggest that shared regulators of both inflammation and angiogenesis may underlie inflammatory conditions. VEGF and the angiopoietins have been demonstrated to play critical roles in the recruitment of inflammatory cells, in addition to the angiogenic roles discussed previously [193] lending more support to the notion that these pathways may be pathogenic in the inflammatory phases of EAE and by extension to MS.

While the initiation of an angiogenic response is an important component of wound healing, this process can become deregulated in disease. Our data demonstrate

that in EAE, infiltrating inflammatory populations are expressing the angiogenic factors Ang-1 and Ang-2. We have shown that T-cells are expressing Ang-1 within areas of inflammation, and elevations of Ang-2 can be attributed to infiltrating macrophages – an observation that has been validated in preliminary observations of human MS tissue.

Our study shows Ang-1 expression by T-cells. The minimal literature that is present on T-cells and Ang-1 demonstrates that overexpression of Ang-1 induced in tetracycline-controlled transgenic model results in significantly elevated recruitment of CD4+ T-cells, as well as Tie-2 expressing macrophages [198]. The expression of Ang-1 by T-cells could promote disease progression in EAE for several reasons. Firstly, as demonstrated by Ward *et al* [198], Ang-1 may serve as a chemotactic signal to other pathogenic T-cell clones, promoting their recruitment into the CNS during EAE. In addition, while Ang-1 has been shown to reduce key players in lymphocyte migration across the barrier (specifically ICAM-1 and VCAM-1), it has been shown *in vitro* to result in upregulation of P-selectin on the vascular endothelium [199]. This may result in increased recruitment not only of T-cells but also of neutrophils, which form a major component of the inflammatory population during EAE. Increased expression of PSGL-1, the ligand for P-selectin [102] has been previously documented in peripheral blood CD4+ T-cells from MS patients, and this cell population was shown to have increased transmigrational capacity [200]. Moreover, neutrophil recruitment to the CNS is also regulated by the interaction between PSGL-1 and P-selectin.

Macrophages produce several angiogenic factors, including VEGF, PlGF, and both angiopoietins in several disease models [201]. In addition to influencing angiogenesis through production of angiogenic regulators, they also express the receptors for several of

these and can therefore be influenced themselves. Macrophages express VEGFR-1 and can migrate toward inflammatory and angiogenic environments in response to VEGF [201]. In other models, Tie-2 expressing macrophages have been shown to be recruited to angiogenic areas in response to Ang-1 where they localize to vessel branch points [193].

In our study we demonstrated that macrophages produce Ang-2 in the CNS during EAE which is likely to promote angiogenesis (although this depends on the ratio of Ang-2 to VEGF, since a high Ang-2/VEGF ratio can result in vessel regression) [154]. Ang-2 has been shown in rheumatoid arthritis to preferentially activate synovial macrophages and significantly increase their production of MIP-1α, a proinflammatory cytokine that plays important roles in the recruitment of other inflammatory populations, as well as induces the release of other pro-inflammatory cytokines [202,203]. This could also be occurring in our model, and warrants further investigation.

6.4 Angiogenesis and CNS Antigen Drainage

An interesting facet of the application of anti-angiogenic therapy in EAE is the reduced peripheral T-cell activation we observe in this study. While we demonstrate this phenomenon *in vivo*, we also show that the anti-angiogenic therapies we applied do not have a direct *in vitro* effect on T-cells. One potential mechanism for this could be that diminished angiogenesis in EAE results in reduced drainage of the inciting antigen from the CNS, leading to subsequent reductions in peripheral T-cell activation in the lymph nodes.

In most tissues of the body, presentation of antigen to T and B cells within the secondary lymphoid organs occurs through the migration of APCs and the drainage of antigen along well defined lymphatic vessels. These lymphatic channels do not exist in

the CNS[204]. However, in addition to directly through the blood, antigen drainage from the CNS can occur via two methods: interstitial fluid can be drained along capillary walls (depicted as the blue perivascular space in Fig. 1.1), and the cerebrospinal fluid can be drained from the subarachnoid space and into the lymphatics of the nasal mucosa[204]. Drainage along the perivascular spaces has been shown to move from the parenchyma to the leptomeningeal vasculature, through the base of the skull to the cervical lymph nodes [102,204,205]. During this transit, the antigens are likely to encounter and be taken up by resident APCs within this space, in addition to draining to the lymph nodes and being taken up by APCs there [102,204] .Several studies have demonstrated the presence of myelin antigens in APCs of the perivascular space, indicating that the antigen is in fact at least partially draining through this route [206,207].

Drainage of antigen through the perivascular spaces to the cervical lymph nodes is thought to play a very important role in reactivating central memory T-cells and perpetuating the autoimmune reaction to myelin[204]. In light of this, by reducing the formation of new blood vessels in EAE using anti-angiogenic therapy we may be restricting the conduits available for both drainage of myelin antigens to lymph nodes, and for interactions of the antigens with APCs within the perivascular space. In addition, by simply reducing the number of blood vessels available for transit, the number of APCs travelling to lymph nodes may be reduced.

6.5 Anti-Angiogenic Strategies

The inflammatory component of MS has long been recognized, and serves as the main target for most currently available DMTs. Our study demonstrates a connection between the pathogenic inflammatory populations known to contribute to MS, and

angiogenesis. This connection appears to involve the VEGF and Ang/Tie signalling pathways which have been implicated in other diseases such as cancer, and asthma [208]. Our attempt to block angiogenesis using both direct and indirect agents resulted in significant improvement of disease indicating that angiogenesis may be a promising therapeutic target in MS.

While bevacizumab had a significant effect on disease scores in EAE, and was useful for exploring the contribution of VEGF, it may not be the ideal therapeutic option. In clinical cancer trials, bevacizumab resulted in significant side effects including hypertension, arterial thromboembolic events, intestinal perforation, and proteinuria [195]. Since VEGF results in the production of the vasodilator substance NO, VEGF blockade can result in vasoconstriction and unwanted cardiovascular side effects such as hypertension. In animal cancer models, inhibition of VEGF results in the upregulation of compensatory pathways such as PlGF [201] which can itself promote pathologic angiogenesis. In light of this, other strategies should be considered instead of, or in conjunction with, this agent. For instance, tyrosine kinase inhibitors (TKIs) have been employed in cancer models with similar effects to bevacizumab, but fewer side effects [193]. While bevacizumab interferes with only VEGFR-2 signaling, TKIs are small molecule antagonists that interfere with the function of receptors for both VEGF and PlGF [195], which reduces the activation of compensatory pathways.

Targeting the angiopoietins is of great interest in cancer, where Ang-2 has been demonstrated to promote tumor development [193,209]. Other disease models have explored the combination of Ang-2 inhibition with agents that target VEGF, and resulted in significantly enhanced disease resolution when compared to monotherapy [193].

Application of a recently developed chimeric decoy receptor that is capable of simultaneously blocking VEGF and both angiopoietins has also been shown to block tumor angiogenesis [210]. Considering the robust Ang-2 expression we noted in EAE, these therapeutic strategies would be intriguing to apply to our model.

6.6 Vascular Permeability and EAE

Despite the strong correlation between angiogenesis and disease activity, we did not demonstrate a direct relationship between angiogenesis and increased vascular permeability. There were early increases in vascular permeability before the onset of clinical signs, but absolute values did not correlate with disease activity and angiogenesis. However, the volume of tissue affected by permeability increases showed a correlation with angiogenesis. Angiogenesis may, therefore, increase leakage as a simple function of increased vessel density without affecting absolute values of permeability that reflect the rate of leakage across individual vessels. New vessels are likely to be capillaries, while permeability changes across the BBB tend to affect larger venules.

6.7 Limitations and Future Directions of This Study

Ongoing experiments are exploring the impact of B20-4.1.1 and angiostatin therapies on the immune populations infiltrating the spinal cord in EAE. This study has focused on VEGF and the Ang/Tie pathways as pathogenic mediators in EAE. Selective targeting of VEGF can result in the upregulation of compensatory pathways so that angiogenesis continues to be promoted as a disease mechanism. In light of this, we are currently evaluating experimental tissue from mice treated with bevacizumab and B20-4.1.1 to determine if they show upregulation of PlGF. Future experiments will also

explore the antigen drainage theory discussed in subsection 6.3 by microinjecting tracers into the CNS of EAE mice to determine how anti-angiogenic therapies effect the rate and speed of their delivery to the peripheral lymph nodes.

As mentioned in previous sections, anti-VEGF treatment may not be the ideal clinical choice. Several studies have demonstrated that VEGF plays a neuroprotective role, influencing neuronal survival, and migration [209]. The long term consequences of interfering with this pathway through anti-VEGF therapy have not been evaluated in the CNS. Demyelination of the myelin sheath around neuronal axons is a hallmark of MS. Early in disease remyelination can occur restoring functional deficits; however, over time it is believed this process becomes limited due to impaired oligodendrocyte recruitment and maturation [210]. Several studies have indicated that VEGF may be able to directly influence the migration of oligodendrocyte precursor cells [211,212]. In light of this, while we demonstrate anti-VEGF therapy results in reduced inflammation and acute disease severity, further exploration is needed into how VEGF blockade impacts long term recovery in EAE by examining important components of repair including remyelination and axonal sparing.

In addition, our data suggests that anti-VEGF therapy may have an immunosuppressive role by reducing T-cell migration from the lymph nodes, as well as peripheral immune activation relevant to T_h-17 and T_h-1 cells. While this is beneficial in EAE, this could also result in unwanted immunosuppression. In light of this, additional angiogenic targets may prove more advantageous. Further studies are needed to delineate the complex effects of angiostatin and its potential to reduce the proliferation of antigen-specific clones without general immune supression.

6.8 Conclusions

This study adds to the evidence that angiogenesis plays a pathogenic role in EAE and by extension MS. We suggest that in MS, angiogenesis is initiated as part of the physiological wound-healing response. This process, however, facilitates the recruitment of pathogenic immune cells into the CNS. These cells in turn, express pro-angiogenic factors which have also been shown to promote inflammation, creating a positive-feedback loop and subsequent pathogenic switch in the angiogenic response.

Angiogenesis inhibitors, like angiostatin, may represent a novel therapeutic option for the more effective treatment of MS, by minimizing immune responses against CNS antigens through the suppression of angiogenesis without general immune suppression when combined with agents like bevacizumab or B20-4.1.1. To the extent that EAE replicates changes occurring in MS, we have demonstrated that modulation of angiogenesis may represent a promising strategy in the management of disease progression.

REFERENCES

1. National Multiple Sclerosis Society. About MS: Who gets MS? . 2012.

2. Compston A, Coles A. Multiple sclerosis. *Lancet*. 2008;372(9648):1502-1517. doi: 10.1016/S0140-6736(08)61620-7.

3. Goldenberg MM. Multiple sclerosis review. *P T*. 2012;37(3):175-184.

4. Hemmer B, Archelos JJ, Hartung HP. New concepts in the immunopathogenesis of multiple sclerosis. *Nat Rev Neurosci*. 2002;3(4):291-301.

5. Robbins SL, Kumar V, Cotran RS. Robbins and cotran pathologic basis of disease. . 2010:1450.

6. Frohman EM, Racke MK, Raine CS. Multiple sclerosis--the plaque and its pathogenesis. *N Engl J Med*. 2006;354(9):942-955.

7. Ransohoff RM. Immunology: In the beginning. *Nature*. 2009;462(7269):41-42.

8. Brinkmann V, Billich A, Baumruker T, et al. Fingolimod (FTY720): Discovery and development of an oral drug to treat multiple sclerosis. *Nat Rev Drug Discov*. 2010;9(11):883-897.

9. Navratil JS, Liu CC, Ahearn JM. Apoptosis and autoimmunity. *Immunol Res*. 2006;36(1-3):3-12.

10. Liu H, Pope RM. The role of apoptosis in rheumatoid arthritis. *Curr Opin Pharmacol*. 2003;3(3):317-322.

11. Ramagopalan SV, Ebers GC. Genes for multiple sclerosis. *Lancet*. 2008;371(9609):283-285.

12. Bernard CC, Kerlero de Rosbo N. Multiple sclerosis: An autoimmune disease of multifactorial etiology. *Curr Opin Immunol*. 1992;4(6):760-765.

13. Pender MP. Genetically determined failure of activation-induced apoptosis of autoreactive T cells as a cause of multiple sclerosis. *Lancet*. 1998;351(9107):978-981.

14. Handel AE, Giovannoni G, Ebers GC, Ramagopalan SV. Environmental factors and their timing in adult-onset multiple sclerosis. *Nat Rev Neurol*. 2010;6(3):156-166.

15. Tremlett H, van der Mei IA, Pittas F, et al. Monthly ambient sunlight, infections and relapse rates in multiple sclerosis. *Neuroepidemiology*. 2008;31(4):271-279.

16. Embry AF, Snowdon LR, Vieth R. Vitamin D and seasonal fluctuations of gadolinium-enhancing magnetic resonance imaging lesions in multiple sclerosis. *Ann Neurol*. 2000;48(2):271-272.

17. O'Gorman C, Lucas R, Taylor B. Environmental risk factors for multiple sclerosis: A review with a focus on molecular mechanisms. *Int J Mol Sci*. 2012;13(9):11718-11752.

18. Munger KL, Levin LI, Hollis BW, Howard NS, Ascherio A. Serum 25-hydroxyvitamin D levels and risk of multiple sclerosis. *JAMA*. 2006;296(23):2832-2838.

19. Lunemann JD, Tintore M, Messmer B, et al. Elevated epstein-barr virus-encoded nuclear antigen-1 immune responses predict conversion to multiple sclerosis. *Ann Neurol*. 2010;67(2):159-169.

20. Farrell RA, Antony D, Wall GR, et al. Humoral immune response to EBV in multiple sclerosis is associated with disease activity on MRI. *Neurology*. 2009;73(1):32-38.

21. Goodin DS. The causal cascade to multiple sclerosis: A model for MS pathogenesis. *PLoS One*. 2009;4(2):e4565.

22. Dean G, Elian M. Age at immigration to england of asian and caribbean immigrants and the risk of developing multiple sclerosis. *J Neurol Neurosurg Psychiatry*. 1997;63(5):565-568.

23. Alter M, Leibowitz U, Speer J. Risk of multiple sclerosis related to age at immigration to israel. *Arch Neurol*. 1966;15(3):234-237.

24. Trapp BD, Nave KA. Multiple sclerosis: An immune or neurodegenerative disorder? *Annu Rev Neurosci*. 2008;31:247-269.

25. Filippi M. MR imaging in white matter diseases of the brain and spinal cord. . 2005:473.

26. McDonald WI, Compston A, Edan G, et al. Recommended diagnostic criteria for multiple sclerosis: Guidelines from the international panel on the diagnosis of multiple sclerosis. *Ann Neurol*. 2001;50(1):121-127.

27. Hawkins CP, Mackenzie F, Tofts P, du Boulay EP, McDonald WI. Patterns of blood-brain barrier breakdown in inflammatory demyelination. *Brain*. 1991;114 (Pt 2)(Pt 2):801-810.

28. Navikas V, Link H. Review: Cytokines and the pathogenesis of multiple sclerosis. *J Neurosci Res*. 1996;45(4):322-333.

29. Kingwell E, Bajdik C, Phillips N, et al. Cancer risk in multiple sclerosis: Findings from british columbia, canada. *Brain*. 2012;135(Pt 10):2973-2979.

30. Murray TJ. Diagnosis and treatment of multiple sclerosis. *BMJ*. 2006;332(7540):525-527.

31. Baker D, Gerritsen W, Rundle J, Amor S. Critical appraisal of animal models of multiple sclerosis. *Mult Scler*. 2011;17(6):647-657.

32. Furlan R, Cuomo C, Martino G. Animal models of multiple sclerosis. *Methods Mol Biol*. 2009;549:157-173.

33. Rivers TM, Sprunt DH, Berry GP. Observations on attempts to produce acute disseminated encephalomyelitis in monkeys. *J Exp Med*. 1933;58(1):39-53.

34. Lavi E, Constantinescu CS, Ebooks Corporation. Experimental models of multiple sclerosis. . 2005:922.

35. Kabat EA, Wolf A, Bezer AE. The rapid production of acute disseminated encephalomyelitis in rhesus monkeys by injection of heterologous and homologous brain tissue with adjuvants. *J Exp Med*. 1947;85(1):117-130.

36. Lee JM, Olitsky PK. Simple method for enhancing development of acute disseminated encephalomyelitis in mice. *Proc Soc Exp Biol Med*. 1955;89(2):263-266.

37. Krishnamoorthy G, Wekerle H. EAE: An immunologist's magic eye. *Eur J Immunol*. 2009;39(8):2031-2035.

38. Owens T. Animal models for multiple sclerosis. *Adv Neurol*. 2006;98:77-89.

39. Baxter AG. The origin and application of experimental autoimmune encephalomyelitis. *Nat Rev Immunol*. 2007;7(11):904-912.

40. Croxford AL, Kurschus FC, Waisman A. Mouse models for multiple sclerosis: Historical facts and future implications. *Biochim Biophys Acta*. 2011;1812(2):177-183.

41. Mix E, Meyer-Rienecker H, Hartung HP, Zettl UK. Animal models of multiple sclerosis--potentials and limitations. *Prog Neurobiol*. 2010;92(3):386-404.

42. Stromnes IM, Goverman JM. Active induction of experimental allergic encephalomyelitis. *Nat Protoc*. 2006;1(4):1810-1819.

43. Staykova MA, Linares D, Fordham SA, Paridaen JT, Willenborg DO. The innate immune response to adjuvants dictates the adaptive immune response to autoantigens. *J Neuropathol Exp Neurol*. 2008;67(6):543-554.

44. Pender MP, Nguyen KB, Willenborg DO. Demyelination and early remyelination in experimental allergic encephalomyelitis passively transferred with myelin basic protein-sensitized lymphocytes in the lewis rat. *J Neuroimmunol*. 1989;25(2-3):125-142.

45. Kuerten S, Kostova-Bales DA, Frenzel LP, et al. MP4- and MOG:35-55-induced EAE in C57BL/6 mice differentially targets brain, spinal cord and cerebellum. *J Neuroimmunol*. 2007;189(1-2):31-40.

46. Bettelli E. Building different mouse models for human MS. *Ann N Y Acad Sci*. 2007;1103:11-18.

47. Baker D, O'Neill JK, Gschmeissner SE, Wilcox CE, Butter C, Turk JL. Induction of chronic relapsing experimental allergic encephalomyelitis in biozzi mice. *J Neuroimmunol*. 1990;28(3):261-270.

48. Stromnes IM, Goverman JM. Passive induction of experimental allergic encephalomyelitis. *Nat Protoc*. 2006;1(4):1952-1960.

49. Steinman L, Zamvil SS. How to successfully apply animal studies in experimental allergic encephalomyelitis to research on multiple sclerosis. *Ann Neurol*. 2006;60(1):12-21.

50. Sriram S, Steiner I. Experimental allergic encephalomyelitis: A misleading model of multiple sclerosis. *Ann Neurol*. 2005;58(6):939-945.

51. Arnason B. Tumour necrosis factor neutralization in MS: A cautionary tale. *Int MS J*. 2011;17(2):63-68.

52. Carmeliet P. Angiogenesis in life, disease and medicine. *Nature*. 2005;438(7070):932-936.

53. Rafii S, Lyden D, Benezra R, Hattori K, Heissig B. Vascular and haematopoietic stem cells: Novel targets for anti-angiogenesis therapy? *Nat Rev Cancer*. 2002;2(11):826-835.

54. Greenberg DA, Jin K. From angiogenesis to neuropathology. *Nature*. 2005;438(7070):954-959.

55. Carmeliet P, Jain RK. Molecular mechanisms and clinical applications of angiogenesis. *Nature*. 2011;473(7347):298-307.

56. Kirk S, Frank JA, Karlik S. Angiogenesis in multiple sclerosis: Is it good, bad or an epiphenomenon? *J Neurol Sci*. 2004;217(2):125-130.

57. Kontos CD, Annex BH. Angiogenesis. *Curr Atheroscler Rep*. 1999;1(2):165-171.

58. Rosenstein JM, Krum JM, Ruhrberg C. VEGF in the nervous system. *Organogenesis*. 2010;6(2):107-114.

59. Phng LK, Gerhardt H. Angiogenesis: A team effort coordinated by notch. *Dev Cell*. 2009;16(2):196-208.

60. Jain RK. Molecular regulation of vessel maturation. *Nat Med*. 2003;9(6):685-693.

61. Gaengel K, Genove G, Armulik A, Betsholtz C. Endothelial-mural cell signaling in vascular development and angiogenesis. *Arterioscler Thromb Vasc Biol*. 2009;29(5):630-638.

62. Rolny C, Mazzone M, Tugues S, et al. HRG inhibits tumor growth and metastasis by inducing macrophage polarization and vessel normalization through downregulation of PlGF. *Cancer Cell*. 2011;19(1):31-44.

63. Ballabh P, Braun A, Nedergaard M. The blood-brain barrier: An overview: Structure, regulation, and clinical implications. *Neurobiol Dis*. 2004;16(1):1-13.

64. Mukouyama YS, Gerber HP, Ferrara N, Gu C, Anderson DJ. Peripheral nerve-derived VEGF promotes arterial differentiation via neuropilin 1-mediated positive feedback. *Development*. 2005;132(5):941-952.

65. Carmeliet P, Tessier-Lavigne M. Common mechanisms of nerve and blood vessel wiring. *Nature*. 2005;436(7048):193-200.

66. Ferrara N. VEGF-A: A critical regulator of blood vessel growth. *Eur Cytokine Netw*. 2009;20(4):158-163..

67. Nagy JA, Dvorak AM, Dvorak HF. VEGF-A and the induction of pathological angiogenesis. *Annu Rev Pathol*. 2007;2:251-275.

68. Neufeld G, Kessler O. The semaphorins: Versatile regulators of tumour progression and tumour angiogenesis. *Nat Rev Cancer*. 2008;8(8):632-645.

69. Iruela-Arispe ML, Davis GE. Cellular and molecular mechanisms of vascular lumen formation. *Dev Cell*. 2009;16(2):222-231.

70. Claesson-Welsh L. VEGF-B taken to our hearts: Specific effect of VEGF-B in myocardial ischemia. *Arterioscler Thromb Vasc Biol*. 2008;28(9):1575-1576.

71. Vlahakis NE, Young BA, Atakilit A, Sheppard D. The lymphangiogenic vascular endothelial growth factors VEGF-C and -D are ligands for the integrin alpha9beta1. *J Biol Chem*. 2005;280(6):4544-4552.

72. Carmeliet P, Moons L, Luttun A, et al. Synergism between vascular endothelial growth factor and placental growth factor contributes to angiogenesis and plasma extravasation in pathological conditions. *Nat Med*. 2001;7(5):575-583.

73. Fischer C, Mazzone M, Jonckx B, Carmeliet P. FLT1 and its ligands VEGFB and PlGF: Drug targets for anti-angiogenic therapy? *Nat Rev Cancer*. 2008;8(12):942-956.

74. Sondell M, Lundborg G, Kanje M. Vascular endothelial growth factor has neurotrophic activity and stimulates axonal outgrowth, enhancing cell survival and schwann cell proliferation in the peripheral nervous system. *J Neurosci*. 1999;19(14):5731-5740.

75. Khaibullina AA, Rosenstein JM, Krum JM. Vascular endothelial growth factor promotes neurite maturation in primary CNS neuronal cultures. *Brain Res Dev Brain Res*. 2004;148(1):59-68.

76. Silverman WF, Krum JM, Mani N, Rosenstein JM. Vascular, glial and neuronal effects of vascular endothelial growth factor in mesencephalic explant cultures. *Neuroscience*. 1999;90(4):1529-1541.

77. Jin KL, Mao XO, Greenberg DA. Vascular endothelial growth factor rescues HN33 neural cells from death induced by serum withdrawal. *J Mol Neurosci*. 2000;14(3):197-203.

78. Sun Y, Jin K, Childs JT, Xie L, Mao XO, Greenberg DA. Increased severity of cerebral ischemic injury in vascular endothelial growth factor-B-deficient mice. *J Cereb Blood Flow Metab*. 2004;24(10):1146-1152.

79. Lee HJ, Cho CH, Hwang SJ, et al. Biological characterization of angiopoietin-3 and angiopoietin-4. *FASEB J*. 2004;18(11):1200-1208.

80. Thurston G. Role of angiopoietins and tie receptor tyrosine kinases in angiogenesis and lymphangiogenesis. *Cell Tissue Res*. 2003;314(1):61-68.

81. Augustin HG, Koh GY, Thurston G, Alitalo K. Control of vascular morphogenesis and homeostasis through the angiopoietin-tie system. *Nat Rev Mol Cell Biol*. 2009;10(3):165-177.

82. De Palma M, Venneri MA, Galli R, et al. Tie2 identifies a hematopoietic lineage of proangiogenic monocytes required for tumor vessel formation and a mesenchymal population of pericyte progenitors. *Cancer Cell*. 2005;8(3):211-226.

83. Folkman J, Shing Y. Angiogenesis. *J Biol Chem*. 1992;267(16):10931-10934.

84. Creamer D, Sullivan D, Bicknell R, Barker J. Angiogenesis in psoriasis. *Angiogenesis*. 2002;5(4):231-236.

85. Gallin JI, Snyderman R. *Inflammation: Basic principles and clinical correlates.* 3rd ed. Philadelphia: Lippincott Williams & Wilkins; 1999:1335.

86. Heissig B, Nishida C, Tashiro Y, et al. Role of neutrophil-derived matrix metalloproteinase-9 in tissue regeneration. *Histol Histopathol*. 2010;25(6):765-770.

87. Du R, Lu KV, Petritsch C, et al. HIF1alpha induces the recruitment of bone marrow-derived vascular modulatory cells to regulate tumor angiogenesis and invasion. *Cancer Cell*. 2008;13(3):206-220.

88. Tvorogov D, Anisimov A, Zheng W, et al. Effective suppression of vascular network formation by combination of antibodies blocking VEGFR ligand binding and receptor dimerization. *Cancer Cell*. 2010;18(6):630-640.

89. Lee S, Chen TT, Barber CL, et al. Autocrine VEGF signaling is required for vascular homeostasis. *Cell*. 2007;130(4):691-703.

90. Schwartz JD, Rowinsky EK, Youssoufian H, Pytowski B, Wu Y. Vascular endothelial growth factor receptor-1 in human cancer: Concise review and rationale for development of IMC-18F1 (human antibody targeting vascular endothelial growth factor receptor-1). *Cancer*. 2010;116(4 Suppl):1027-1032.

91. Gupta PK, Prabhakar S, Sharma S, Anand A. Vascular endothelial growth factor-A (VEGF-A) and chemokine ligand-2 (CCL2) in amyotrophic lateral sclerosis (ALS) patients. *J Neuroinflammation*. 2011;8:47-2094-8-47.

92. Rindfleisch E. *Pathological histology:An introduction to the study of pathological anatomy.* London: Trubner & Co.; 1872.

93. Proescholdt MA, Jacobson S, Tresser N, Oldfield EH, Merrill MJ. Vascular endothelial growth factor is expressed in multiple sclerosis plaques and can induce inflammatory lesions in experimental allergic encephalomyelitis rats. *J Neuropathol Exp Neurol*. 2002;61(10):914-925.

94. Ludwin S, Henry J, McFarland H. Vascular proliferation and angiogenesis in MS: Clinical and pathogenic implications. *Journal of Neuropathology and Experimental Neurology*. 2001;60:505.

95. Noseworthy JH, Lucchinetti C, Rodriguez M, Weinshenker BG. Multiple sclerosis. *N Engl J Med*. 2000;343(13):938-952.

96. Griffioen AW, Molema G. Angiogenesis: Potentials for pharmacologic intervention in the treatment of cancer, cardiovascular diseases, and chronic inflammation. *Pharmacol Rev*. 2000;52(2):237-268.

97. Van Meir EG. Cytokines and tumors of the central nervous system. *Glia*. 1995;15(3):264-288.

98. Giovannoni G, Miller DH, Losseff NA, et al. Serum inflammatory markers and clinical/MRI markers of disease progression in multiple sclerosis. *J Neurol*. 2001;248(6):487-495.

99. Ziche M, Morbidelli L. Nitric oxide and angiogenesis. *J Neurooncol*. 2000;50(1-2):139-148.

100. Wuerfel J, Bellmann-Strobl J, Brunecker P, et al. Changes in cerebral perfusion precede plaque formation in multiple sclerosis: A longitudinal perfusion MRI study. *Brain*. 2004;127(Pt 1):111-119.

101. Plumb J, McQuaid S, Mirakhur M, Kirk J. Abnormal endothelial tight junctions in active lesions and normal-appearing white matter in multiple sclerosis. *Brain Pathol*. 2002;12(2):154-169.

102. Engelhardt B, Ransohoff RM. Capture, crawl, cross: The T cell code to breach the blood-brain barriers. *Trends Immunol*. 2012;33(12):579-589.

103. Joice SL, Mydeen F, Couraud PO, et al. Modulation of blood-brain barrier permeability by neutrophils: In vitro and in vivo studies. *Brain Res*. 2009;1298:13-23.

104. Rapoport SI. A mathematical model for vasogenic brain edema. *J Theor Biol*. 1978;74(3):439-467.

105. Go KG. The normal and pathological physiology of brain water. *Adv Tech Stand Neurosurg*. 1997;23:47-142.

106. Costa C, Incio J, Soares R. Angiogenesis and chronic inflammation: Cause or consequence? *Angiogenesis*. 2007;10(3):149-166.

107. Szekanecz Z, Besenyei T, Paragh G, Koch AE. Angiogenesis in rheumatoid arthritis. *Autoimmunity*. 2009;42(7):563-573.

108. Szekanecz Z, Koch AE. Mechanisms of disease: Angiogenesis in inflammatory diseases. *Nat Clin Pract Rheumatol*. 2007;3(11):635-643.

109. Holley JE, Newcombe J, Whatmore JL, Gutowski NJ. Increased blood vessel density and endothelial cell proliferation in multiple sclerosis cerebral white matter. *Neurosci Lett*. 2010;470(1):65-70.

110. Kirk SL, Karlik SJ. VEGF and vascular changes in chronic neuroinflammation. *J Autoimmun*. 2003;21(4):353-363.

111. Roscoe WA, Welsh ME, Carter DE, Karlik SJ. VEGF and angiogenesis in acute and chronic MOG((35-55)) peptide induced EAE. *J Neuroimmunol*. 2009;209(1-2):6-15.

112. Seabrook TJ, Littlewood-Evans A, Brinkmann V, Pollinger B, Schnell C, Hiestand PC. Angiogenesis is present in experimental autoimmune encephalomyelitis and pro-angiogenic factors are increased in multiple sclerosis lesions. *J Neuroinflammation*. 2010;7:95-2094-7-95.

113. Pardridge WM. Blood-brain barrier delivery. *Drug Discov Today*. 2007;12(1-2):54-61. doi: 10.1016/j.drudis.2006.10.013.

114. Daniel PM, Lam DK, Pratt OE. Relation between the increase in the diffusional permeability of the blood-central nervous system barrier and other changes during the development of experimental allergic encephalomyelitis in the lewis rat. *J Neurol Sci*. 1983;60(3):367-376.

115. Juhler M, Barry DI, Offner H, Konat G, Klinken L, Paulson OB. Blood-brain and blood-spinal cord barrier permeability during the course of experimental allergic encephalomyelitis in the rat. *Brain Res*. 1984;302(2):347-355.

116. Kermode AG, Thompson AJ, Tofts P, et al. Breakdown of the blood-brain barrier precedes symptoms and other MRI signs of new lesions in multiple sclerosis. pathogenetic and clinical implications. *Brain*. 1990;113 (Pt 5)(Pt 5):1477-1489.

117. Floris S, Blezer EL, Schreibelt G, et al. Blood-brain barrier permeability and monocyte infiltration in experimental allergic encephalomyelitis: A quantitative MRI study. *Brain*. 2004;127(Pt 3):616-627.

118. Spitsin S, Portocarrero C, Phares TW, et al. Early blood-brain barrier permeability in cerebella of PLSJL mice immunized with myelin basic protein. *J Neuroimmunol*. 2008;196(1-2):8-15.

119. Bennett J, Basivireddy J, Kollar A, et al. Blood-brain barrier disruption and enhanced vascular permeability in the multiple sclerosis model EAE. *J Neuroimmunol*. 2010;229(1-2):180-191.

120. Rumjanek VM, Leyton J, Morley J. Mononuclear cell accumulation and plasma protein extravasation (PPE) during induction, remission and re-challenge of experimental allergic encephalomyelitis in the rat. *J Neurol Sci*. 1984;65(1):81-92.

121. Fabis MJ, Scott GS, Kean RB, Koprowski H, Hooper DC. Loss of blood-brain barrier integrity in the spinal cord is common to experimental allergic encephalomyelitis in knockout mouse models. *Proc Natl Acad Sci U S A*. 2007;104(13):5656-5661.

122. Schlageter KE, Molnar P, Lapin GD, Groothuis DR. Microvessel organization and structure in experimental brain tumors: Microvessel populations with distinctive structural and functional properties. *Microvasc Res*. 1999;58(3):312-328.

123. Easton AS, Sarker MH, Fraser PA. Two components of blood-brain barrier disruption in the rat. *J Physiol*. 1997;503 (Pt 3)(Pt 3):613-623.

124. Tham E, Gielen AW, Khademi M, Martin C, Piehl F. Decreased expression of VEGF-A in rat experimental autoimmune encephalomyelitis and in cerebrospinal fluid

mononuclear cells from patients with multiple sclerosis. *Scand J Immunol*. 2006;64(6):609-622.

125. Sondell M, Sundler F, Kanje M. Vascular endothelial growth factor is a neurotrophic factor which stimulates axonal outgrowth through the flk-1 receptor. *Eur J Neurosci*. 2000;12(12):4243-4254.

126. Papavassiliou E, Gogate N, Proescholdt M, et al. Vascular endothelial growth factor (vascular permeability factor) expression in injured rat brain. *J Neurosci Res*. 1997;49(4):451-460.

127. Alvarez JA, Baird A, Tatum A, et al. Localization of basic fibroblast growth factor and vascular endothelial growth factor in human glial neoplasms. *Mod Pathol*. 1992;5(3):303-307.

128. Mor F, Quintana FJ, Cohen IR. Angiogenesis-inflammation cross-talk: Vascular endothelial growth factor is secreted by activated T cells and induces Th1 polarization. *J Immunol*. 2004;172(7):4618-4623.

129. Plate KH. Mechanisms of angiogenesis in the brain. *J Neuropathol Exp Neurol*. 1999;58(4):313-320.

130. Marti HJ, Bernaudin M, Bellail A, et al. Hypoxia-induced vascular endothelial growth factor expression precedes neovascularization after cerebral ischemia. *Am J Pathol*. 2000;156(3):965-976.

131. Stratmann A, Risau W, Plate KH. Cell type-specific expression of angiopoietin-1 and angiopoietin-2 suggests a role in glioblastoma angiogenesis. *Am J Pathol*. 1998;153(5):1459-1466.

132. Beck H, Acker T, Wiessner C, Allegrini PR, Plate KH. Expression of angiopoietin-1, angiopoietin-2, and tie receptors after middle cerebral artery occlusion in the rat. *Am J Pathol*. 2000;157(5):1473-1483.

133. Nourhaghighi N, Teichert-Kuliszewska K, Davis J, Stewart DJ, Nag S. Altered expression of angiopoietins during blood-brain barrier breakdown and angiogenesis. *Lab Invest*. 2003;83(8):1211-1222.

134. Ohab JJ, Fleming S, Blesch A, Carmichael ST. A neurovascular niche for neurogenesis after stroke. *J Neurosci*. 2006;26(50):13007-13016.

135. Valable S, Bellail A, Lesne S, et al. Angiopoietin-1-induced PI3-kinase activation prevents neuronal apoptosis. *FASEB J*. 2003;17(3):443-445.

136. Ward NL, Putoczki T, Mearow K, Ivanco TL, Dumont DJ. Vascular-specific growth factor angiopoietin 1 is involved in the organization of neuronal processes. *J Comp Neurol*. 2005;482(3):244-256.

137. Poncet S, Gasc JM, Janzer RC, Meyer S, Juillerat-Jeanneret L. Expression of tie-2 in human peripheral and autonomic nervous system. *Neuropathol Appl Neurobiol*. 2003;29(4):361-369.

138. Kosacka J, Figiel M, Engele J, Hilbig H, Majewski M, Spanel-Borowski K. Angiopoietin-1 promotes neurite outgrowth from dorsal root ganglion cells positive for tie-2 receptor. *Cell Tissue Res*. 2005;320(1):11-19.

139. Hansen TM, Moss AJ, Brindle NP. Vascular endothelial growth factor and angiopoietins in neurovascular regeneration and protection following stroke. *Curr Neurovasc Res*. 2008;5(4):236-245.

140. Kobayashi H, Lin PC. Angiopoietin/Tie2 signaling, tumor angiogenesis and inflammatory diseases. *Front Biosci*. 2005;10:666-674.

141. Huang H, Bhat A, Woodnutt G, Lappe R. Targeting the ANGPT-TIE2 pathway in malignancy. *Nat Rev Cancer*. 2010;10(8):575-585.

142. Huang YF, Yang CH, Huang CC, Tai MH, Hsu KS. Pharmacological and genetic accumulation of hypoxia-inducible factor-1alpha enhances excitatory synaptic transmission in hippocampal neurons through the production of vascular endothelial growth factor. *J Neurosci*. 2010;30(17):6080-6093.

143. Lisak RP, Nedelkoska L, Studzinski D, Bealmear B, Xu W, Benjamins JA. Cytokines regulate neuronal gene expression: Differential effects of Th1, Th2 and monocyte/macrophage cytokines. *J Neuroimmunol*. 2011;238(1-2):19-33.

144. Folcik VA, Smith T, O'Bryant S, et al. Treatment with BBB022A or rolipram stabilizes the blood-brain barrier in experimental autoimmune encephalomyelitis: An additional mechanism for the therapeutic effect of type IV phosphodiesterase inhibitors. *J Neuroimmunol*. 1999;97(1-2):119-128.

145. Bolton C, Paul C. MK-801 limits neurovascular dysfunction during experimental allergic encephalomyelitis. *J Pharmacol Exp Ther*. 1997;282(1):397-402.

146. Kean RB, Spitsin SV, Mikheeva T, Scott GS, Hooper DC. The peroxynitrite scavenger uric acid prevents inflammatory cell invasion into the central nervous system in experimental allergic encephalomyelitis through maintenance of blood-central nervous system barrier integrity. *J Immunol*. 2000;165(11):6511-6518.

147. Schreibelt G, Musters RJ, Reijerkerk A, et al. Lipoic acid affects cellular migration into the central nervous system and stabilizes blood-brain barrier integrity. *J Immunol*. 2006;177(4):2630-2637.

148. Lu C, Diehl SA, Noubade R, et al. Endothelial histamine H1 receptor signaling reduces blood-brain barrier permeability and susceptibility to autoimmune encephalomyelitis. *Proc Natl Acad Sci U S A*. 2010;107(44):18967-18972.

149. Gobel K, Pankratz S, Schneider-Hohendorf T, et al. Blockade of the kinin receptor B1 protects from autoimmune CNS disease by reducing leukocyte trafficking. *J Autoimmun*. 2011;36(2):106-114.

150. Gavard J, Patel V, Gutkind JS. Angiopoietin-1 prevents VEGF-induced endothelial permeability by sequestering src through mDia. *Dev Cell*. 2008;14(1):25-36.

151. Sarker MH, Easton AS, Fraser PA. Regulation of cerebral microvascular permeability by histamine in the anaesthetized rat. *J Physiol*. 1998;507 (Pt 3)(Pt 3):909-918.

152. Inglis VI, Jones MP, Tse AD, Easton AS. Neutrophils both reduce and increase permeability in a cell culture model of the blood-brain barrier. *Brain Res*. 2004;998(2):218-229.

153. Hu DE, Easton AS, Fraser PA. TRPV1 activation results in disruption of the blood-brain barrier in the rat. *Br J Pharmacol*. 2005;146(4):576-584.

154. MacMillan CJ, Starkey RJ, Easton AS. Angiogenesis is regulated by angiopoietins during experimental autoimmune encephalomyelitis and is indirectly related to vascular permeability. *J Neuropathol Exp Neurol*. 2011;70(12):1107-1123.

155. Bar-Or A. Immunology of multiple sclerosis. *Neurol Clin*. 2005;23(1):149-75, vii.

156. Peterson JW, Trapp BD. Neuropathobiology of multiple sclerosis. *Neurol Clin*. 2005;23(1):107-29, vi-vii.

157. Presta LG, Chen H, O'Connor SJ, et al. Humanization of an anti-vascular endothelial growth factor monoclonal antibody for the therapy of solid tumors and other disorders. *Cancer Res*. 1997;57(20):4593-4599.

158. Ferrara N, Hillan KJ, Gerber HP, Novotny W. Discovery and development of bevacizumab, an anti-VEGF antibody for treating cancer. *Nat Rev Drug Discov*. 2004;3(5):391-400.

159. Ferrara N, Hillan KJ, Novotny W. Bevacizumab (avastin), a humanized anti-VEGF monoclonal antibody for cancer therapy. *Biochem Biophys Res Commun*. 2005;333(2):328-335.

160. Bock F, Onderka J, Dietrich T, et al. Bevacizumab as a potent inhibitor of inflammatory corneal angiogenesis and lymphangiogenesis. *Invest Ophthalmol Vis Sci*. 2007;48(6):2545-2552.

161. Avisar I, Weinberger D, Kremer I. Effect of subconjunctival and intraocular bevacizumab injections on corneal neovascularization in a mouse model. *Curr Eye Res*. 2010;35(2):108-115.

162. Bock F, Onderka J, Rummelt C, et al. Safety profile of topical VEGF neutralization at the cornea. *Invest Ophthalmol Vis Sci*. 2009;50(5):2095-2102.

163. Dastjerdi MH, Saban DR, Okanobo A, et al. Effects of topical and subconjunctival bevacizumab in high-risk corneal transplant survival. *Invest Ophthalmol Vis Sci*. 2010;51(5):2411-2417.

164. Dastjerdi MH, Sadrai Z, Saban DR, Zhang Q, Dana R. Corneal penetration of topical and subconjunctival bevacizumab. *Invest Ophthalmol Vis Sci*. 2011;52(12):8718-8723.

165. Dratviman-Storobinsky O, Lubin BC, Hasanreisoglu M, Goldenberg-Cohen N. Effect of subconjuctival and intraocular bevacizumab injection on angiogenic gene expression levels in a mouse model of corneal neovascularization. *Mol Vis*. 2009;15:2326-2338.

166. Teixeira LR, Vargas FS, Acencio MM, et al. Blockage of vascular endothelial growth factor (VEGF) reduces experimental pleurodesis. *Lung Cancer*. 2011;74(3):392-395.

167. Rezaeian F, Wettstein R, Egger JF, et al. Erythropoietin-induced upregulation of endothelial nitric oxide synthase but not vascular endothelial growth factor prevents musculocutaneous tissue from ischemic damage. *Lab Invest*. 2010;90(1):40-51.

168. Yang H, Jager MJ, Grossniklaus HE. Bevacizumab suppression of establishment of micrometastases in experimental ocular melanoma. *Invest Ophthalmol Vis Sci*. 2010;51(6):2835-2842.

169. Barzelay A, Lowenstein A, George J, Barak A. Influence of non-toxic doses of bevacizumab and ranibizumab on endothelial functions and inhibition of angiogenesis. *Curr Eye Res*. 2010;35(9):835-841.

170. Eveno C, Gaujoux S, Tobelem G, Pocard M. Did animal offer relevant model for bevacizumab testing? *Br J Cancer*. 2008;99(9):1555; author reply 1556.

171. Liang WC, Wu X, Peale FV, et al. Cross-species vascular endothelial growth factor (VEGF)-blocking antibodies completely inhibit the growth of human tumor xenografts and measure the contribution of stromal VEGF. *J Biol Chem*. 2006;281(2):951-961.

172. Yu L, Wu X, Cheng Z, et al. Interaction between bevacizumab and murine VEGF-A: A reassessment. *Invest Ophthalmol Vis Sci*. 2008;49(2):522-527.

173. MacMillan CJ, Furlong SJ, Doucette CD, Chen PL, Hoskin DW, Easton AS. Bevacizumab diminishes experimental autoimmune encephalomyelitis by inhibiting spinal cord angiogenesis and reducing peripheral T-cell responses. *J Neuropathol Exp Neurol*. 2012;71(11):983-999.

174. Jorgensen SH, Jensen PE, Laursen H, Sorensen PS. Intravenous immunoglobulin ameliorates experimental autoimmune encephalomyelitis and reduces neuropathological abnormalities when administered prophylactically. *Neurol Res*. 2005;27(6):591-597.

175. Fonsatti E, Sigalotti L, Arslan P, Altomonte M, Maio M. Emerging role of endoglin (CD105) as a marker of angiogenesis with clinical potential in human malignancies. *Curr Cancer Drug Targets*. 2003;3(6):427-432.

176. Duff SE, Li C, Garland JM, Kumar S. CD105 is important for angiogenesis: Evidence and potential applications. *FASEB J*. 2003;17(9):984-992.

177. Easton AS, Fraser PA. Variable restriction of albumin diffusion across inflamed cerebral microvessels of the anaesthetized rat. *J Physiol*. 1994;475(1):147-157.

178. Zhang ZG, Zhang L, Jiang Q, et al. VEGF enhances angiogenesis and promotes blood-brain barrier leakage in the ischemic brain. *J Clin Invest*. 2000;106(7):829-838.

179. El-behi M, Rostami A, Ciric B. Current views on the roles of Th1 and Th17 cells in experimental autoimmune encephalomyelitis. *J Neuroimmune Pharmacol*. 2010;5(2):189-197.

180. Fuh G, Wu P, Liang, W-C., Ultsch, M., Lee CV, Moffat B, Wiesmann C. Structure-function studies of two synthetic anti-VEGF fabs and comparison with avastin. *Journal of Biological Chemistry*. 2006;281:6625-6631.

181. Weller RO, Galea I, Carare RO, Minagar A. Pathophysiology of the lymphatic drainage of the central nervous system: Implications for pathogenesis and therapy of multiple sclerosis. *Pathophysiology*. 2010;17(4):295-306.

182. Stefanini MO, Wu FT, Mac Gabhann F, Popel AS. Increase of plasma VEGF after intravenous administration of bevacizumab is predicted by a pharmacokinetic model. *Cancer Res*. 2010;70(23):9886-9894.

183. Cao Y. Antiangiogenic cancer therapy. *Semin Cancer Biol*. 2004;14(2):139-145.

184. Moser TL, Stack MS, Asplin I, et al. Angiostatin binds ATP synthase on the surface of human endothelial cells. *Proc Natl Acad Sci U S A*. 1999;96(6):2811-2816.

185. Moser TL, Kenan DJ, Ashley TA, et al. Endothelial cell surface F1-F0 ATP synthase is active in ATP synthesis and is inhibited by angiostatin. *Proc Natl Acad Sci U S A*. 2001;98(12):6656-6661.

186. Troyanovsky B, Levchenko T, Mansson G, Matvijenko O, Holmgren L. Angiomotin: An angiostatin binding protein that regulates endothelial cell migration and tube formation. *J Cell Biol*. 2001;152(6):1247-1254.

187. Griscelli F, Li H, Bennaceur-Griscelli A, et al. Angiostatin gene transfer: Inhibition of tumor growth in vivo by blockage of endothelial cell proliferation associated with a mitosis arrest. *Proc Natl Acad Sci U S A*. 1998;95(11):6367-6372.

188. Claesson-Welsh L, Welsh M, Ito N, et al. Angiostatin induces endothelial cell apoptosis and activation of focal adhesion kinase independently of the integrin-binding motif RGD. *Proc Natl Acad Sci U S A*. 1998;95(10):5579-5583.

189. Lu H, Dhanabal M, Volk R, et al. Kringle 5 causes cell cycle arrest and apoptosis of endothelial cells. *Biochem Biophys Res Commun*. 1999;258(3):668-673.

190. Lucas R, Holmgren L, Garcia I, et al. Multiple forms of angiostatin induce apoptosis in endothelial cells. *Blood*. 1998;92(12):4730-4741.

191. Hayes AJ, Li LY, Lippman ME. Anti-vascular therapy: A new approach to cancer treatment. *West J Med*. 2000;172(1):39-42.

192. Granger JP. Vascular endothelial growth factor inhibitors and hypertension: A central role for the kidney and endothelial factors? *Hypertension*. 2009;54(3):465-467.

193. Fagiani E, Christofori G. Angiopoietins in angiogenesis. *Cancer Lett*. 2013;328(1):18-26.

194. Distler JH, Hirth A, Kurowska-Stolarska M, Gay RE, Gay S, Distler O. Angiogenic and angiostatic factors in the molecular control of angiogenesis. *Q J Nucl Med*. 2003;47(3):149-161.

195. Birk DM, Barbato J, Mureebe L, Chaer RA. Current insights on the biology and clinical aspects of VEGF regulation. *Vasc Endovascular Surg*. 2008;42(6):517-530.

196. Su JJ, Osoegawa M, Matsuoka T, et al. Upregulation of vascular growth factors in multiple sclerosis: Correlation with MRI findings. *J Neurol Sci*. 2006;243(1-2):21-30.

197. Hanahan D. Signaling vascular morphogenesis and maintenance. *Science*. 1997;277(5322):48-50.

198. Ward NL, Hatala DA, Wolfram JA, Knutsen DA, Loyd CM. Cutaneous manipulation of vascular growth factors leads to alterations in immunocytes, blood

vessels and nerves: Evidence for a cutaneous neurovascular unit. *J Dermatol Sci*. 2011;61(1):14-22.

199. Brindle NP, Saharinen P, Alitalo K. Signaling and functions of angiopoietin-1 in vascular protection. *Circ Res*. 2006;98(8):1014-1023.

200. Bahbouhi B, Berthelot L, Pettre S, et al. Peripheral blood CD4+ T lymphocytes from multiple sclerosis patients are characterized by higher PSGL-1 expression and transmigration capacity across a human blood-brain barrier-derived endothelial cell line. *J Leukoc Biol*. 2009;86(5):1049-1063.

201. Noonan DM, De Lerma Barbaro A, Vannini N, Mortara L, Albini A. Inflammation, inflammatory cells and angiogenesis: Decisions and indecisions. *Cancer Metastasis Rev*. 2008;27(1):31-40.

202. Maurer M, von Stebut E. Macrophage inflammatory protein-1. *Int J Biochem Cell Biol*. 2004;36(10):1882-1886.

203. Krausz S, Garcia S, Ambarus CA, et al. Angiopoietin-2 promotes inflammatory activation of human macrophages and is essential for murine experimental arthritis. *Ann Rheum Dis*. 2012;71(8):1402-1410.

204. Weller RO, Galea I, Carare RO, Minagar A. Pathophysiology of the lymphatic drainage of the central nervous system: Implications for pathogenesis and therapy of multiple sclerosis. *Pathophysiology*. 2010;17(4):295-306.

205. Szentistvanyi I, Patlak CS, Ellis RA, Cserr HF. Drainage of interstitial fluid from different regions of rat brain. *Am J Physiol*. 1984;246(6 Pt 2):F835-44.

206. Li LY, Barlow KD, Metheny-Barlow LJ. Angiopoietins and Tie2 in health and disease. *Pediatr Endocrinol Rev*. 2005;2(3):399-408.

207. Bach F, Uddin FJ, Burke D. Angiopoietins in malignancy. *Eur J Surg Oncol*. 2007;33(1):7-15.

208. Koh YJ, Kim HZ, Hwang SI, et al. Double antiangiogenic protein, DAAP, targeting VEGF-A and angiopoietins in tumor angiogenesis, metastasis, and vascular leakage. *Cancer Cell*. 2010;18(2):171-184.

209. Merrill MJ, Oldfield EH. A reassessment of vascular endothelial growth factor in central nervous system pathology. *J Neurosurg*. 2005;103(5):853-868.

210. Fancy SP, Kotter MR, Harrington EP, et al. Overcoming remyelination failure in multiple sclerosis and other myelin disorders. *Exp Neurol*. 2010;225(1):18-23.

211. Hayakawa K, Pham LD, Som AT, et al. Vascular endothelial growth factor regulates the migration of oligodendrocyte precursor cells. *J Neurosci*. 2011;31(29):10666-10670.

212. Sun J, Sha B, Zhou W, Yang Y. VEGF-mediated angiogenesis stimulates neural stem cell proliferation and differentiation in the premature brain. *Biochem Biophys Res Commun*. 2010;394(1):146-152.

APPENDIX A: COPYRIGHT PERMISSION LETTERS

Copyright Clearance Center

Confirmation Number: 11063835
Order Date: 01/23/2013

Customer Information

Customer: Carolyn MacMillan
Account Number: 3000611027
Organization: Carolyn MacMillan
Email: cj.macmillan@hotmail.com
Phone: +1 (902) 494-6653
Payment Method: Invoice

Order Details

Trends in immunology

Billing Status: **N/A**

Order detail ID:	63373594
Article Title:	Capture, crawl, cross: the T cell code to breach the blood–brain barriers
Author(s):	Engelhardt, Britta ; Ransohoff, Richard M.
DOI:	10.1016/J.IT.2012.07.004
Date:	Dec 01, 2012
ISSN:	1471-4906
Publication Type:	Journal
Volume:	33
Issue:	12
Start page:	579
Publisher:	ELSEVIER LTD.

Permission Status: Granted
Permission type: Republish or display content
Type of use: reuse in a thesis/dissertation
Order License Id: 3074860145782

Number of pages	11
Portion	figures/tables/illustrations
Number of figures/tables/illustrations	1
Format	both print and electronic
Are you the author of this Elsevier article?	No
Will you be translating?	No
Order reference number	
Title of your thesis/dissertation	Angiogenesis as a Pathologic Mechanism and Novel Therapeutic Target in an Animal Model of Multiple Sclerosis
Expected completion date	Mar 2013
Estimated size (number of pages)	200
Elsevier VAT number	GB 494 6272 12
Permissions price	0.00 USD
VAT/Local Sales Tax	0.00 USD

Note: This item was invoiced separately through our **RightsLink service.** More info **$ 0.00**

Total order items: 1 **Order Total: $0.00**

WOLTERS KLUWER HEALTH LICENSE TERMS AND CONDITIONS

Jan 11, 2013

This is a License Agreement between Carolyn J MacMillan ("You") and Wolters Kluwer Health ("Wolters Kluwer Health") provided by Copyright Clearance Center ("CCC"). The license consists of your order details, the terms and conditions provided by Wolters Kluwer Health, and the payment terms and conditions.

All payments must be made in full to CCC. For payment instructions, please see information listed at the bottom of this form.

License Number	3066080024692
License date	Jan 11, 2013
Licensed content publisher	Wolters Kluwer Health
Licensed content publication	Journal of Neuropathology and Experimental Neurology
Licensed content title	Angiogenesis is Regulated by Angiopoietins During Experimental Autoimmune Encephalomyelitis and is Indirectly Related to Vascular Permeability
Licensed content author	Carolyn MacMillan, Ryan Starkey, and Alexander Easton
Licensed content date	Jan 1, 2011
Volume Number	70
Issue Number	12
Type of Use	Dissertation/Thesis
Requestor type	Individual
Title of your thesis / dissertation	Angiogenesis as a Pathologic Mechanism and Novel Therapeutic Target in an Animal Model of Multiple Sclerosis
Expected completion date	Mar 2013
Estimated size(pages)	200
Billing Type	Invoice
Billing address	5850 College Street 11J1 Sir Charles Tupper Building Halifax, NS B3H4R2 Canada
Customer reference info	
Total	0.00 USD
Terms and Conditions	

Terms and Conditions

1. A credit line will be prominently placed and include: for books - the author(s), title of book, editor, copyright holder, year of publication; For journals - the author(s), title of article, title of journal, volume number, issue number and inclusive pages.

2. The requestor warrants that the material shall not be used in any manner which may be considered derogatory to the title, content, or authors of the material, or to Wolters Kluwer.
3. Permission is granted for a one time use only within 12 months from the date of this invoice. Rights herein do not apply to future reproductions, editions, revisions, or other derivative works. Once the 12-month term has expired, permission to renew must be submitted in writing.
4. Permission granted is non-exclusive, and is valid throughout the world in the English language and the languages specified in your original request.
5. Wolters Kluwer cannot supply the requestor with the original artwork or a "clean copy."
6. The requestor agrees to secure written permission from the author (for book material only).
7. Permission is valid if the borrowed material is original to a Wolters Kluwer imprint (Lippincott-Raven Publishers, Williams & Wilkins, Lea & Febiger, Harwal, Igaku-Shoin, Rapid Science, Little Brown & Company, Harper & Row Medical, American Journal of Nursing Co, and Urban & Schwarzenberg - English Language).
8. If you opt not to use the material requested above, please notify Rightslink within 90 days of the original invoice date.
9. Please note that articles in the ahead-of-print stage of publication can be cited and the content may be re-used by including the date of access and the unique DOI number. Any final changes in manuscripts will be made at the time of print publication and will be reflected in the final electronic version of the issue.
   Disclaimer: Articles appearing in the Published Ahead-of-Print section have been peer-reviewed and accepted for publication in the relevant journal and posted online before print publication. Articles appearing as publish ahead-of-print may contain statements, opinions, and information that have errors in facts, figures, or interpretation. Accordingly, Lippincott Williams & Wilkins, the editors and authors and their respective employees are not responsible or liable for the use of any such inaccurate or misleading data, opinion or information contained in the articles in this section.
10. This permission does not apply to images that are credited to publications other than Wolters Kluwer journals. For images credited to non-Wolters Kluwer journal publications, you will need to obtain permission from the journal referenced in the figure or table legend or credit line before making any use of the image(s) or table(s).
11. Other Terms and Conditions:

v1.4

If you would like to pay for this license now, please remit this license along with your payment made payable to "COPYRIGHT CLEARANCE CENTER" otherwise you will be invoiced within 48 hours of the license date. Payment should be in the form of a check or money order referencing your account number and this invoice number RLNK500932665.
Once you receive your invoice for this order, you may pay your invoice by credit card. Please follow instructions provided at that time.

Make Payment To:
Copyright Clearance Center
Dept 001
P.O. Box 843006
Boston, MA 02284-3006

For suggestions or comments regarding this order, contact RightsLink Customer Support: customercare@copyright.com or +1-877-622-5543 (toll free in the US) or +1-978-646-2777.

Gratis licenses (referencing $0 in the Total field) are free. Please retain this printable license for your reference. No payment is required.

WOLTERS KLUWER HEALTH LICENSE TERMS AND CONDITIONS

Jan 11, 2013

This is a License Agreement between Carolyn J MacMillan ("You") and Wolters Kluwer Health ("Wolters Kluwer Health") provided by Copyright Clearance Center ("CCC"). The license consists of your order details, the terms and conditions provided by Wolters Kluwer Health, and the payment terms and conditions.

All payments must be made in full to CCC. For payment instructions, please see information listed at the bottom of this form.

License Number	3066071145327
License date	Jan 11, 2013
Licensed content publisher	Wolters Kluwer Health
Licensed content publication	Journal of Neuropathology and Experimental Neurology
Licensed content title	Bevacizumab Diminishes Experimental Autoimmune Encephalomyelitis by Inhibiting Spinal Cord Angiogenesis and Reducing Peripheral T-Cell Responses
Licensed content author	Carolyn MacMillan, Suzanne Furlong, Carolyn Doucette, et al
Licensed content date	Jan 1, 2012
Volume Number	71
Issue Number	11
Type of Use	Dissertation/Thesis
Requestor type	Individual
Title of your thesis / dissertation	Angiogenesis as a Pathologic Mechanism and Novel Therapeutic Target in an Animal Model of Multiple Sclerosis
Expected completion date	Mar 2013
Estimated size(pages)	200
Billing Type	Invoice
Billing address	5850 College Street 11J1 Sir Charles Tupper Building Halifax, NS B3H4R2 Canada
Customer reference info	
Total	0.00 USD
Terms and Conditions	

Terms and Conditions

1. A credit line will be prominently placed and include: for books - the author(s), title of book, editor, copyright holder, year of publication; For journals - the author(s), title of article, title of journal, volume number, issue number and inclusive pages.

2. The requestor warrants that the material shall not be used in any manner which may be considered derogatory to the title, content, or authors of the material, or to Wolters Kluwer.
3. Permission is granted for a one time use only within 12 months from the date of this invoice. Rights herein do not apply to future reproductions, editions, revisions, or other derivative works. Once the 12-month term has expired, permission to renew must be submitted in writing.
4. Permission granted is non-exclusive, and is valid throughout the world in the English language and the languages specified in your original request.
5. Wolters Kluwer cannot supply the requestor with the original artwork or a "clean copy."
6. The requestor agrees to secure written permission from the author (for book material only).
7. Permission is valid if the borrowed material is original to a Wolters Kluwer imprint (Lippincott-Raven Publishers, Williams & Wilkins, Lea & Febiger, Harwal, Igaku-Shoin, Rapid Science, Little Brown & Company, Harper & Row Medical, American Journal of Nursing Co, and Urban & Schwarzenberg - English Language).
8. If you opt not to use the material requested above, please notify Rightslink within 90 days of the original invoice date.
9. Please note that articles in the ahead-of-print stage of publication can be cited and the content may be re-used by including the date of access and the unique DOI number. Any final changes in manuscripts will be made at the time of print publication and will be reflected in the final electronic version of the issue.
   Disclaimer: Articles appearing in the Published Ahead-of-Print section have been peer-reviewed and accepted for publication in the relevant journal and posted online before print publication. Articles appearing as publish ahead-of-print may contain statements, opinions, and information that have errors in facts, figures, or interpretation. Accordingly, Lippincott Williams & Wilkins, the editors and authors and their respective employees are not responsible or liable for the use of any such inaccurate or misleading data, opinion or information contained in the articles in this section.
10. This permission does not apply to images that are credited to publications other than Wolters Kluwer journals. For images credited to non-Wolters Kluwer journal publications, you will need to obtain permission from the journal referenced in the figure or table legend or credit line before making any use of the image(s) or table(s).
11. Other Terms and Conditions:

v1.4

If you would like to pay for this license now, please remit this license along with your payment made payable to "COPYRIGHT CLEARANCE CENTER" otherwise you will be invoiced within 48 hours of the license date. Payment should be in the form of a check or money order referencing your account number and this invoice number RLNK500932657.
Once you receive your invoice for this order, you may pay your invoice by credit card. Please follow instructions provided at that time.

Make Payment To:
Copyright Clearance Center
Dept 001
P.O. Box 843006
Boston, MA 02284-3006

For suggestions or comments regarding this order, contact RightsLink Customer Support: customercare@copyright.com or +1-877-622-5543 (toll free in the US) or +1-978-646-2777.

Gratis licenses (referencing $0 in the Total field) are free. Please retain this printable license for your reference. No payment is required.